VOL.107 NO.HY6. JUNE 1981

JOURNAL OF THE HYDRAULICS DIVISION

PROCEEDINGS OF
THE AMERICAN SOCIETY
OF CIVIL ENGINEERS

VOL.107 NO.HY6. JUNE 1981

JOURNAL OF THE HYDRAULICS DIVISION

PROCEEDINGS OF
THE AMERICAN SOCIETY
OF CIVIL ENGINEERS

ISSN 0044-796X

Melvin W. Anderson, Editor
University of South Florida

AMERICAN SOCIETY OF CIVIL ENGINEERS

CONTENTS

This Journal is published monthly by the American Society of Civil Engineers. Publications office is at 345 East 47th Street, New York, N.Y. 10017. Address all ASCE correspondence to the Editorial and General Offices at 345 East 47th Street, New York, N.Y. 10017. Allow six weeks for change of address to become effective. Subscription price to members is $16.50. Nonmember subscriptions available; prices obtainable on request. Second-class postage paid at New York, N.Y. and at additional mailing offices. HY.

The Society is not responsible for any statement made or opinion expressed in its publications.

DISCUSSION

Proc. Paper 16282

*Discussion period closed for this paper. Any other discussion received during this discussion period will be published in subsequent Journals.

16313 SUSPENDED SEDIMENT TRANSPORT

KEY WORDS: Continuum hypothesis; Diffusion; Drag; **Fluid dynamics;** Fluid mechanics; Mixtures; **Sediments; Suspended sediments;** Theoretical analysis; **Turbulent diffusion; Turbulent flow**

ABSTRACT: The transport of suspended sediment in a turbulent flow is examined through the continuum theory of mixtures. Turbulent averaging, applied to the mixture momentum balances, yields a correlation representing the effect on the particles of the drag associated with velocity fluctuations in the fluid. This correlation balances the buoyant weight of the sediment in a plane uniform mean flow. Thus, classical results for "turbulent diffusion" of particles may be reinterpreted as models for this correlation, and the source of the diffusion process is clearly identified in view of the dynamics of fluid-particle interaction. This viewpoint leads to a multi-layer model for the mass transport in a turbulent boundary layer and results in a significant improvement in the accuracy of predicted concentration profiles in steady plane flows.

REFERENCE: McTigue, David F., "Mixture Theory for Suspended Sediment Transport," *Journal of the Hydraulics Division,* ASCE, Vol. 107, No. HY6, **Proc. Paper 16313**, June, 1981, pp. 659-673

16349 SIMULATION OF RIVERINE TRANSPORT

KEY WORDS: **Advection; Dispersion;** Dyes; Hydrodynamics; **Hydrologic models; Mississippi River;** Mixing; **Rivers;** Simulation; Solutes; Transport theory; Water pollution; **Water quality**

ABSTRACT: The transport (advection and dispersion) of a slug of soluble or suspendable material in a river is analyzed by two mathematical descriptions. The models are compared and are applied to a dye study on a 10.7-mile (17.2-km) long reach of the Upper Mississippi River upstream from pool no.2. One model is a mixed cells-in-series (CIS) model and the other is an advection-dispersion (AD) model. Bulk parameters used in both models are related to each other and three sets of field data. The CIS model is simpler in formulation and application than the AD model. Both models give very similar results for the field study. Both models show good agreement for nearly symmetrical time-concentration distribution, but give only a fair description of skewed time-concentration curves. An explanation is provided.

REFERENCE: Stefan, Heinz G., and Demetracopoulos, Alexander C., "Cells-In-Series Simulation of Riverine Transport," *Journal of the Hydraulics Division,* ASCE, Vol. 107, No. HY6, **Proc. Paper 16349**, June, 1981, pp. 675-697

16292 SPECIFIC ENERGY IN COMPOUND OPEN CHANNEL

KEY WORDS: Critical depth; Flow profiles; **Fluid flow; Froude number;** Gradually varied flow; **Open channels; Specific energy;** Subcritical flow

ABSTRACT: A compound-channel Froude number is derived to reflect correctly the occurrence of minimum specific energy in open channels with overbank flow. The limitations of conventional Froude-number formulations are described and comparisons with the proposed compound-channel Froude number are presented. The results of a laboratory investigation into the occurrence of two points of minimum specific energy are presented, and this phenomenon can occur for certain compound-channel geometries as predicted by the compound-channel Froude number. The experimental investigation indicates that the upper point of minimum specific energy can properly be considered the limit of subcritical flow.

REFERENCE: Blalock, Merritt E., and Sturm, Terry W., "Minimum Specific Energy in Compound Open Channel," *Journal of the Hydraulics Division,* ASCE, Vol. 107, No. HY6, **Proc. Paper 16292**, June, 1981, pp. 699-717

16299 DIFFUSION-WAVE FLOOD ROUTING IN CHANNEL NETWORKS

KEY WORDS: Backwater; Channels (waterways); **Flood routing;** Floods; Hydrography; **Networks; Open channels;** Rivers; **Unsteady flow;** Water flow

ABSTRACT: A nonlinear diffusion-wave model is developed for routing of floods in dendritic open-channel networks. The model considers backwater effects from both upstream and downstream ends of a channel. An overlapping-segment technique is adopted to decompose the network. The nonlinear algebraic finite-difference equations are solved through a special formulation of tridiagonal banded matrices. Comparison of the results of the proposed model to those of the dynamic-wave and nonlinear kinematic wave models indicates that the proposed model is nearly as accurate as, and computationally much cheaper, than the dynamic-wave model. It is computationally as inexpensive but more accurate than the nonlinear kinematic-wave model.

REFERENCE: Akan, Ali Osman, and Yen, Ben Chie, "Diffusion-Wave Flood Routing in Channel Networks," *Journal of the Hydraulics Division,* ASCE, Vol. 107, No. HY6, **Proc. Paper 16299**, June, 1981, pp. 719-732

16307 MODELS OF SUSPENDED SEDIMENT DISPERSION

KEY WORDS: **Dispersion; Mathematical models;** Open channels; Probability theory; Sedimentation; **Stochastic processes;** Streams; **Suspended sediments; Turbulent flow**

ABSTRACT: Existing probabilistic methods for predicting turbulent dispersion of suspended sediments are reviewed, starting with the early theory of particle diffusion by continuous movements, and proceeding to more recent random walk simulations. The evolutions of these models are explored along with their limiting assumptions. The methods are basically equivalent. The random walk procedure is not restricted in principle to stationary flows, but it imposes probability distribution restrictions that are not present in the continuous movements technique. A basic problem common to both techniques is that detailed information is needed about the turbulent features of the carrying flow. The sediment diffusivity can be obtained from either Lagrangian or Eulerian information provided that the particle properties and turbulent velocity scales satisfy certain specific relationships.

REFERENCE: Alonso, Carlos V., "Stochastic Models of Suspended-Sediment Dispersion," *Journal of the Hydraulics Division,* ASCE, Vol. 107, No. HY6, **Proc. Paper 16307**, June, 1981, pp. 733-757

16324 RUN HYDROGRAPHS FOR FLOODS

KEY WORDS: Bivariate analysis; Damage; **Dams; Floods;** Hydrograph analysis; **Hydrographs; Hydrology;** Peak floods; Probability distribution functions; **Spillways;** Truncation errors; Volume

ABSTRACT: A bivariate lognormal probability distribution in flood peaks and flood volumes describes families of flood hydrographs, each family with a desired return period. Truncated series of floods are used to estimate the underlying population parameters. The method provides more information on floods than conventional methods, and the theory is illustrated with a worked example. Run hydrograph theory was developed and demonstrated for application on fully-gaged catchments. The method allows for the synthesis of the whole family of design hydrographs for each desired return period. In the development of the theory, hydrographs were analyzed as they occur in the record; thus the sample of hydrographs contains many composite hydrographs. This should result in realistic design hydrographs for practical applications. In the estimation of the necessary parameters it was demonstrated how straightforward it can be to calculate the underlying probability distribution parameters from a truncated sample. The run hydrograph technique may also be amenable towards extrapolation to ungaged catchments.

REFERENCE: Hiemstra, Lourens A.V., and Francis, David M., "Run Hydrographs for Prediction of Flood Hydrographs," *Journal of the Hydraulics Division,* ASCE, Vol. 107, No. HY6, **Proc. Paper 16324**, June, 1981, pp. 759-775

MIXTURE THEORY FOR SUSPENDED SEDIMENT TRANSPORT

By David F. McTigue[1]

INTRODUCTION

The transport of fine particulate matter in turbulent fluid flows is of fundamental importance in a broad range of disciplines. Examples include the movement of dust and pollutants in atmospheric flows, sediment transport in natural waters, and various industrial processes such as the piping of suspensions.

A steady mean rectilinear flow carrying particles denser than the fluid poses an obvious problem: one must appeal to some mechanism to balance the buoyant weight of the particles. It was long ago suggested that this balancing mechanism could be found in "turbulent diffusion" of particles down mean concentration gradients. Indeed, results from diffusion models in various forms compare quite well with both laboratory and field data for concentration profiles in plane turbulent flows.

The success of such models has led to a considerable body of work directed toward identifying the origin of the "diffusion" process and toward generalizing the governing equations so that more complex flows can be analyzed. Most of these efforts, however, assume a priori a gradient diffusion-type process, and yield little physical insight into the balance they attempt to elucidate.

This paper invokes the continuum theory of mixtures to examine the problem described in the previous paragraphs. Mixture theory has been available for a number of years and has in fact been applied to the suspended sediment problem in the past. However, the balance identified here has apparently been overlooked, and leads to a very simple and intuitively appealing result. Equilibrium is struck between the buoyant weight of the particles and a correlation associated with the fluid drag due to vertical velocity fluctuations. The classical "diffusion" term may be interpreted as a *model* for this correlation.

Having identified this correlation with the diffusion process, the scaling of the diffusion coefficients is clarified. A two-layer model is suggested, in which the inner layer (near the bed) is dominated by the length scale y, the distance from the boundary, and the outer layer is dominated by the scale h, the flow

[1]Postdoctoral Research Assoc., Dept. of Earth and Planetary Sci., Massachusetts Inst. of Tech., Cambridge, Mass. 02139.

Note.—Discussion open until November 1, 1981. To extend the closing date one month, a written request must be filed with the Manager of Technical and Professional Publications, ASCE. Manuscript was submitted for review for possible publication on September 3, 1980. This paper is part of the Journal of the Hydraulics Division, Proceedings of the American Society of Civil Engineers, ©ASCE, Vol. 107, No. HY6, June, 1981. ISSN 0044-796X/81/0006-0659/$01.00.

depth. The predicted concentration profile, actually a combination of previously known results, agrees very well with available data.

Previous Work

Schmidt (18) first posed the governing equation for the suspended sediment distribution in a plane rectilinear flow by noting that the net vertical flux of particles must be everywhere zero. The downward flux due to gravitational settling must then be exactly balanced by an upward diffusive flux, giving (see Fig. 1):

$$cU_{\infty} + \epsilon_s \frac{dc}{dy} = 0 \quad \text{(1)}$$

in which c = concentration or volume fraction of solids; U_{∞} = settling velocity of particles; and ϵ_s = diffusion coefficient for sediment. Eq. 1 is presented

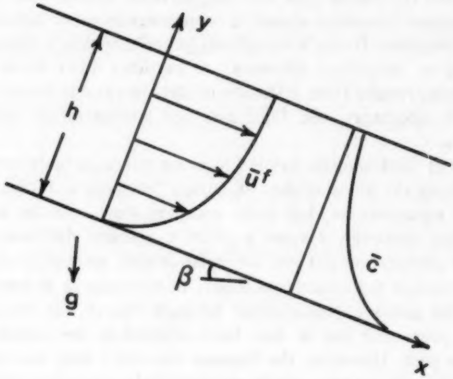

FIG. 1.—Definition Sketch for Gravity Flow

in virtually all standard texts on sedimentation (e.g., 9, 16, 21), and various choices of the coefficient, ϵ_s, in general taken to be a function of y, are explored. Considerable effort has been given to developing a more general theory that will yield Eq. 1 as a special case. Several approaches are considered briefly below.

Convection-Diffusion Theories.—Sediment dispersal in turbulent flows having been observed to exhibit diffusion-like characteristics, it has often been suggested that a classical convection-diffusion model for the concentration is an appropriate generalization. This can be motivated in the following manner. The mass balance for the fluid, of constant density, ρ^f, is given by

$$\frac{\partial}{\partial t}(1 - c) + \nabla \cdot [(1 - c)\mathbf{u}^f] = 0 \quad \text{(2)}$$

in which $\mathbf{u}^f$ = fluid velocity. Introducing the Reynolds decompositions, $c = \bar{c} + c'$, $\mathbf{u}^f = \bar{\mathbf{u}}^f + \mathbf{u}^{f\prime}$, where overbars indicate mean quantities and primes indicate fluctuating quantities, and averaging gives

$$\frac{\partial \bar{c}}{\partial t} + \bar{\mathbf{u}}^f \cdot \nabla \bar{c} = -\nabla \cdot (\overline{c' \mathbf{u}^{f\prime}}) + (1 - \bar{c}) \nabla \cdot \bar{\mathbf{u}}^f \quad \ldots \ldots \ldots \ldots \ldots \ldots \ldots \ldots \ldots (3)$$

For $c << 1$, Eq. 2 gives $\nabla \cdot \mathbf{u}^f \simeq 0$, and the last term in 3 may be neglected. If a Boussinesq model for the correlation is now introduced, such that

$$\overline{c' \mathbf{u}^{f\prime}} \equiv -\boldsymbol{\epsilon} \cdot \nabla \bar{c} \quad \ldots \ldots \ldots \ldots \ldots \ldots \ldots \ldots \ldots \ldots \ldots \ldots \ldots \ldots \ldots \ldots \ldots (4)$$

in which $\boldsymbol{\epsilon}$ is a second-order tensor of diffusion coefficients, Eq. 3 becomes the classical convection-diffusion equation:

$$\frac{\partial \bar{c}}{\partial t} + \bar{\mathbf{u}}^f \cdot \nabla \bar{c} = \nabla \cdot (\boldsymbol{\epsilon} \cdot \nabla \bar{c}) \quad \ldots \ldots \ldots \ldots \ldots \ldots \ldots \ldots \ldots \ldots \ldots \ldots \ldots \ldots \ldots \ldots (5)$$

Eq. 5 does not reduce to Eq. 1 for plane rectilinear flow, although that assertion has erroneously been made (9). Furthermore, Eq. 5 is motivated entirely by kinematic arguments, and provides no insight into the dynamic process of sediment dispersal.

Two-Phase Flow Theories.—Soo and co-workers (20) have developed an extensive body of theory and analysis based in part on the dynamics of the particulate phase. This theory is able to reproduce the balance given by Eq. 1, but, in its present form, the theory exhibits several shortcomings.

First, the gradient diffusion term introduced by, for example, Soo and Tung (20) again has no dynamic significance. It arises through the Reynolds decomposition and averaging applied to the particulate phase mass balance (19), in a fashion similar to that shown in Eqs. 2–5. It is further noted here that, although the averaging scheme is applied to the mass balance to obtain the diffusion term, it is not then applied to the momentum balance. Thus, other correlations of fluctuating quantities that should be accounted for are neglected. Also, this leads to a situation where *averaged* velocities are equated with *exact* velocities. If the averaging is carried out consistently throughout the derivation of the two-phase theory, results very similar to those that follow can be obtained.

Finally, the two-phase theory leads to a second-order equation for the concentration in plane rectilinear flow, the first integral of which gives Eq. 1 when the integration constant is taken to be zero. This introduces further ambiguity to the problem already present in determining an appropriate condition for even the first-order equation given by Eq. 1.

Mixture Theory

The approach adopted here is grounded in the formalism of the continuum theory of mixtures [see Atkin and Craine (1,2) for a general review]. A few studies of particulate transport in turbulent flows have been made in view of mixture theory, but have led to significantly different results (4,5,15). Comparisons will be noted where appropriate in the following developments.

The theory assumes that the fluid and the dispersed solid particles can each be treated as continuous media. For fluid and solid densities ρ^f and ρ^s, respectively,

and particle volume fraction (concentration) c, the bulk densities of the fluid and particulate phases *in the mixture* are $\rho^f(1-c)$ and $\rho^s c$, respectively. The mass balance equations, for constant ρ^f and ρ^s, are then

$$\frac{\partial}{\partial t}(1-c) + \nabla\cdot[(1-c)\mathbf{u}^f] = 0 \quad \ldots\ldots\ldots\ldots\ldots\ldots\ldots\ldots\ldots\ldots (6)$$

$$\frac{\partial c}{\partial t} + \nabla\cdot(c\mathbf{u}^s) = 0 \quad \ldots\ldots\ldots\ldots\ldots\ldots\ldots\ldots\ldots\ldots\ldots\ldots (7)$$

in which $\mathbf{u}^s$ = velocity of dispersed solid phase. The momentum balances are (11):

$$\rho^f(1-c)\left(\frac{\partial \mathbf{u}^f}{\partial t} + \mathbf{u}^f\cdot\nabla\mathbf{u}^f\right) = \nabla\cdot[(1-c)\mathbf{T}^f] + \rho^f(1-c)\mathbf{g} - \mathbf{F} \quad \ldots\ldots\ldots (8)$$

$$\rho^s c\left(\frac{\partial \mathbf{u}^s}{\partial t} + \mathbf{u}^s\cdot\nabla\mathbf{u}^s\right) = \nabla\cdot(c\mathbf{T}^s) + \rho^s c\mathbf{g} + \mathbf{F} \quad \ldots\ldots\ldots\ldots\ldots\ldots (9)$$

in which $\mathbf{T}^f$ = fluid phase stress; $\mathbf{T}^s$ = dispersed solid phase stress; $\mathbf{g}$ = acceleration of gravity; and $\mathbf{F}$ = force of the fluid on the particulate phase per unit volume. Note that the interaction term, $\mathbf{F}$, vanishes when Eqs. 8 and 9 are added to obtain a momentum balance for the mixture. Also, in the limit as c vanishes, Eqs. 8 and 9 reduce properly to the momentum balance for a single fluid.

Closure to the system of Eqs. 6–9 is obtained by posing constitutive equations for the stresses, $\mathbf{T}^f$ and $\mathbf{T}^s$, and the interaction force, $\mathbf{F}$. For simplicity, the independent constitutive variables assumed here are

$$\mathbf{u}^f - \mathbf{u}^s \quad \text{and} \quad \nabla c \quad \ldots\ldots\ldots\ldots\ldots\ldots\ldots\ldots\ldots\ldots\ldots\ldots (10)$$

both of which are properly invariant (14). Neglect of any dependence on the rate of deformation of the fluid, the rate of deformation of the particulate phase, and the relative rotation rate anticipates that concern is limited here to flows in which inertia dominates the flow behavior. Thus, the detailed form of the rate-dependent terms in the constitutive equations is unimportant, an assumption that is clearly valid in the limit of very small concentrations ($c << 1$) and high mean flow Reynolds numbers. The neglected dissipative stress terms are crucial, of course, to *energy* balance considerations (5), which are not addressed here.

The linear, isotropic constitutive equations based on the assumptions of Eq. 10 are

$$\mathbf{T}^f = -p^f\mathbf{1} \quad \ldots\ldots\ldots\ldots\ldots\ldots\ldots\ldots\ldots\ldots\ldots\ldots\ldots\ldots (11)$$

$$\mathbf{T}^s = -p^s\mathbf{1} \quad \ldots\ldots\ldots\ldots\ldots\ldots\ldots\ldots\ldots\ldots\ldots\ldots\ldots\ldots (12)$$

$$\mathbf{F} = f_1(\mathbf{u}^f - \mathbf{u}^s) + f_2\nabla c \quad \ldots\ldots\ldots\ldots\ldots\ldots\ldots\ldots\ldots\ldots (13)$$

in which p^f and p^s = the fluid and dispersed solid phase pressures, respectively; and f_1 and f_2 = in general, scalar functions of the concentration, c. Thus, each phase is modeled as an ideal fluid.

It is assumed that the pressure of each phase is identical; that is, $p^f = p^s$

$= p$ (7,11). Thus, $-p$ is simply the mean normal stress of the mixture, (1/3) tr $\mathbf{T}^m$, in which $\mathbf{T}^m = (1 - c)\mathbf{T}^f + c\mathbf{T}^s$. The terms appearing in Eq. 13 are readily identifiable with well-known fluid-particle interaction forces. The term in the relative velocity, $\mathbf{u}^f - \mathbf{u}^s$, is the drag force. In its linear form, the drag term is limited to the Stokes range (small particle Reynolds numbers), and, for noninteracting ($c << 1$) spherical particles, is given by

$$f_1 = \frac{9\mu}{2a^2} c \quad (14)$$

in which a = particle radius; and μ = fluid viscosity. The validity of the drag term may easily be extended to larger particle Reynolds numbers by allowing nonlinear terms in Eq. 13, in which case f_1 can be a function of the invariant $|\mathbf{u}^f - \mathbf{u}^s|$ (20). The second term in Eq. 13 is identified with the force of the fluid pressure on the dispersed solid phase, giving (6)

$$f_2 = p \quad (15)$$

The form of the term $f_2 \nabla c$ is suggestive of a gradient diffusion process, and indeed, a diffusivity, D, might be included in f_2 to represent Brownian diffusion. Peddieson (15) has suggested that such a term may also represent "turbulent diffusion" of the particles. However, simply inserting a turbulent diffusivity into the constitutive model is somewhat ad hoc, insofar as such a process cannot be readily identified in the exact equations of motion. Reynolds decomposition and averaging of the Brownian diffusion term does not result in an additional "turbulent diffusion" term, and the effect of Brownian motion on large particles is exceedingly small.

Collecting the results of Eqs. 8–15

$$\rho^f(1 - c)\left(\frac{\partial \mathbf{u}^f}{\partial t} + \mathbf{u}^f \cdot \nabla \mathbf{u}^f\right) = -(1 - c)\nabla p + \rho^f(1 - c)\mathbf{g} - \frac{9\mu}{2a^2} c\,(\mathbf{u}^f - \mathbf{u}^s) \quad (16)$$

$$\rho^s c\left(\frac{\partial \mathbf{u}^s}{\partial t} + \mathbf{u}^s \cdot \nabla \mathbf{u}^s\right) = -c\nabla p + \rho^s c\mathbf{g} + \frac{9\mu}{2a^2} c\,(\mathbf{u}^f - \mathbf{u}^s) \quad (17)$$

Eqs. 6, 7, 16, and 17 give a complete set of eight equations for the eight unknowns, $\mathbf{u}^f$, $\mathbf{u}^s$, p, and c. Identical equations of motion have been used by Drew (4) and derived by Hinze (10), neglecting viscous terms and virtual mass effects.

Turbulent Fluctuations and Averaging

The decomposition and averaging scheme adopted here is from Drew (4), and is only briefly outlined in the following. The velocities and concentration are decomposed into mean and fluctuating parts: $\mathbf{u}^f = \bar{\mathbf{u}}^f + \mathbf{u}^{f\prime}$, $\mathbf{u}^s = \bar{\mathbf{u}}^s + \mathbf{u}^{s\prime}$, $c = \bar{c} + c'$. The mean velocities, $\bar{\mathbf{u}}^f$ and $\bar{\mathbf{u}}^s$, are defined in terms of mean momenta, such that

$$\rho^f(1 - \bar{c})\bar{\mathbf{u}}^f = \overline{\rho^f(1 - c)\mathbf{u}^f} \quad (18)$$

$$\rho^s \bar{c}\,\bar{\mathbf{u}}^s = \overline{\rho^s c \mathbf{u}^s} \quad (19)$$

Thus, the average of the velocity fluctuations does not vanish. Rather, $\overline{\mathbf{u}^{f\prime}}$

$= \overline{c\mathbf{u}^{f\prime}}$ and $\overline{c\mathbf{u}^{s\prime}} = 0$. This scheme, originally developed for treating compressible fluid flows, yields only one correlation from the inertial terms in Eqs. 16 or 17. Applying these definitions to Eqs. 6, 7, 16, and 17 gives the mass and momentum balances for the fluid and particulate phases:

$$\frac{\partial}{\partial t}(1-\bar{c}) + \nabla\cdot[(1-\bar{c})\bar{\mathbf{u}}^f] = 0 \quad \ldots\ldots\ldots\ldots\ldots\ldots\ldots\ldots \quad (20)$$

$$\frac{\partial \bar{c}}{\partial t} + \nabla\cdot(\bar{c}\,\bar{\mathbf{u}}^s) = 0 \quad \ldots\ldots\ldots\ldots\ldots\ldots\ldots\ldots\ldots\ldots \quad (21)$$

$$\rho^f(1-\bar{c})\left(\frac{\partial \bar{\mathbf{u}}^f}{\partial t} + \bar{\mathbf{u}}^f\cdot\nabla\bar{\mathbf{u}}^f\right) = -(1-\bar{c})\nabla\bar{p} + \overline{c'\nabla p'} - \frac{9\mu}{2a^2}\bar{c}(\bar{\mathbf{u}}^f - \bar{\mathbf{u}}^s)$$

$$-\frac{9\mu}{2a^2}\overline{c'\mathbf{u}^{f\prime}} + \rho^f(1-\bar{c})\mathbf{g} + \rho^f\nabla\cdot[\overline{(1-c)\mathbf{u}^{f\prime}\mathbf{u}^{f\prime}}] \quad \ldots\ldots\ldots\ldots \quad (22)$$

$$\rho^s\bar{c}\left(\frac{\partial \bar{\mathbf{u}}^s}{\partial t} + \bar{\mathbf{u}}^s\cdot\nabla\bar{\mathbf{u}}^s\right) = -\bar{c}\nabla\bar{p} - \overline{c'\nabla p'} + \frac{9\mu}{2a^2}\bar{c}(\bar{\mathbf{u}}^f - \bar{\mathbf{u}}^s)$$

$$+\frac{9\mu}{2a^2}\overline{c'\mathbf{u}^{f\prime}} + \rho^s\bar{c}\mathbf{g} + \rho^s\nabla\cdot(\overline{c\mathbf{u}^{s\prime}\mathbf{u}^{s\prime}}) \quad \ldots\ldots\ldots\ldots\ldots\ldots \quad (23)$$

in which $p = \bar{p} + p'$ has been introduced; and $\overline{p'} = 0$. Identical equations were obtained by Drew (4).

Plane Rectilinear Flow

Consider now the classical problem of steady plane gravity flow with a free surface (Fig. 1). Solutions are sought for the flow when $\bar{\mathbf{u}}^f = \{\bar{u}^f(y), 0, 0\}$, $\bar{\mathbf{u}}^s = \{\bar{u}^s(y), 0, 0\}$, $\mathbf{u}^{f\prime} = \{u^{f\prime}, v^{f\prime}, w^{f\prime}\}$, $\mathbf{u}^{s\prime} = \{u^{s\prime}, v^{s\prime}, w^{s\prime}\}$, $\partial/\partial x = \partial/\partial z = 0$, and $\bar{c} = \bar{c}(y)$. Eqs. 20 and 21 are then identically satisfied, and 22 and 23 each reduce to an x and a y component:

$$0 = (1-\bar{c})\rho^f g\sin\beta - \frac{9\mu}{2a^2}\bar{c}(\bar{u}^f - \bar{u}^s) - \frac{9\mu}{2a^2}\overline{c'u^{f\prime}}$$

$$+\rho^f\frac{\partial}{\partial y}[\overline{(1-c)u^{f\prime}v^{f\prime}}] \quad \ldots\ldots\ldots\ldots\ldots\ldots\ldots\ldots \quad (24)$$

$$0 = -(1-\bar{c})\frac{\partial \bar{p}}{\partial y} + \overline{c'\frac{\partial p'}{\partial y}} - (1-\bar{c})\rho^f g\cos\beta$$

$$-\frac{9\mu}{2a^2}\overline{c'v^{f\prime}} + \rho^f\frac{\partial}{\partial y}[\overline{(1-c)v^{f\prime}v^{f\prime}}] \quad \ldots\ldots\ldots\ldots\ldots\ldots \quad (25)$$

$$0 = \bar{c}\rho^s g\sin\beta + \frac{9\mu}{2a^2}\bar{c}(\bar{u}^f - \bar{u}^s) + \frac{9\mu}{2a^2}\overline{c'u^{f\prime}} + \rho^s\frac{\partial}{\partial y}(\overline{cu^{s\prime}v^{s\prime}}) \quad \ldots \quad (26)$$

$$0 = -\bar{c}\frac{\partial \bar{p}}{\partial y} - \overline{c'\frac{\partial p'}{\partial y}} - \bar{c}\rho^s g\cos\beta + \frac{9\mu}{2a^2}\overline{c'v^{f\prime}} + \rho^s\frac{\partial}{\partial y}(\overline{cv^{s\prime}v^{s\prime}}) \quad (27)$$

Adding the two x-momentum equations, Eqs. 24 and 26:

$$0 = [(1 - \bar{c})\rho^f + \bar{c}\rho^s]\, g \sin\beta + \rho^f \frac{\partial}{\partial y}\left[\overline{(1-c)u^{f\prime} v^{f\prime}}\right]$$

$$+ \rho^s \frac{\partial}{\partial y}\left(\overline{cu^{s\prime} v^{s\prime}}\right) \quad \ldots\ldots\ldots\ldots\ldots\ldots\ldots\ldots\ldots\ldots\ldots\ldots \quad (28)$$

When ρ^f and ρ^s are of the same order, as is the case for, say, quartz particles in water, and assuming that the fluid and particle velocity fluctuations are of the same order, Eq. 28 may be approximated for $c << 1$ by

$$0 \simeq \rho^f g \sin\beta + \rho^f \frac{\partial}{\partial y}\left(\overline{u^{f\prime} v^{f\prime}}\right) \quad \ldots\ldots\ldots\ldots\ldots\ldots\ldots\ldots\ldots\ldots \quad (29)$$

the classical balance between the gravitational driving force and the gradient of the Reynolds stress in a pure fluid. Note that Eq. 29 suggests that the characteristic scale of the velocity fluctuations is of the order of $(gh \sin\beta)^{1/2}$, in which h = the flow depth, leading to the usual definition of a shear velocity; $u_* \equiv (\tau_0/\rho^f)^{1/2}$, where $\tau_0 = \rho^f gh \sin\beta \simeq \rho^f gh\beta$ for small β. Solution of Eq. 29, of course, requires the adoption of a model for the correlation $\overline{u^{f\prime} v^{f\prime}}$. The most common choice is a mixing-length model, which leads in the present case to the familiar logarithmic "defect-law" profile for $\bar{u}^f$ (16), and requires no further consideration here.

Now consider the y-momentum balances, Eqs. 25 and 27. Eliminating the mean pressure gradient between the two equations and again approximating for small concentrations ($1 - \bar{c} \simeq 1$) and small slopes ($\cos\beta \simeq 1$) gives

$$0 = -\overline{c' \frac{\partial p'}{\partial y}} - \bar{c}(\rho^s - \rho^f)g + \frac{9\mu}{2a^2}\overline{c' v^{f\prime}}$$

$$+ \rho^s \frac{\partial}{\partial y}\left(\overline{cv^{s\prime} v^{s\prime}}\right) - \bar{c}\rho^f \frac{\partial}{\partial y}\left(\overline{v^{f\prime} v^{f\prime}}\right) \quad \ldots\ldots\ldots\ldots\ldots\ldots\ldots \quad (30)$$

The second term is the buoyant weight of the dispersed particulate phase, and the term or terms that balance this are sought. In order to examine this balance, Eq. 30 is nondimensionalized assuming that c scales with a characteristic concentration c_0, $v^{f\prime}$ and $v^{s\prime}$ with u_* (see aforementioned identity), and $\partial/\partial y$ with $1/h$. Rearranging so that the buoyant weight term is of order unity, Eq. 30 becomes

$$0 = -\bar{c} + \frac{u_*}{U_\infty}\overline{c' v^{f\prime}} + \left(\frac{U^2}{g'h}\right)\left(\frac{u_*}{U}\right)^2 \left(-\overline{c' \frac{\partial p'}{\partial y}}\right.$$

$$\left. + \frac{\rho^s}{\rho^f}\frac{\partial}{\partial y}\left(\overline{cv^{s\prime} v^{s\prime}}\right) - \bar{c}\frac{\partial}{\partial y}\left(\overline{v^{f\prime} v^{f\prime}}\right)\right) \quad \ldots\ldots\ldots\ldots\ldots\ldots \quad (31)$$

in which $U_\infty = 2a^2(\rho^s - \rho^f)g/9\mu$ = settling velocity of particle in still fluid; U = characteristic mean flow velocity; $g' = (\rho^s - \rho^f)g/\rho^f$; and all variables are now dimensionless and of order unity. Note that the group $U^2/g'h$ is the square of the "densiometric" Froude number.

Consider a typical wide stream carrying very fine quartz sand [$a = 5.0 \times 10^{-5}$ m (2.0×10^{-3} in.), $U_\infty \simeq 1.0 \times 10^{-2}$ m/s (3.3×10^{-2} fps)] over a flat bottom. For slope $\beta \simeq 10^{-4}$ and depth $h \simeq 1.0$ m (39 in.), the mean flow velocity is about 1.0 m/s (3.3 fps) and it is found that the second term in Eq. 31 is of order unity, while the terms in brackets are of order 10^{-4}. Thus, returning to dimensional variables, it is clear that the buoyant weight of the particles in Eq. 30 is balanced by the drag associated with the vertical velocity fluctuations in the fluid:

$$\bar{c}(\rho^s - \rho^f)g \simeq \frac{9\mu}{2a^2}\,\overline{c'\,v^{f'}} \quad \text{(32)}$$

Note that Drew (4) examined the identical problem in view of the same governing equations, but discarded the term in $\overline{c'\,\mathbf{u}^{f'}}$ early in his analysis. He was thus forced to find the balance with the Reynolds stress terms appearing in Eq. 30.

The foregoing arguments assume that the characteristic length scale of the flow is h, the total depth. Near the bed, however, the relevant scale is y, the distance from the bed. This suggests, based on Eq. 29, that the velocity fluctuations scale with $u_*(y/h)^{1/2}$ very near the bed. The dimensionless group scaling the second term in Eq. 31 then becomes $(u_*/U_\infty)(y/h)^{1/2}$. Thus, the terms in brackets in Eq. 31 may dominate over the second term in a region very close to the lower boundary. For the sample parameters cited previously, however, these additional terms would be important only in a vanishingly thin layer, and the balance given by Eq. 32 appears to be valid over virtually the entire flow depth.

Dividing Eq. 32 by $9\mu/2a^2$ recovers the balance in terms of the flux of settling particles,

$$\bar{c}\,U_\infty - \overline{c'\,v^{f'}} = 0 \quad \text{(33)}$$

and comparison with Eq. 1 shows immediately that the classical "turbulent diffusion" may be regarded as a *model* for the correlation $\overline{c'\,v^{f'}}$. Similar balances have been noted before, based simply on the kinematics of particle fluxes. For example, both the ASCE (21, pp. 69–71) and Lumley (12, p. 309) obtain expressions like Eq. 33, but with $v^{f'}$ replaced by $v^{s'}$. It is nonetheless particularly satisfying to discover this balance in the *dynamics* of the fluid-particle interactions.

The interpretation of Eq. 32 is straightforward. Due to viscous drag on the particles, vertical turbulent motions of fluid parcels carry sediment. This process tends to smooth out large-scale concentration gradients, thus appearing as "diffusion." The correlation $\overline{c'\,v^{f'}}$ in Eq. 32 is clearly nonzero in the presence of a vertical gradient in the mean concentration. For $\bar{c}$ increasing downward, an upward (+) fluid velocity fluctuation carries with it a concentration larger (+) than the local mean, and a downward (−) velocity fluctuation carries a concentration deficit (−).

Models for $\overline{c'\,\mathbf{u}^{f'}}$

In view of the foregoing results, various expressions for "turbulent diffusion" of sediment are interpreted here as models for the correlation $\overline{c'\,\mathbf{u}^{f'}}$. This

term arises from Reynolds decomposition and averaging applied to the fluid-particle interaction force appearing in the mixture momentum balances (Eqs. 8 and 9). Although originally motivated in different ways, a number of well-known theories for "turbulent diffusion" exist, and three are reviewed briefly here in light of the preceding reinterpretation. All are variations on the Boussinesq model for the correlation given by Eq. 4, noting that the averaging scheme is now that defined in Eqs. 18 and 19.

The simplest expression for the diffusion coefficient tensor $\boldsymbol{\epsilon}$ is

$$\boldsymbol{\epsilon} \equiv \epsilon_s \mathbf{1} \quad \ldots \quad (34)$$

in which ϵ_s is a scalar. Then Eq. 4 becomes

$$\overline{c' \mathbf{u}^{f\prime}} \equiv -\epsilon_s \nabla \bar{c} \quad \ldots \quad (35)$$

and substitution into Eq. 33 for the plane uniform flow retrieves the classical balance of Eq. 1. By inspection of Eq. 35, it can be anticipated that the diffusivity, ϵ_s, scales with the product of the characteristic velocity and length scales of the flow. By direct analogy with models for *momentum* transport in a turbulent boundary layer, it is expected that the *concentration* profile will exhibit an inner and an outer region because of the dominance of different length scales near the bed and far away.

The outer region is commonly taken (8) to include about 80% of the boundary layer (in the present case, the boundary layer occupies the entire flow depth). In this region, the characteristic velocity scale is u_* and the dominant length scale is h, the flow depth. Thus

$$\epsilon_s \equiv \kappa_1 u_* h \quad \ldots \quad (36)$$

in which κ_1 = a dimensionless constant of order unity. For the outer region, then, ϵ_s is a constant, and Eq. 1 is easily solved, yielding the familiar result:

$$\bar{c} = c_\lambda \exp\left[-\left(\frac{U_\infty}{\kappa_1 u_* h}\right)(y - \lambda)\right] \quad \ldots \quad (37)$$

The boundary condition $\bar{c}(\lambda) = c_\lambda$ has been used here, where λ is some arbitrary height above the bed. Classically, this arbitrariness is due to a lack of anything in the theory that would suggest the appropriate condition at a true boundary. In the context of the multilayer model presented here, the problem of identifying an appropriate condition on the near-bed concentration resides in the *inner* layer, while c_λ in Eq. 37 is obtained by matching with the inner solution at some level, say at $\lambda = 0.2h$.

Eq. 37 is shown in Fig. 2, fitted to data from Montes and Ippen (13) for fine quartz sand in water [$a = 6.5 \times 10^{-4}$ m (2.6×10^{-2} in.), $U_\infty = 1.3 \times 10^{-2}$ m/s (4.3×10^{-2} fps), $u_* = 6.3 \times 10^{-2}$ m/s (2.1×10^{-1} fps), $U = 1.4$ m/s (4.6 fps), $h = 5.7 \times 10^{-2}$ m (2.2 in.)]. Note that the particle Reynolds number falls slightly outside of the Stokes range, so that the drag term linear in $\mathbf{u}^f - \mathbf{u}^s$ in the theory is not strictly valid. Nonetheless, the agreement is excellent in the outer 80% of the flow, while, as anticipated, Eq. 37 fails near the bed. A value of $\kappa_1 = 0.11$, which is of the correct order of magnitude, is obtained for this example.

The constant ϵ_s given by Eq. 36 implies isotropic, homogeneous turbulence,

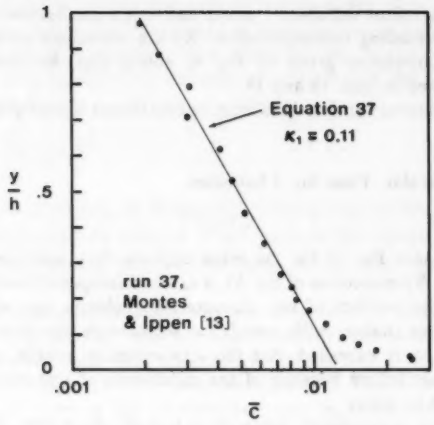

FIG. 2.—Concentration Profile for Outer Region

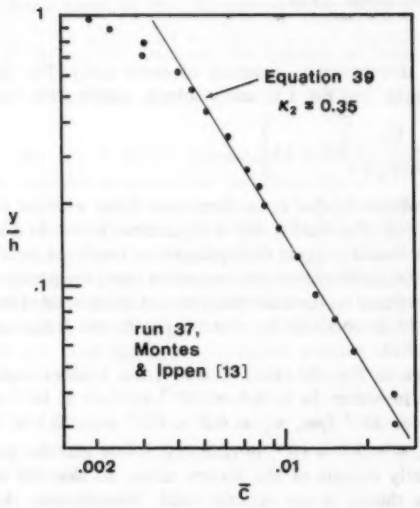

FIG. 3.—Concentration Profile for Inner Region

and must clearly break down near solid boundaries where the correlation $\overline{c' u^{f'}}$ must vanish as $u^{f'}$ vanishes. Just as in the usual arguments for momentum transport, the appropriate length scale near the bed is y, while the velocity scale is u_*, giving for the inner layer

$$\epsilon_s \equiv \kappa_2 u_* y \quad \ldots \quad (38)$$

in which κ_2 is again a dimensionless constant of order unity. This model has been suggested by Batchelor (3) and Lumley (12), and gives, with Eq. 33

$$\bar{c} = c_\lambda \left(\frac{y}{\lambda}\right)^{-U_\infty/\kappa_2 u_*} \quad \ldots \quad (39)$$

in which the condition $\bar{c}(\lambda) = c_\lambda$ has again been imposed. This result is appealing in that the concentration becomes more uniform for increasing bottom shear stress, τ_0, and for decreasing settling velocity. Note that Eq. 39 gives $\bar{c} \to \infty$ as $y \to 0$. Eq. 39 is shown in Fig. 3 for comparison with the same experimental data of Montes and Ippen (13), redrawn for ease of interpretation on a log-log plot. A value of $\kappa_2 = 0.35$ is obtained for the fit shown. The agreement is again excellent, in this case for the *inner* 50% of the flow. Thus, by dividing

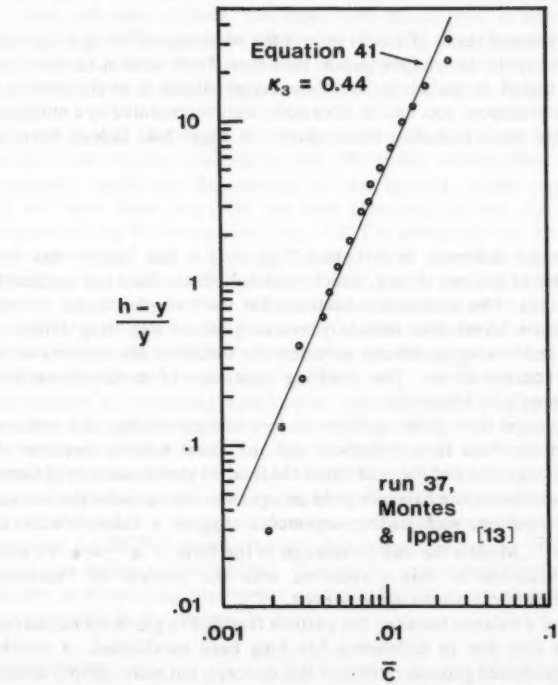

FIG. 4.—Concentration Profile from Rouse (17) Theory

the flow into inner and outer layers characterized by different length scales, very good predictions are obtained for each region, and they can be matched in their broad overlap region.

Finally, a third expression for ϵ_s was given by Rouse (17), who supposed that the "sediment diffusivity" in Eq. 1 must be similar to the eddy diffusivity introduced in considering the fluid velocity field. Thus, taking

$$\epsilon_s \equiv \kappa_3 u_* y \left(1 - \frac{y}{h}\right) \quad \ldots \ldots \ldots \ldots \ldots \ldots \ldots \ldots \ldots \ldots \quad (40)$$

the resulting concentration profile, from Eq. 33, is

$$\bar{c} = c_\lambda \left(\frac{h-y}{h-\lambda}\frac{\lambda}{y}\right)^{U_\infty/\kappa_3 u_*} \quad \ldots \ldots \ldots \ldots \ldots \ldots \ldots \ldots \ldots \ldots \quad (41)$$

Eq. 41 is shown in Fig. 4, again with the same data for comparison, the fit shown giving $\kappa_3 = 0.44$. The model of Eq. 40 cannot be motivated unambiguously from dimensional arguments as in Eqs. 36 and 38. However, recognizing that both h and y are important length scales, Eq. 40 might be taken as the simplest model that ensures that the correlation vanishes both at the bed and at the free surface.

The widely accepted result of Eq. 41 enjoys the advantage of being a "global" solution, valid over the entire flow depth. However, from what is known about momentum transport in turbulent boundary layers, there is every reason to expect that mass transport, too, can be more accurately represented by a multilayer model. Available data, including those shown in Figs. 2–4, indeed bear this out.

Summary

The transport of sediment in turbulent flow over a flat bottom has been examined in view of mixture theory, which models both the fluid and particulate phases as continua. The momentum balances for the two phases are coupled through interaction terms that include pressure gradient and drag forces. A decomposition and averaging scheme accounts for turbulent fluctuations of the velocities and concentrations. The resulting equations of motion have been presented previously by Drew (4).

For plane uniform flow down a slope at low concentrations, the sediment does not affect the bulk flow behavior, and the usual balance between the gravitational driving force and the gradient of the fluid Reynolds stress is obtained. The cross-stream momentum balances yield an equation that includes the buoyant weight of the particles, and scaling arguments suggest a balance with the correlation $\overline{c' v^{f\prime}}$. Models for this correlation in the form $\overline{c' \mathbf{u}^{f\prime}} \equiv \boldsymbol{\epsilon} \cdot \nabla \bar{c}$ complete the identification of this correlation with the process of "turbulent diffusion," and classical results are retrieved.

The concept of a balance between the particle flux due to gravitational settling and a diffusive flux due to turbulence has long been established. A number of studies have proposed generalizations of this concept, but many simply assume a priori the existence of a Fickian diffusion-like process. Such theories can only model an observation, rather than offering any insight into its source. Other studies identify a correlation similar to that of Eq. 4 from purely kinematic

arguments, again providing no information on the dynamics of the dispersal process.

The theory presented here has identified the "diffusion" process in terms of a correlation that arises from the decomposition and averaging of the fluid-particle interaction terms in the momentum balances. The result is simple and intuitively appealing. The correlation represents the effect of the drag on the particles associated with turbulent velocity fluctuations in the fluid. In the case of plane flow over a flat bed in the presence of a mean concentration gradient, it is clear that the concentration and vertical velocity fluctuations are highly correlated. The result will appear to be a diffusion-like process, tending to obliterate the mean concentration gradient.

Thus, mixture theory offers a clear *dynamic* interpretation of the "turbulent diffusion" of sediment. The diffusion process, successfully treated by Rouse (17) and others, may then be viewed as a *model* for the correlation identified here.

Review of previous representations (Eqs. 36, 38, 40) of the "sediment diffusivity," ϵ_s, in light of the present theory suggests that more accurate results can be obtained by combining them in a multilayer model. Just as in momentum transport processes in a turbulent boundary layer, mass transport can be divided into inner and outer regions. The outer part of the flow is dominated by the length scale h, while the inner part, near the bed, is dominated by y. Joining the solutions for these two layers in an overlap region yields results that compare more favorably to available data than the widely accepted Rouse equation (Eq. 41).

For clarity and simplicity, the data presented here are confined to a single example from Montes and Ippen (13). However, examination of other data consistently reinforces the success of the layered model considered here. This has been done, e.g., for the data presented by the ASCE (21, p. 80) in support of the Rouse equation (Eq. 41). The prediction for the concentration in the outer layer (Eq. 37) is significantly larger than a few measured values very near a free surface. This might be anticipated, since the correlation $c' v'$ does not vanish at the free surface under the assumption of Eq. 36, while Rouse's formulation (Eq. 40) assures this. In the context of the multilayer model presented here, this difficulty can easily be accommodated by introducing a third layer dominated by the length scale $h - y$.

In addition to recovering well-known classical results, the present theory is, from the outset, fully three-dimensional (Eqs. 20–23). A further advantage is that, at the level of Eqs. 16 and 17, the structure of the theory is completely general. Thus, directions for future refinement are immediately apparent. First, the constitutive equations used are based on the greatest possible simplifications. Considerable work is needed to develop appropriate forms for the stresses and interaction forces that include the rate-dependent constitutive variables and that are valid at higher concentrations. The second major area for further research is clearly in developing appropriate scaling relations and models for the correlations appearing in the theory.

Acknowledgment

This work was carried out while the writer was supported by a grant from

the Petroleum Research Fund, PRF 11459-AC2, administered by the American Chemical Society.

Appendix I.—References

1. Atkin, R. J., and Craine, R. E., "Continuum Theories of Mixtures: Basic Theory and Historical Development," *Quarterly Journal of Mechanics and Applied Mathematics*, Vol. 29, 1976, pp. 209–244.
2. Atkin, R. J., and Craine, R. E., "Continuum Theories of Mixtures: Applications," *Journal of the Institute of Mathematics and its Applications*, Vol. 17, 1976, pp. 153–207.
3. Batchelor, G. K., "The Motion of Small Particles in Turbulent Flow," *Proceedings of the Second Australasian Conference on Hydraulics and Fluid Mechanics*, 1965, pp. O19–O41.
4. Drew, D. A., "Turbulent Sediment Transport Over a Flat Bottom Using Momentum Balance," *Journal of Applied Mechanics*, Vol. 42, 1975, pp. 38–44.
5. Drew, D. A., "Production and Dissipation of Energy in the Turbulent Flow of a Particle-Fluid Mixture, With Some Results on Drag Reduction," *Journal of Applied Mechanics*, Vol. 43, 1976, pp. 543–547.
6. Drew, D. A., and Segal, L. A., "Averaged Equations for Two-Phase Flows," *Studies in Applied Mathematics*, Vol. 50, 1971, pp. 205–231.
7. Drew, D. A., and Segal, L. A., "Analysis of Fluidized Beds and Foams Using Averaged Equations," *Studies in Applied Mathematics*, Vol. 50, 1971, pp. 233–257.
8. Fernholz, H.-H., "External Flows," *Turbulence*, P. Bradshaw, ed., Springer-Verlag, Berlin, Germany, 1978, pp. 45–107.
9. Graf, W. H., *Hydraulics of Sediment Transport*, McGraw-Hill, New York, N.Y., 1971.
10. Hinze, J. O., "Momentum and Mechanical-Energy Balance Equations for a Flowing Homogeneous Suspension with Slip Between the Two Phases," *Applied Scientific Research*, Section A., Vol. 11, 1961, pp. 33–46.
11. Ishii, M., *Thermo-Fluid Dynamic Theory of Two-Phase Flow*, Eyrolles, Paris, France, 1975.
12. Lumley, J. L., "Two-Phase and Non-Newtonian Flows," *Turbulence*, P. Bradshaw, ed., Springer-Verlag, Berlin, Germany, 1978, pp. 289–331.
13. Montes, J. S., and Ippen, A. T., "Interaction of Two-Dimensional Turbulent Flow with Suspended Particles," *Ralph M. Parsons Laboratory for Water Resources and Hydrodynamics Report No. 164*, Massachusetts Institute of Technology, Cambridge, Mass., 1973.
14. Müller, I., "A Thermodynamic Theory of Mixtures of Fluids," *Archive for Rational Mechanics and Analysis*, Vol. 28, 1968, pp. 1–39.
15. Peddieson, J., "On Continuum Description of Solid-Fluid Suspensions," *Developments in Theoretical and Applied Mechanics*, Vol. 7, 1974, pp. 355–368.
16. Raudkivi, A. J., *Loose Boundary Hydraulics*, Pergamon, Oxford, England, 1976.
17. Rouse, H., "Modern Conceptions of the Mechanics of Fluid Turbulence," *Transactions*, ASCE, Vol. 102, 1937, pp. 463–543.
18. Schmidt, W., "Der Massenaustausch in freier Luft und verwandte Erscheinungen," *Probleme der kosmischen Physik*, Vol. 7, 1925.
19. Soo, S. L., "Diffusion in Multiphase Flow," *Iranian Journal of Science and Technology*, Vol. 7, 1978, pp. 31–35.
20. Soo, S. L., and Tung, S. K., "Deposition and Entrainment in Pipe Flow of a Suspension," *Powder Technology*, Vol. 6, 1972, pp. 283–294.
21. *Sedimentation Engineering*, V. A. Vanoni, ed., ASCE, New York, N.Y., 1975.

Appendix II.—Notation

The following symbols are used in this paper:

a = particle radius;

c = concentration (volume fraction of solids);
c_0 = reference concentration;
D = Brownian diffusivity ($=3\kappa\theta/4\pi a^3$, κ = Boltzmann's constant, θ = absolute temperature);
$\mathbf{F}$ = force of fluid on particulate phase per unit volume;
f_1, f_2 = scalar functions of c;
$\mathbf{g}$ = acceleration of gravity;
g' = $(\rho^s - \rho^f)g/\rho^f$;
h = flow depth;
p = pressure;
p^f = fluid phase pressure;
p^s = dispersed particulate phase pressure;
t = time;
$\mathbf{T}^f$ = fluid phase stress;
$\mathbf{T}^s$ = dispersed particulate phase stress;
$\mathbf{u}^f$ = fluid phase velocity;
U = characteristic mean flow velocity;
U_∞ = single-particle settling velocity;
$\mathbf{u}^s$ = dispersed particulate phase velocity;
u_* = shear velocity;
$u^\alpha, v^\alpha, w^\alpha$ = components of $\mathbf{u}^\alpha$;
x, y = Cartesian coordinates;
β = bed slope;
$\boldsymbol{\epsilon}$ = diffusion coefficient tensor;
ϵ_s = sediment diffusivity;
$\kappa_1, \kappa_2, \kappa_3$ = dimensionless constants of order unity;
λ = arbitrary distance above bed;
μ = fluid viscosity;
ρ^f = fluid density;
ρ^s = solid density; and
τ_0 = bottom shear stress.

Symbols

overbar = averaged quantity; and
prime = fluctuating quantity.

CELLS-IN-SERIES SIMULATION OF RIVERINE TRANSPORT

By Heinz G. Stefan,[1] M. ASCE and Alexander C. Demetracopoulos[2]

INTRODUCTION

A cells-in-series (CIS) formulation to simulate riverine transport of dissolved material in water quality models will be presented. The characteristics of the model will be compared to one using the conventional one-dimensional advection-dispersion (AD) equation, and the advantages and disadvantages of the CIS model will be illustrated. Both models will be applied to a 10.7-mile (17.2-km) reach of the Upper Mississippi River in which dye tracing experiments have been conducted by the United States Geological Survey (USGS).

A CIS model for the transport of a conservative material in a river was previously presented by Banks (1). A basic description of CIS modeling for chemical reactors can be found in Levenspiel (14).

Major discrepancies between observed dispersion in rivers and predictions with the classical AD equation have been acknowledged and explained in the literature (16,20). Some investigators have therefore proposed other models to predict mass transport in natural streams and rivers. Examples are those given by Thackston and Schnelle (24), Jobson and Yotsukura (12), McQuivey and Keefer (17,18), Pedersen (19), Sabol and Nordin (20), Beltaos (2), and Liu (16). Some of the alternative models are expansions of the AD equation and include entrapment in dead zones (19,24,27), or multidimensionality (12), or time-dependent (or distance) dispersion coefficients (16). Models which do not use the AD equation at all emphasize convective transport (18) or a combination of convective transport and stochastic processes (20). The convective model (18) was shown to give very good results for the first one-sixth of the convective period as defined by Fischer (5).

The approach taken in this paper is a more radical deviation from the classical AD equation. The CIS formulation used herein has been recognized as an alternative way for mass transport modeling in essentially one-dimensional

[1]Prof. Dept. of Civ. and Mineral Engrg., St. Anthony Falls Hydraulic Lab., Univ. of Minnesota, Minneapolis, Minn. 55455.

[2]Asst. Prof., Dept. of Civ. Engrg., Rutgers State Univ., The State Univ. of New Jersey, New Brunswick, N.J. 08854.

Note.—Discussion open until November 1, 1981. To extend the closing date one month, a written request must be filed with the Manager of Technical and Professional Publications, ASCE. Manuscript was submitted for review for possible publication on July 23, 1980. This paper is part of the Journal of the Hydraulics Division, Proceedings of the American Society of Civil Engineers, ©ASCE, Vol. 107, No. HY6, June, 1981. ISSN 0044-796X/81/0006-0675/$01.00.

systems (14). Only the fundamental aspects of the CIS theory and its relation to AD models will be considered herein. The question of how to relate the CIS model parameter, k (number of cells), to the hydraulic characteristics of a stream or river will not be covered in detail.

The physical process of mass transport and dispersion in a natural river is quite complex. Any mathematical description of natural systems requires simplifications and abstractions. The search for a simple yet appropriate description has led to the CIS model which has a basic equation that is an ordinary first-order differential equation instead of a partial differential equation, as used in AD models. This is advantageous when the basic transport equation is used in a water quality model for an extensive river reach, or to a branching system, as is the case in shallow river impoundments, estuarine networks, ship canals, etc.

It has also been suggested by a reviewer that a CIS simulation may be applied as an approximation to river reaches where the one-dimensional AD equation cannot be used because the initial convective period (5) has not been exceeded. In that case, a two-dimensional model should really be used. However, if the complexity of the river geometry or the time and expense do not justify development of a two-dimensional model for such a river reach, it has been suggested that a CIS model with site-specific parameters may provide approximate answers.

Transport Parameters of River

The following presentation will consider the transport of a slug of material in a river because it illustrates the riverine transport features which are of interest in water quality modeling. A somewhat idealized but typical concentration versus time record which describes the passage of a slug of dissolved or fine suspended material at two consecutive stations in a river is shown in Fig. 1. Without specifying the mass concentration functions, $C(t)$, analytically, some important bulk features of these functions can be described by the moments of $C(t)$. We shall consider the first four moments of $C(t)$ because they suffice for a fairly accurate summary of the $C(t)$ curves for water quality modeling purposes.

The four moments of interest are:

$$A = \int_o^{+\infty} C\,dt \quad \text{(zero moment)} \qquad (1)$$

$$\bar{t} = \frac{1}{A}\int_o^{+\infty} C\,t\,dt \quad \text{(first moment)} \qquad (2)$$

$$\nu = \sigma^2 = \frac{1}{A}\int_o^{+\infty} C(t-\bar{t})^2\,dt \quad \text{(second moment)} \qquad (3)$$

$$\mu = \frac{1}{A}\int_o^{+\infty} C(t-\bar{t})^3\,dt \quad \text{(third moment)} \qquad (4)$$

Each of the four moments is related to or descriptive of a particular feature or characteristic or riverine transport.

Parameter $A = M/Q$, in which Q = the steady-state volumetric river flow rate; and M = the total mass of material in the slug. If applied to two stations, 1 and 2, respectively, along a stream, $(A_1 - A_2)\,Q$ represents the loss of material between the two stations. Such loss may be produced by chemical or biological reactions, settling, evaporation, etc. If the mass is conservative, a concentration versus time function should give the same value of A at all stations along a river reach.

The first moment, $\bar{t}$, specifies the location (in time) of the centroid of the slug of mass. A differential, $\bar{t}_2 - \bar{t}_1$, between two stations (1 and 2) is the mean advective travel time or residence time of the material in the river reach between these two stations.

The variance, σ^2, reflects the longitudinal spread of material along the river. It is a measure of the width (in time) of the two curves, $C(t)$, shown in Fig. 1, but does not account for the lack of symmetry about the mean travel time, $\bar{t}_1$ and $\bar{t}_2$. A change, $\sigma_2^2 - \sigma_1^2$, from station 1 to station 2 is usually called

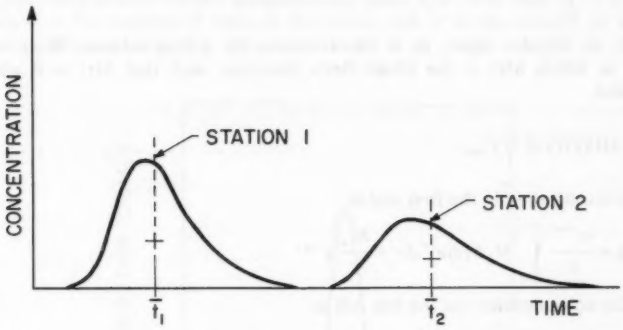

FIG. 1.—Schematic Concentration Versus Time Curves for Slug of Dissolved (or Suspended) Material Traveling Past Two River Sampling Stations

longitudinal dispersion, which in turn depends on such flow characteristics as velocity distributions and turbulence.

Finally, the third moment of skewness, μ, describes the asymmetry of the curve, $C(t)$. This asymmetry can be caused by the velocity distribution in a real river or by entrapment of materials, in separated flow regions and backwaters and subsequent release. Entrapment usually causes a large degree of skewness. The last three of the aforementioned features are functions of river morphology and flow rate, while the first (zero moment) is simply the mass, M, divided by the discharge, Q.

It can be shown how a CIS model, and by comparison, the AD equation, describe the aforementioned four features.

CIS Model

A CIS model assumes that a river is composed of a sequence of elements of equal volume, called cells. Complete mixing occurs in each cell. The general

mass transport equation for a CIS model is

$$V\frac{dC}{dt} = W(t) - QC - KVC \quad (5)$$

in which V = the volume of a cell; C = the concentration in the cell; t = time; $W(t)$ = an external mass input rate into the cell, including that advected into the cell from the neighboring cell upstream, and that through direct injection; Q = the volumetric flow rate out of the cell; and K = a kinetic rate of material removal. With $\alpha = (Q / V) + K$ and $I = W/V$, Eq. 5 transforms to

$$\frac{dC}{dt} + \alpha C = I(t) \quad (6)$$

With an initial condition, $C = C_o = 0$ for $t < 0$, the solution is

$$C = e^{-\alpha t}\int_o^t I(\tau)e^{\alpha\tau}\,d\tau \quad (7)$$

For an impulse input, as is characteristic for a slug release, $W(t) = M_o\,\delta(t)$, in which $\delta(t)$ = the Dirac Delta function, such that $\delta(t) = 0$ when $t \neq 0$ and

$$\int_{-\infty}^{\infty} \delta(t) f(t)\,dt = f_{t=0} \quad (8)$$

The concentration in the first cell is

$$C_1(t) = \frac{e^{-\alpha t}}{V}\int_o^t M_o\delta(\tau)e^{\alpha\tau}\,d\tau = \frac{M_o}{V}e^{-\alpha t} \quad (9)$$

and the concentration for the kth cell is

$$C_k(t) = \frac{M_o Q^{k-1}}{V^k}e^{-\alpha t}\frac{t^{k-1}}{(k-1)!} \quad (10)$$

The four transport characteristics defined in Eqs. 1–4 can now be computed. In the process, the gamma function

$$\Gamma(k+1) = \int_o^{\infty} e^{-\tau}\tau^k\,d\tau, \quad k \geq 0 \quad (11)$$

and $\Gamma(k+1) = k!$ (12)

if k is an integer, will be used. The material conservation coefficient is found to be

$$A = \frac{M_o}{Q}\left[1 + \left(\frac{VK}{Q}\right)\right]^{-k} = \frac{M_o}{Q}\left(\frac{Q}{V}\right)^k\frac{1}{\alpha^k} \quad (13)$$

The mean and the variance of the gamma-type concentration distribution are

$$\bar{t} = \frac{k}{\alpha} \quad (14)$$

and $\sigma^2 = \frac{k}{\alpha^2}$ . . . . (15)

respectively. The skewness is found to be

$$\mu = \frac{2k}{\alpha^3} \quad \text{(16a)}$$

or the skewness coefficient is

$$S = \frac{\mu}{\sigma^3} = 2k^{-1/2} \quad \text{(16b)}$$

Eqs. 13–16 are simple functions of the number of cells used. This characteristic of the CIS model is more directly shown in Fig. 2, in which the dimensionless concentration, CV_t/M_o, in the effluent from a river reach of constant volume, V_t, has been plotted versus dimensionless time, $t/\bar{t}$. Note that $V_t = kV$, in which k = the number of cells in the reach; and V = the volume of a cell. The normalized form of Eq. 10 is

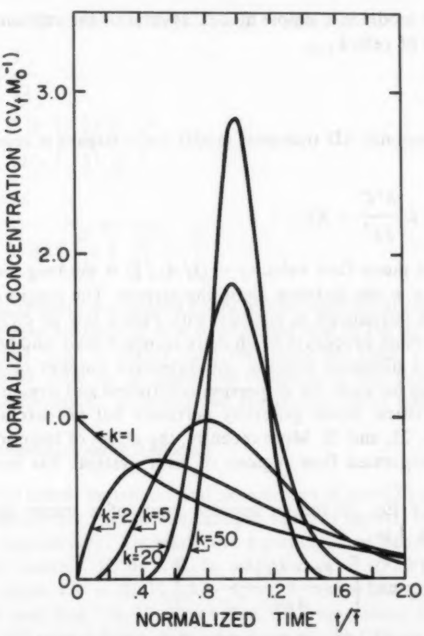

FIG. 2.—Dimensionless (Normalized) Concentration Versus Time Curves for Different Numbers of Cells in River Reach (Eq. 17)

$$\frac{CV_t}{M_o} = \left(1 - \frac{K\bar{t}}{k}\right)^{k-1} \left(\frac{t}{\bar{t}}\right)^{k-1} \frac{k^k}{(k-1)!} \exp\left(-\frac{kt}{\bar{t}}\right) \quad \ldots\ldots\ldots\ldots (17)$$

Fig. 2 was plotted for $K = 0$.

The loss of mass, the mean residence time, and the changes in variance and skewness between two stations (1 and 2) can be expressed as simple functions of the number of cells in the river reach $k_{1-2} = k_2 - k_1$

$$\frac{A_1 - A_2}{A_1} = 1 - \left(\frac{Q}{V\alpha}\right)^{k_{1-2}} \quad \ldots\ldots\ldots\ldots\ldots\ldots\ldots\ldots\ldots\ldots (18)$$

$$\bar{t}_2 - \bar{t}_1 = \frac{k_{1-2}}{\alpha} \quad \ldots\ldots\ldots\ldots\ldots\ldots\ldots\ldots\ldots\ldots\ldots\ldots (19)$$

$$\sigma_2^2 - \sigma_1^2 = \frac{k_{1-2}}{\alpha^2} \quad \ldots\ldots\ldots\ldots\ldots\ldots\ldots\ldots\ldots\ldots\ldots\ldots (20)$$

$$\mu_2 - \mu_1 = \frac{2k_{1-2}}{\alpha^3} \quad \ldots\ldots\ldots\ldots\ldots\ldots\ldots\ldots\ldots\ldots\ldots\ldots (21)$$

Because the CIS model is a simple model, several of the relationships are linear with the number of cells k_{1-2}.

AD Model

The one-dimensional AD transport model for a stream is represented by the relationship

$$\frac{\partial C}{\partial t} = -U\frac{\partial C}{\partial x} + D\frac{\partial^2 C}{\partial x^2} - KC \quad \ldots\ldots\ldots\ldots\ldots\ldots\ldots\ldots (22)$$

in which U = the mean flow velocity = Q/A_s; D = the longitudinal dispersion coefficient; and x = the distance along the stream. The longitudinal dispersion coefficient, D, is introduced in analogy with Fick's law of diffusion, although the riverine dispersion process is much more complex than, and has little physical resemblance to, a diffusion process. An extensive amount of literature exists on the relationship between the dispersion coefficient and stream and hydrologic stream characteristics. Some generally pertinent but not exclusive references are Refs. 3, 7, 15, 23, and 28. More recently, the effect of temporary entrapment of materials in separated flow regions of river systems has been studied (19, 20, 25, and 27).

The solution of Eq. 22 for an impulse input of a tracer described earlier and shown in Fig. 1 is

$$C = \frac{M_o}{A_s(4\pi D t)^{1/2}} \exp\left[-\frac{(x - Ut)^2}{4Dt} - Kt\right] \quad \ldots\ldots\ldots\ldots\ldots (23)$$

If the river flow rate, Q, and the total volume of the river reach downstream from the injection point, V_t, are introduced, the equation can be rewritten as

$$C(t) = \frac{M_o}{2V_t} \cdot \left[\pi\left(\frac{D}{Ux}\right)\left(\frac{Qt}{V_t}\right)\right]^{-1/2} \exp\left[\frac{-\left(1-\frac{Qt}{V_t}\right)^2}{4\left(\frac{D}{Ux}\right)\left(\frac{Qt}{V_t}\right)} - Kt\right] \quad \ldots \quad (24)$$

This equation gives the concentration of a tracer as a function of dimensionless time. The time is normalized by the mean residence time, V_t/Q. The parameter D/Ux = the inverse of a Peclet Number, *Pe*. The skewness of the $C(t)$ curve increases with D/Ux and Kt. The parameter D/Ux can also be expressed as DV_t/Qx^2 for practical evaluations. For $K = 0$, and very small values of D/Ux (large Peclet numbers), the concentration distribution approaches a Gaussian function. The skewness predicted by Eq. 24 is usually much less than that observed in a river and stream and expanded versions of Eq. 22 with additional parameters (i.e., Eqs. 16, 19, and 24) are required to account for the real skewness.

For a conservative tracer ($K = 0$), Eq. 24 can be used to evaluate the transport parameters introduced by Eqs. 1–4. Eq. 1 gives

$$A = \frac{M_o}{Q} \quad \ldots \quad (25)$$

According to Levenspiel and Smith (13), Eqs. 2 and 3 give

$$\bar{t} = \left(1 + 2\frac{D}{Ux}\right)\frac{V_t}{Q} \quad \ldots \quad (26)$$

$$\sigma^2 = \left[2\frac{D}{Ux} + 8\left(\frac{D}{Ux}\right)^2\right]\left(\frac{V_t}{Q}\right)^2 \quad \ldots \quad (27)$$

Finally, Eq. 4 gives

$$\mu = \left[12\left(\frac{D}{Ux}\right)^2 + 64\left(\frac{D}{Ux}\right)^3\right]\left(\frac{V_t}{Q}\right)^3 \quad \ldots \quad (28)$$

The last three parameters are related to the Peclet number of the flow.

Eqs. 25–28 are also obtained if $K \neq 0$, provided that in Eq. 24, K is multiplied by a constant time, e.g., $\bar{t}$, rather than instantaneous time, t. The foregoing analysis is therefore valid for all dissolved materials in the water (conservative as well as nonconservative), provided that the kinetic decay rates are low.

Comparison of Mixed-Cells and AD Models

The mean travel times, variances, and skewnesses of the CIS model expressed in Eq. 14–16, respectively, can be compared to those of the AD model, expressed in Eqs. 26–28, respectively. To relate the equations one needs to replace the total river reach volume V_t by kV. In addition, $\alpha = (Q/V) + K$, and for a conservative tracer ($K = 0$) $V_t/Q = k/\alpha$. A comparison of the two sets, i.e., Eqs. 14–16 and Eqs. 26–28 shows that the expressions for $\bar{t}$, σ^2, and μ derived for the AD model degenerate into those of the CIS model if the tracer is conservative and if the Peclet number Ux/D is sufficiently large. Otherwise, the two models provide somewhat different results.

In a given river reach of volume, V_t, and at a given river flow, Q, the mean travel time is independent of the subdivision (number of cells) in the CIS model (Eq. 14), because $k/\alpha = V_t/Q$. It is slightly dependent on the dispersion coefficient, D, in the AD models (Eq. 26).

The spread in the arrival times of the dissolved (or suspended) material at any one station is related to the number of cells into which the river reach is subdivided in the CIS model. A larger number of cells provides less dispersion, as shown in Fig. 2. The longitudinal dispersion coefficient, D, in the AD model and the number of cells, k, in the CIS model therefore describe similar transport features and are related to each other through

$$\frac{1}{k} = 2\frac{D}{Ux} + 8\left(\frac{D}{Ux}\right)^2 \qquad (29)$$

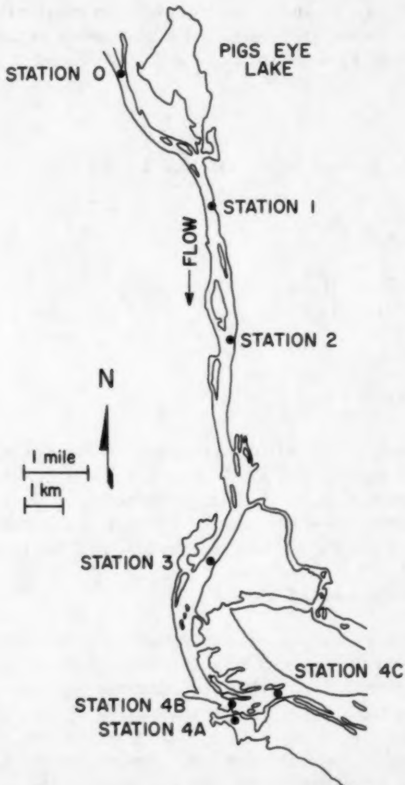

FIG. 3.—Upper Mississippi River Reach Downstream from St. Paul

The number of cells also affects the skewness of the $C(t)$ curve. So does the longitudinal dispersion coefficient in the AD models. Typically, the CIS model can provide a larger degree of skewness than the AD model, which is often more realistic. In both the CIS and the AD models, skewness is not described by an independent parameter but is determined by the choice of parameters, k or D, respectively.

Other parameters can also be selected to describe the riverine transport features of a particular river reach, e.g., the maximum concentration of the $C(t)$ curve. For the CIS model it is found to be

$$C_{\max} = \frac{M_o}{V} e^{-(k-1)} \frac{(k-1)^{k-1}}{(k-1)!} \left(\frac{\alpha - K}{\alpha}\right)^{k-1} \quad \ldots\ldots\ldots\ldots\ldots\ldots (30)$$

and for the AD model it is

$$C_{\max} = \frac{M_o}{2V_t} \left[\frac{\pi}{2}(1 - F^2)\right]^{-1/2} \exp\left[\frac{F-1}{2(F+1)} - K\bar{t}\right] \quad \ldots\ldots\ldots\ldots (31)$$

with the times of arrival of the maximum concentrations given by

$$t_{\max} = \frac{k-1}{\alpha} \quad \ldots\ldots\ldots\ldots\ldots\ldots\ldots\ldots\ldots\ldots\ldots\ldots (32)$$

and $$t_{\max} = \frac{V_t}{Q} F \quad \ldots\ldots\ldots\ldots\ldots\ldots\ldots\ldots\ldots\ldots\ldots\ldots (33)$$

for the CIS and the AD model, respectively. Eqs. 31 and 33 are for $Kt = K\bar{t} = \text{const.}$; and the function $F = [(D/Ux)^2 + 1]^{1/2} - D/Ux$.

Application of CIS and AD Models to Upper Mississippi River

In July 1976, May 1977, and October 1977, the USGS St. Paul District traced the passage of dye releases in the Upper Mississippi in the vicinity of Minneapo-

TABLE 1.—Location of Sampling Sites on Upper Mississippi River

USGS site number (1)	Station number (2)	Location (3)	Miles above Ohio River (4)	Length of subreach, in kilometers (5)
7.6	0	Pigs Eye Metropolitan Waste Treatment Plant	835.2	
8	1	I-494 Bridge	832.5	4.3
9	2	County Road 22 Bridge	830.3	3.5
10	3	Shieley Commercial Dock	826.5	6.1
11	4A	Spring Lake Inlet Channel (July 1976)	823.8	4.3
	4B	Main channel at Lower Gray Cloud Island (May 1977)	823.8	
	4C	Downstream from Spring Lake Entrance (October 1977)	823.0	1.3

TABLE 2.—Upper Mississippi Transport Parameters

Parameter (1)	July 1976[a] Station 1 (2)	Station 2 (3)	Station 3 (4)	Station 4 (5)
M, in kilograms	36.66	36.01	39.50	39.35
M/M_o, in kilograms	0.702	0.690	0.757	0.754
$\bar{t}$, in hours	27.2	41.6	62.9	84.1
σ^2, in square hours	75.69	124.2	213.3	226.5
S (−)	0.616	1.009	1.147	0.651
C_{max}, in micrograms per liter	6.0	4.4	3.7	3.45
t_{max}, in hours	18.0	32.0	60.0	82.0

[a] Q = 3,260 cfs (92.32 m^3 s); M_o = 52.19 kg.
[b] Q = 4,670 cfs (132.3 m^3 s); M_o = 49.92 kg.
[c] Q = 9,470 cfs (268.2 m^3 s); M_o = 43.12.

TABLE 3.—Upper Mississippi Transport Parameters Calculated

Parameter (1)	July 1976 Station 1 (2)	Station 2 (3)	Station 3 (4)	Station 4 (5)
k (−)	9.75	13.94	18.55	31.19
k, as an integer	10	14	19	31
α, per hour	0.359	0.335	0.295	0.371
K, per hour	0.013	0.009	0.005	0.003
$\alpha - K/\alpha$	0.965	0.972	0.984	0.991
V, in 1×10^6 cubic feet (1×10^5 cubic meters)	33.9 (9.6)	36.0 (10.2)	40.5 (11.5)	31.9 (9.03)
S (−)	0.641	0.536	0.464	0.358
C_{max}, in milligrams per liter	6.7	4.2	3.1	2.7
t_{max}, in hours	24.4	38.6	59.5	81.4
kV, in 1×10^6 cubic feet (1×10^5 cubic meters)	331 (93.7)	502 (142)	751 (213)	995 (282)

[a] The average kV values for the three surveys are 664 × 10^6 cu ft (183 × 10^5 m^3).
Note: Values of Q, M_o, M, $\bar{t}$, and σ^2 are the same as in Table 2.

lis/St. Paul. The procedures and basic data were described in Ref. 26. Rhodamine WT was injected at three different locations on the river upstream from Station 0 (Fig. 3) and traced downstream. The river reach from mile 835.2 to mile 823.8 downstream from the Metropolitan Waste Treatment Plant was covered in all three experiments. (The mileage is with reference to the mouth of the Ohio River.) For orientation, the Wabasha Bridge near downtown St. Paul is at river mile 839.5; Lock and Dam No. 2 is at river mile 815.4. Fig. 3 shows the Mississippi River reach of interest in this study and the locations of the sampling stations. Table 1 provides some additional information on the sampling stations.

from Dye Release Data for Three Field Surveys

May 1977[b]				October 1977[c]	
Station				Station	
1 (6)	2 (7)	3 (8)	4 (9)	2 (10)	4 (11)
45.95	43.68	45.04	41.72	27.24	25.43
0.921	0.875	0.902	0.836	0.632	0.590
11.9	20.2	34.4	47.4	9.58	28.3
14.4	30.1	37.3	66.4	3.64	34.3
2.46	1.94	1.38	1.31	1.61	1.48
22.0	14.4	9.4	6.4	10.5	4.0
10.3	17.0	30.0	42.0	8.0	24.8

from CIS Model by Section for Three Field Surveys

May 1977				October 1977	
Station				Station	
1 (6)	2 (7)	3 (8)	4 (9)	2 (10)	4 (11)
9.83	13.62	31.69	33.84	25.3	23.31
10	14	32	34	25	23
0.825	0.673	0.922	0.714	2.64	0.824
0.007	0.007	0.003	0.004	0.049	0.019
0.991	0.990	0.997	0.995	0.981	0.977
20.6	25.2	18.3	23.7	13.2	42.4
(5.8)	(7.14)	(5.18)	(6.71)	(3.74)	(12.0)
0.638	0.542	0.355	0.344	0.398	0.414
10.8	8.1	6.5	4.5	7.9	1.9
10.7	18.8	33.3	46.0	9.2	27.1
202	343	580	802	334	988
(57)	(97)	(164)	(227)	(95)	(280)

600×10^6 cu ft (136×10^5 m^3), and 654×10^6 cu ft (187×10^5 m^3), respectively.

Riverine transport parameters presented in the preceding sections were calculated from the dye concentration versus time data measured at each station. The numerical results are presented in Table 2. The CIS model and the AD model were applied to the field data as follows.

CIS Model

Analysis of Data by River Cross Section.—If only river flow and dye study data but no river morphologic data are used, the observed values of $\bar{t}$, σ^2, and M in Table 2 can be used to find the time constant, α, the number of cells, k, and the kinetic rate, K, section by section. For this purpose Eqs.

13, 14, and 15 are rewritten in the form:

$$\alpha = \frac{\bar{t}}{\sigma^2} \quad \ldots \quad (34)$$

$$k = \frac{\bar{t}^2}{\sigma^2} \quad \ldots \quad (35)$$

$$\text{and} \quad K = \alpha \left[1 - \left(\frac{M}{M_o} \right)^{1/k} \right] \quad \ldots \quad (36)$$

The results of such computations for the Upper Mississippi River are shown in Table 3. Concentrations down to 0.1 $\mu g/L$ were considered on the receding limb of the measured $C(t)$ curves. With these parameters, other values such as S, C_{max}, and t_{max} can be calculated using Eqs. 16*b*, 30, and 32, respectively.

The kinetic rates, K, computed from Eq. 36 were found to be virtually identical with those obtained by the conventional method in which measured values of M and $\bar{t}$ are fitted to an equation

$$\text{or} \quad K = \frac{1}{\bar{t}} \ln \left(-\frac{M}{M_o} \right) \quad \ldots \quad (37)$$

in which M/M_o = the recovery ratio of the tracer.

Analysis of Data by River Reach.—If Stations 1 and 4 in the Mississippi River are chosen, e.g., the pertinent relationship derived from Eqs. 13, 14, and 15 are

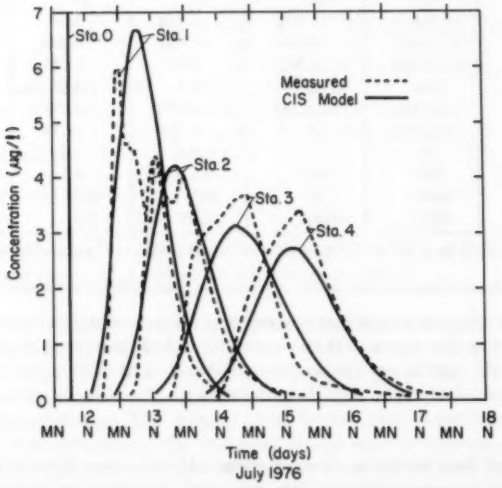

FIG. 4.—Measured and Predicted (CIS Model) Concentration Versus Time and Station 1–Station 4; Dye Release Study, July 1976

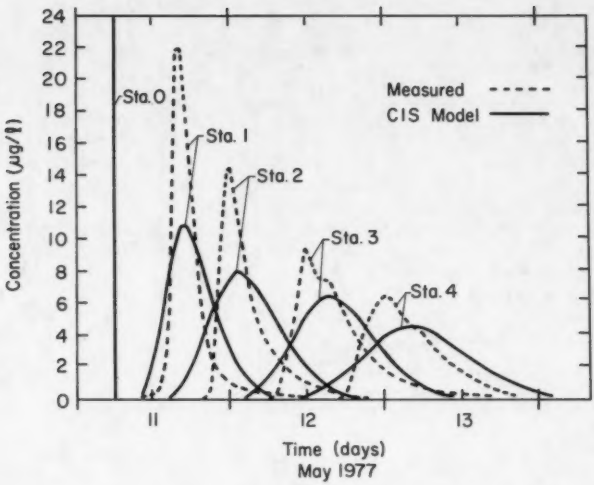

FIG. 5.—Measured and Predicted (CIS Model) Concentration Versus Time at Station 1–Station 4; Dye Release Study, May 1977

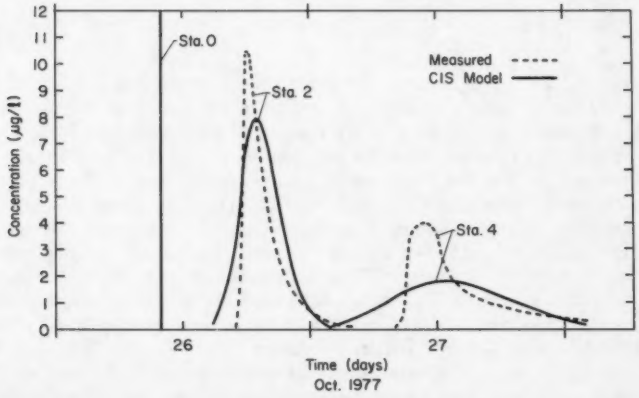

FIG. 6.—Measured and Predicted (CIS Model) Concentration Versus Time at Station 1–Station 4; Dye Release Study, October 1977

TABLE 4.—Upper Mississippi Transport Parameters Calculated

Parameter (1)	July 1976			
	Station			
	1 (2)	2 (3)	3 (4)	4A (5)
V_t/Q, in hours	24.7	38.8	59.7	81.5
Y, per hour	0.00205	0.00093	0.00045	0.000196
x, in feet (meters)	14,250 (4,340)	25,870 (7,880)	45,930 (14,000)	60,190 (18,340)
D, in square feet per second (square meters per second)	115.7 (10.75)	172.9 (16.06)	263.7 (24.50)	197.2 (18.33)
V_t, in 1×10^6 cubic feet (1×10^5 cubic meters)	289.9 (82.0)	455.4 (128.9)	700.6 (198.4)	956.5 (270.8)
C_{max}, in micrograms per liter	5.67	4.17	3.33	2.84
t_{max}, in hours	23.5	37.4	58.1	80.2
D/Q, per foot (per meter)	0.057 (0.189)	0.057 (0.189)	0.057 (0.189)	0.057 (0.189)

Note: Values of $\bar{t}$ and σ^2 are the same as in Table 2.

$$\alpha_{1-4} = \frac{\bar{t}_4 - \bar{t}_1}{\sigma_4^2 - \sigma_1^2} \quad \text{(38)}$$

$$k_{1-4} = \alpha_{1-4}(\bar{t}_4 - \bar{t}_1) = \frac{(\bar{t}_4 - \bar{t}_1)^2}{\sigma_4^2 - \sigma_1^2} \quad \text{(39)}$$

$$K_{1-4} = \alpha_{1-4}\left[1 - \left(\frac{M_4}{M_1}\right)^{1/k_{1-4}}\right] \quad \text{(40)}$$

The variable k_{1-4} = the number of mixed cells between Stations 1 and 4 or $k_{1-4} = k_4 - k_1$. Numerical values are not shown for lack of space. The results were comparable to those obtained by analysis by cross section in Table 3.

Predicted $C(t)$ Curves.—With the parameters α, k, and K established, one may proceed to calculate $C(t)$ curves and to compare them with the actually observed ones. This was done for all three field survey dates and each station.

Predicted (CIS model) and measured concentration versus time distributions at station 1–station 4 are shown in Figs. 4, 5, and 6. The July 1976 concentrations in Fig. 4, and the October 1977 concentrations in Fig. 6 are reasonably well-predicted, except for some irregular features in Fig. 4 which can be neither explained nor modeled. The predictions in Fig. 4 are good because the parameters K, k, and α were selected station by station from Table 3. The May 1977 data in Fig. 5 produce an apparent poorer match between predicted and measured concentration versus time curves. In particular, the maximum concentration is poorly-predicted. The same discrepancy will be seen to occur for the AD model (see a later figure) and explanation will be provided later.

AD Model

Analysis of Data by River Cross Section.—From Eqs. 26 and 27, relationships

from AD Model by Section for Three Field Surveys

May 1977				October 1977	
Station				Station	
1 (6)	2 (7)	3 (8)	4B (9)	2 (10)	4C (11)
10.8	18.8	33.3	46.0	9.2	27.1
0.00472	0.00198	0.000496	0.000331	0.00224	0.000817
16,890	28,510	48,570	62,830	28,510	67,050
(5,150)	(8,690)	(14,800)	(19,150)	(8,690)	(20,430)
374.2	447.1	325.1	362.9	505.8	1,020.4
(34.77)	(41.54)	(30.20)	(33.72)	(47.00)	(94.80)
181.6	316.1	559.8	773.3	313.6	923.9
(51.4)	(89.5)	(158.5)	(219.0)	(88.8)	(261.6)
11.3	7.14	6.26	4.33	6.00	1.84
10.3	18.1	32.8	45.3	9.0	26.5
0.081	0.081	0.081	0.081	0.081	0.081
(0.265)	(0.265)	(0.265)	(0.265)	(0.265)	(0.265)

for the dispersion coefficient, D, and the total hydraulic residence time, V_t/Q, as functions of the measured parameters, t and σ^2 can be developed. It is found that

$$\frac{V_t}{Q} = \frac{3\bar{t}}{2} - \frac{1}{2}\sqrt{\bar{t}^2 + 4\sigma^2} \quad \ldots\ldots\ldots\ldots\ldots\ldots\ldots\ldots\ldots\ldots \quad (41)$$

and

$$\frac{D}{x^2} = \frac{-\bar{t} + \sqrt{\bar{t}^2 + 4\sigma^2}}{(3\bar{t} - \sqrt{\bar{t}^2 + 4\sigma^2})^2} = Y \quad \ldots\ldots\ldots\ldots\ldots\ldots\ldots\ldots \quad (42)$$

Numerical results are shown in Table 4.

Analysis of Dye Release Data by River Reach.—Given the preceding analysis one can write for two stations, e.g., 1 and 4

$$Y_1 = \frac{D}{x_1^2} \quad \text{and} \quad Y_4 = \frac{D}{x_4^2} \quad \ldots\ldots\ldots\ldots\ldots\ldots\ldots\ldots\ldots\ldots \quad (43a)$$

$$\text{or} \quad D = (Y_1 - Y_4)\frac{x_1^2 x_4^2}{x_4^2 - x_1^2} \quad \ldots\ldots\ldots\ldots\ldots\ldots\ldots\ldots\ldots\ldots \quad (43b)$$

Numerical results are not shown for lack of space, but results were comparable to those in Table 4, except for the October 1977 data.

For dispersion to be described by a diffusion equation, it is necessary for the motion of a tracer particle not to be correlated with its initial velocity (5). On this basis an initial convective period (5) or length (18) is defined. For the Mississippi River reach below St. Paul, the initial convective length is about 1.9 miles considering only gravity-driven flow and no wind effects. The measurements used herein were taken at a distance more than the convective length downstream from the injection point. Distances from the dye injection

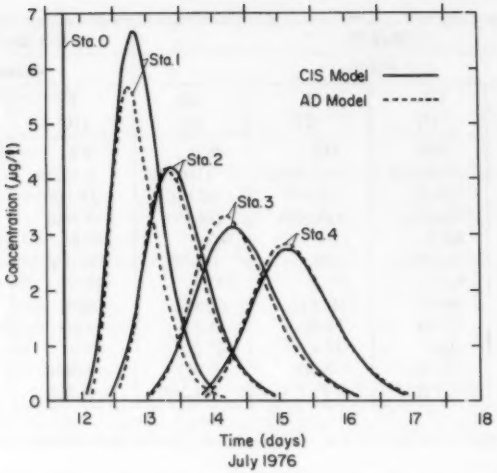

FIG. 7.—Concentration Versus Time Predicted by CIS and AD Models; Dye Release Study, July 1976

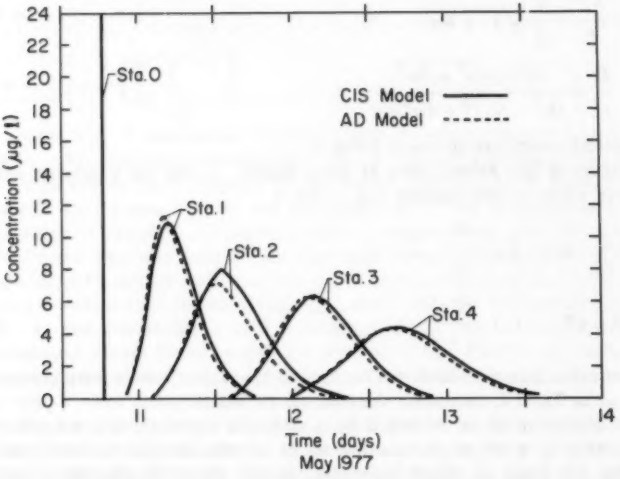

FIG. 8.—Concentration Versus Time Predicted by CIS and AD Models; Dye Release Study, May 1977

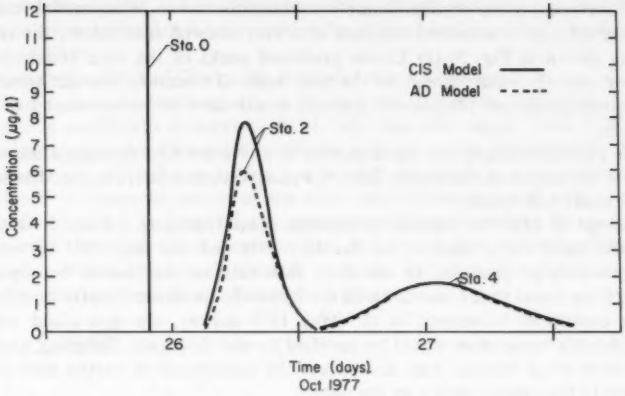

FIG. 9.—Concentration Versus Time Predicted by CIS and AD Models; Dye Release Study, October 1977

point to station 1 (Fig. 3 and Tables 2 and 4) were 2.7 mile, 3.2 mile, and 5.4 mile in July 1976, May 1977, and October 1977, respectively (1 mile = 1.609 km).

Predicted $C(t)$ Curves.—The parameters x, D, and V_t used in Eq. 24 for the AD model predictions are those listed in Table 4 station by station. The loss rate, K, was that given in Table 3 station by station. Predictions based on the AD model are very similar to those made by the CIS model as shown in Figs. 7, 8, and 9. The predictive capabilities of both models for the three case studies on the Upper Mississippi are about equal.

Comparison of CIS and AD Models and Their Relationship to Observed Features of Riverine Concentration Versus Time Curves

Skewness.—The CIS and AD models simulate concentrations versus time curves based on bulk parameters derived or estimated from observed concentrations, i.e., mean travel time and variance. Neither provides a sufficient description of the skewness of the time concentration curves.

The skewness in the CIS and AD models is directly related to variance (see Eqs. 15 and 16 or 27 and 28) and cannot be adjusted independently. This deficiency is more serious as the observed time concentration curves become more skewed, as seen in the May 1977 data versus the July 1976 data for the Mississippi River study. The model results may very well agree with each other but differ from actual measurements when the distribution is very skewed. The agreements and discrepancies shown in Figs. 4, 5, and 6 are directly related to the magnitude of the skewness coefficients shown in Tables 2 and 3.

In a strongly skewed distribution the time lag from the time of maximum concentration to the mean travel time (centroid) contributes heavily to the magnitude of the variance. Both the CIS and the AD model impose a relatively

small skewness of the predicted time concentration curves. When model variance is matched with a measured variance of a very skewed distribution, the results are as shown in Fig. 5: (1) Lower predicted peaks of the time concentration curves; and (2) wider spread on the time scale. To remedy this deficiency an additional parameter (degree-of-freedom) would have to be introduced in both models.

The physical reasons for the skewness of a riverine time concentration curve are not the subject of this paper, but a few observations relative to the Mississippi River study will follow.

Concept of Effective Volume in Riverine Mass-Transport.—First, it is noted that the mean travel time, t, for the July 1976 and the May 1977 survey are not inversely proportional to the river flow rate as they would be expected to be, if the travel time coincided with the hydraulic residence time (river volumes being essentially constant). In the May 1977 survey, the dye cloud travels considerably faster than would be justified by the flow rate. Sampling location in a river cross section may also affect the concentration versus time curve but not to the degree shown by the data.

The volumes, V and kV, resulting from the application of the CIS model to the data and shown in Table 3 vary considerably from the July 1976 to the May 1977 survey. This is in direct disagreement with the real river volumes, which according to stage-discharge relationships are nearly identical. One is therefore led to consider some sort of short-circuiting effect in the system, which can be described by introduction of the "effective volume." The effective volume is the volume obtained from the field dye experiment by application of the CIS model. It is a measure of that portion of a river system through which the dye travels. It will normally be less than the real volume of the river system.

In the Mississippi River reach used in this case study, vertical temperature stratification during the daytime has been observed under low flow (20). This daytime stratification accelerates transport in the surface layer where the dye was originally introduced and measured. (All water samples for dye concentration measurements were retrieved within less than 8 in. from the water surface.)

It is believed that intermittent (daytime) stratification is also responsible for the unusually high skewness of the observed May 1977 time concentration curves. Stratification allows transport in one layer while material is left behind in the other layers.

Estimation of Parameter k from River Parameters.—If dye tracings are not available or cannot be obtained for a river reach, an estimate of the parameter, k, in the CIS model can be made at present from river geometry and flow parameters as follows. Equating the relationships, Eqs. 15 and 27, and substituting $\alpha = (Q/V) + K$ and $V = V_r/k$ gives the relationship

$$\left(k + \frac{KV_r}{Q}\right)^2 \left[2\frac{D}{Ux} + 8\left(\frac{D}{Ux}\right)^2\right] - k = 0 \quad \ldots\ldots\ldots\ldots\ldots\ldots \quad (44)$$

The solution of this quadratic equation for k depends on the numerical values of the two dimensionless numbers, $K\ V_r/Q$ and D/Ux. The former can be calculated knowing the volume of the river reach to be modeled, the kinetic rate coefficient of the material, and the flow rate. The numerical value of the

Peclet numer, Ux/D, can be found from river characteristics using any of the empirical or semi-empirical relationships for D proposed by other investigators (11,15,16,17,19).

For example, Liu and Cheng (16) proposed the relationship $D = \gamma u_* A_s^2/h^3$, in which A_s = cross-sectional area = V_r/x; h = mean depth of the river reach; and γ = a coefficient determined from field data and ranges from 0.27–1.25 according to Liu and Cheng (16), with an average on the order of 0.6. Then, $D/Ux = \gamma u_* B^3/xQ$ and with $u_* = \sqrt{gRS}$, in which g = acceleration of gravity; R = hydraulic radius of the river, approximately equal to the depth for wide rivers; S = slope of the energy gradeline; and B = the width of the river in the reach under consideration, $B = A_s/h$. The preceding equation holds only if dispersion is dominated by lateral variation of velocity and not by vertical velocity gradients. Substitution gives

$$\frac{D}{Ux} = \gamma \frac{B^3 \sqrt{ghS}}{xQ} \quad \ldots\ldots\ldots\ldots\ldots\ldots\ldots\ldots\ldots\ldots\ldots\ldots\ldots\ldots \quad (45)$$

which can be used in Eq. 44 to compute a value for k. A simplified solution for a conservative tracer ($K = 0$) would be

$$k \simeq \frac{1}{2}\frac{Ux}{D} = \frac{1}{\gamma}\frac{xQ}{B^3\sqrt{ghS}} \quad \ldots\ldots\ldots\ldots\ldots\ldots\ldots\ldots\ldots\ldots\ldots\ldots\ldots\ldots \quad (46)$$

Further studies of the relationships between k and river characteristics are needed.

Summary and Conclusions

Riverine transport of dissolved or suspended material is a composite of advection along a river thalweg, transverse mixing towards the river banks, entrapment in backwaters, and other separated flow regions created by shoreline and bottom irregularities and other not well-identified processes. The prediction and analysis of riverine transport for water quality modeling has been preoccupied with the application of the AD equation, probably because early on, Taylor (23) showed how the AD equation can be used to analyze mass transport in pipes. Elder (4) expanded its applicability to wide and straight open channels and others later added transverse mixing (7,9,28) entrapment and dead zones (10,19,27), bends (6,8), etc. The geometry of a natural river is often complicated. Spatial and time variations of velocities and turbulence in natural riverine flow systems are usually very pronounced. Simple one-dimensional AD models have been applied to riverine systems incorporating the complicated aforementioned processes in only one parameter, the longitudinal dispersion coefficient. Other models using expanded forms of the AD equation or lump parameters other than a dispersion coefficient are worth consideration to describe natural systems. To this end, a mixed CIS model has been explored in this paper.

The lump parameter in the CIS model is the number of cells into which a river reach is subdivided. Each cell is well-mixed. Dissolved material and water cascade from cells in a given river reach was kept constant in the case study described herein but can be made a function of flow rate where required. For water quality modeling, it is worth noting that biological or chemical kinetics

are easily incorporated into a CIS model. The mathematical form of the governing equation, Eq. 6, which is an ordinary linear differential equation with constant coefficients, makes it possible to express the response of any function, $I(t)$, by means of the convolution of $I(t)$ with the response to a unit impulse (21). Physically, this means that a concentration cloud of an arbitrary shape can be traced downstream by superposition of a number of unit impulses simulating the concentration cloud. Such an application becomes very important in the numerical analysis of hydrologic transport in branching systems, such as shallow river impoundments, estuarine networks, ship canals, etc.

It has been shown in this study that a CIS model provides as good a description of riverine transport as a one-dimensional AD model. Either model reproduces bulk features of the mass transport (mean travel time and variance) without necessarily particular success in the prediction of instantaneous concentrations. The bulk parameters are the total mass of dissolved or suspended material, the mean travel time, the variance and the skewness, respectively, of the time concentration curves. The definitions of these four parameters have been given in Eqs. 1–4 and explicit forms applicable to the CIS and the AD models, in Eqs. 13–16 and Eqs. 25–28, respectively.

If time-variable flow rates are to be used in a water quality model, the CIS model can be easily expanded to handle that feature.

Numerical solutions of the AD equation have similarity to results from a CIS model, because in both cases a river reach is subdivided into finite, well-mixed volumes, and concentrations are obtained as discrete values. Dispersion (numerical dispersion) then becomes an undesirable by-product of the solution. In CIS models, the dispersion due to discretizing of concentrations is used to simulate real dispersion.

CIS models produce skewness without additional terms in the transport equation. Retention of material in the cells is an integral part of the model formulation. Skewness is directly related to the number of cells used.

The CIS model does not use a diffusion-type term to describe the dispersion process which introduces a second-order derivative in the conservation of mass equation. The dispersion process is related to simple parameters such as number of cells, effective cell volume, and volumetric flow rate in the CIS model.

The actual volumes of a river reach are not required for the application of the CID model. Instead, the necessary parameters, i.e., number of cells and effective volume, can be derived from a dye-tracing experiment. In fact, the use of actual volumes based on river geometry instead of effective volumes may lead to erroneous results of travel times and longitudinal spread.

If dye tracings have not or cannot be performed on a river reach, estimates of the parameter k required for a CIS model can be made from river parameters using Eq. 44 and any of the empirical or semi-empirical relationships proposed in the literature for D (e.g., Refs. 15, 16, 17, 19). Results such as given in Eq. 46 can be used until further studies have been conducted.

The CIS models may be most useful for slowly moving and highly dispersive rivers.

Acknowledgments

The writers thank the USGS, St. Paul District, and particularly Gregory Payne for providing dye study data from their open file reports.

Appendix I.—References

1. Banks, R. B., "A Mixing-Cell Model for Longitudinal Dispersion in Open Channels," *Water Resources Research*, Vol. 10, No. 2, Apr., 1974, pp. 357–358.
2. Beltaos, S., "An Interpretation of Longitudinal Dispersion Data in Rivers," *Report No. SWE-78/03*, Alberta Research Council, Alberta, Canada, July, 1978, 55 p.
3. Day, T. J., "Longitudinal Dispersion in Natural Channels," *Water Resources Research*, Vol. 11, No. 6, 1975.
4. Elder, J. W., "The Dispersion of Marked Fluid in Turbulent Shear Flow," *Journal of Fluid Mechanics*, London, England, Vol. 5, No. 4, 1954, pp. 544–560.
5. Fischer, H. B., "The Mechanics of Dispersion in Natural Streams," *Journal of the Hydraulics Division*, ASCE, Vol. 93, No. HY6, Proc. Paper 5992, Nov., 1967, pp. 187–216.
6. Fischer, H. B., "The Effect of Bends on Dispersion in Streams," *Water Resources Research*, Vol. 5, No. 5, Oct., 1969.
7. Fischer, H., "Longitudinal Dispersion and Turbulent Mixing in Open Channel Flow," *Annual Reviews of Fluid Mechanics*, 1973, pp. 59–78.
8. Fukuoka, S., and Sayre, W. W., "Longitudinal Dispersion in Sinusoidal Channels," *Journal of the Hydraulics Division*, ASCE, Vol. 99, No. 1, Proc. Paper 9479, Jan., 1973, pp. 195–217.
9. Holley, E. R., and Abraham, G., "Field Tests on Transverse Mixing in Rivers," *Journal of the Hydraulic Division*, ASCE, Vol. 99, No. HY12, Proc. Paper 10241, Dec., 1973, pp. 2313–2331.
10. Holley, E. R., and Tsai, Y. H., "Effects of Separation Zones on Temporal Moments for Longitudinal Mixing in Rivers," E. E. Driver and W. O. Wunderlich, eds., *Proceedings of the International Symposium on Environmental Effects of Hydraulic Engineering Works*, Sept. 12–14, 1978.
11. Jain, S. C., "Longitudinal Dispersion Coefficients for Streams," *Journal of the Environmental Engineering Division*, ASCE, Vol. 102, No. EE2, Proc. Paper 12037, Apr., 1976, pp. 465–474.
12. Jobson, H. E., and Yotsukura, N., "Mechanics of Heat Transfer in Non-Stratified Open-Channel Flow," *Environmental Impact on Rivers*, H. W. Shen, ed., Fort Collins, Colo., 1972, chapter 8.
13. Levenspiel, O., and Smith, W. K., "Notes of the Diffusion-Type Model for the Longitudinal Mixing of Fluids in Flow," *Chemical Engineering Science*, Vol. 6, 1957, p. 227.
14. Levenspiel, O., *Chemical Reaction Engineering*, John Wiley & Sons, Inc., New York, N.Y., 1972, 578 p.
15. Liu, H., "Predicting Dispersion Coefficient of Streams," *Journal of the Environmental Engineering Division*, ASCE, Vol. 103, No. EE1, Proc. Paper 12724, Feb., 1977, pp. 59–69.
16. Liu, H., and Cheng, A. H. D., "Modified Fickian Model for Dispersion," *Journal of the Hydraulic Division*, ASCE, Vol. 106, No. HY6, Proc. Paper 15454, June, 1980, pp. 1021–1040.
17. McQuivey, R. S., and Keefer, T. N., "Simple Method for Predicting Dispersion in Streams," *Journal of the Environmental Engineering Division*, ASCE, Vol. 100, No. EE4, Proc. Paper 10708, Aug., 1974, pp. 997–1011.
18. McQuivey, R. S., and Keefer, T. N., "Convective Model of Longitudinal Dispersion," *Journal of the Hydraulics Division*, ASCE, Vol. 102, No. HY10, Proc. Paper 12478, Oct., 1976, pp. 1409–1424.
19. Pedersen, F. B., "Prediction of Longitudinal Dispersion in Natural Streams," *Series Paper 14*, Institute of Hydrodynamics and Hydraulic Engineering, Technical University of Denmark, Copenhagen, Denmark, Feb., 1977, 69 p.
20. Sabol, G. V., and Nordin, C. F., "Dispersion in Rivers as Related to Storage Zones," *Journal of the Hydraulics Division*, ASCE, Vol. 104, No. HY5, Proc. Paper 13758, May, 1978, pp. 695–708.
21. Salvadori, M. G., and Schwarz, R. J., *Differential Equations in Engineering Problems*, Prentice-Hall, Inc., New York, N.Y., 1954.
22. Stefan, H., and Wood, A., "Field Investigations of Water Temperature Stratification

and Wind Effects on Dissolved Oxygen in Pool No. 2 of the Mississippi River," *Project Report No. 163*, St. Anthony Falls Hydraulic Laboratory, University of Minnesota, Minneapolis, Minn., Dec., 1976, 116 p.
23. Taylor, G. I., "The Dispersion of Matter in Turbulent Flow Through a Pipe," *Proceedings of the Royal Society of London*, Vol. 223A, 1954, pp. 446–468.
24. Thackston, E. L., and Schnelle, K. B., Jr., "Predicting Effects of Dead Zones on Stream Mixing," *Journal of the Sanitary Engineering Division*, ASCE, Vol. 96, No. SA2, Proc. Paper 7218, Apr., 1970, pp. 319–331.
25. Tsai, Y. H., and Holley, E. R., "Temporal Moments for Longitudinal Dispersion," *Journal of the Hydraulics Division*, ASCE, Vol. 104, No. HY12, Proc. Paper 14266, Dec., 1978, pp. 1617–1634.
26. "Time of Travel and Dispersion Data for Mississippi and Minnesota Rivers, Minneapolis-St. Paul Area. Basic Data Report," prepared in cooperation with the Metropolitan Waste Control Commission by the United States Geological Survey, St. Paul, Minn., 1978.
27. Valentine, E. M., and Wood, I. R., "Longitudinal Dispersion with Dead Zones," *Journal of the Hydraulics Division*, ASCE, Vol. 103, No. HY9, Proc. Paper 13208, Sept., 1977, pp. 975–990.
28. Yotsukura, N., Fischer, H. G., and Sayre, W. W., "Measurements of Mixing Characteristics of the Missouri River Between Sioux City, Iowa and Plattsmouth, Nebraska," *Water Supply Paper 1899-G*, United States Geological Survey, 1970.

Appendix II.—Notation

The following symbols are used in this paper:

A = area under concentration versus time curve in (kilograms second per cubic meter);
A_s = cross-sectional area (in square meters);
B = width (in meters);
C = concentration of dissolved (tracer) or suspended material (in kilograms second per cubic meter);
C_{max} = maximum value of C (in kilograms per cubic meter);
D = longitudinal dispersion coefficient (in square meters per second);
F = dimensionless parameter, function of Peclet number;
h = mean depth (in meters);
I = W/V (in kilograms per cubic meters per second);
K = kinetic rate of material removal (in seconds);
k = number of cells in river reach (−);
M = total dissolved (or suspended) mass (in kilograms);
M_o = initially released mass (in kilograms);
Pe = Peclet number = Ux/D;
Q = volumetric river flow rate (in cubic meters per second);
S = skewness coefficient = μ/σ^3;
t = time since material release (in hours);
$\bar{t}$ = time to centroid of $C(t)$ curve (in hours);
t_{max} = time to C_{max};
U = mean river velocity (in meters per second);
V = mixed cell volume (in cubic meters);
V_t = total volume of river reach = kV;
W = rate of external material input into cell (in kilograms per second);
x = distance from point of material release (in meters);

Y = D/x^2;
α = $(Q/V) + K$;
γ = coefficient;
δ = Dirac delta function;
μ = skewness of $C(t)$ function (in cubic hours); and
σ = standard deviation of $C(t)$ function (in hours).

Subscripts

0, 1, 2, 3, ... = refer to river station number; and
1–2, 1–4, ... = refer to river reach between stations.

Minimum Specific Energy in Compound Open Channel

By Merritt E. Blalock,[1] M. ASCE and Terry W. Sturm,[2] A. M. ASCE

Introduction

Analysis of open channel flow by the application of the energy principle is often clarified and aided by the concept of specific energy, which was introduced by Bakhmeteff (1) in 1912. Specific energy is defined for one-dimensional open-channel flow as the height of the energy grade line above the channel bottom. It leads to a classification of open-channel flow into subcritical and supercritical flow regimes, distinguished by flow depths that are respectively greater or less than the depth at which specific energy is minimum (critical depth). A mathematical consideration of minimum specific energy gives rise to the definition of a Froude number having a value of unity at critical depth. The value of the Froude number is greater than unity for supercritical flow and less than unity for subcritical flow.

The occurrence of critical depth and its associated minimum specific energy is of considerable practical importance to hydraulic engineers. It is one type of channel control which may provide the boundary condition for computation of water-surface profiles in steady, gradually varied flow. Water-surface profile computations are an integral part of water resources investigations involving flood-plain delineations, evaluation of flood control measures, and the design of irrigation and drainage channels.

Petryk and Grant (9) show that the determination of critical depth in channels with overbank or flood-plain flow (compound channels) can be troublesome. Customary definitions of the Froude number generally do not indicate critical depth at the point of minimum specific energy. In addition, there are some compound-channel geometries which produce specific-energy diagrams with two points of minimum specific energy. It is the purpose of this paper to present an analytical formulation of a compound-channel Froude number which correctly identifies the occurrence of points of minimum specific energy for flow in compound open channels. The proposed compound-channel Froude number can

[1]Hydrologist, United States Geological Survey, Atlanta, Ga.; formerly President's Fellow, Georgia Inst. of Tech., Atlanta, Ga. 30332.

[2]Asst. Prof., School of Civ. Engrg., Georgia Inst. of Tech., Atlanta, Ga. 30332.

Note.—Discussion open until November 1, 1981. To extend the closing date one month, a written request must be filed with the Manager of Technical and Professional Publications, ASCE. Manuscript was submitted for review for possible publication on September 26, 1980. This paper is part of the Journal of the Hydraulics Division, Proceedings of the American Society of Civil Engineers, ©ASCE, Vol. 107, No. HY6, June, 1981. ISSN 0044-796X/81/0006-0699/$01.00.

be used in conjunction with existing computer programs for water-surface profile computation (5,13,16), and is necessarily limited by the same simplifying assumptions that are associated with the conventionally used, one-dimensional equation of steady, gradually varied flow (17). The results of an experimental investigation in a laboratory flume are also presented, demonstrating the existence of two points of minimum specific energy and identifying these points by the proposed compound-channel Froude number.

Froude Number-Flow Regime Discrepancies

For a simple channel of nonrectangular section and uniform cross-sectional velocity distribution, the Froude number F is defined by

$$F = \left(\frac{Q^2 T}{gA^3}\right)^{1/2} \quad \ldots\ldots\ldots\ldots\ldots\ldots\ldots\ldots\ldots\ldots\ldots\ldots\ldots\ldots\ldots\ldots (1)$$

in which Q = discharge; T = the top width of the water surface; g = acceleration of gravity; and A = the cross-sectional area of flow. For a compound channel it is customary to include the kinetic energy flux correction coefficient, α, in the definition of specific energy. As a result, α appears as follows in the definition of the Froude number assuming α is constant with depth:

$$F_\alpha = \left(\frac{\alpha Q^2 T}{gA^3}\right)^{1/2} \quad \ldots\ldots\ldots\ldots\ldots\ldots\ldots\ldots\ldots\ldots\ldots\ldots\ldots\ldots\ldots\ldots (2)$$

For natural channels with overbank flow, it is often assumed that the major contribution to α is the large difference in mean velocity between main channel and overbank sections. By comparison the nonuniformity of the velocity distribution within each subsection can be neglected.

Two major problems arise in the computation of one-dimensional, steady, gradually varied flow profiles in compound channels as a result of using the Froude numbers F or F_α. First, incorrect solutions are generated when numerical methods are used to solve the gradually varied flow equation written in a form involving the Froude number F_α. Second, incorrect solutions may be accepted when the standard step method is used to compute water-surface profiles near critical depth. These difficulties are the result of neglecting the variation of α with depth in compound-channel flows.

Consider the equation of gradually varied flow in the following form:

$$\frac{dy}{dx} = \frac{S_0 - S_e}{1 - F_\alpha^2} \quad \ldots\ldots\ldots\ldots\ldots\ldots\ldots\ldots\ldots\ldots\ldots\ldots\ldots\ldots\ldots\ldots (3)$$

in which dy/dx = the rate of change in depth of flow with respect to distance along the channel; S_0 = the bed slope of the channel; and S_e = the slope of the energy grade line. Prasad (10) has proposed a numerical solution procedure for Eq. 3 which can be applied to natural channels. In addition to the assumption that α is constant, the assumptions involved in obtaining Eq. 3 include: no lateral flow, a hydrostatic pressure distribution, a constant bed slope, and a straight, very wide channel, or alternatively, an approximately prismatic channel (17). Because the variation in α with depth and thus with distance along the channel has been neglected, application of Eq. 3 to a gradually varied flow

in a compound channel will lead to incorrect water-surface elevations. The denominator of the term on the right-hand side in Eq. 3 arises from a consideration of the variation of specific energy with depth, a portion of which is due to changes in α with depth in compound-channel flow. Furthermore, the use of F_α can cause the right-hand side of Eq. 3 to become indefinite at a depth that does not correspond to the actual critical depth.

As an alternative to Eq. 3, water-surface profiles are computed in natural channels by the standard step method (6) in which the specific energy is computed explicitly. In this case, F_α does not appear in the equation to be solved, but is used instead to indicate whether the solution is in the supercritical or subcritical flow regime. For compound channels, neither F nor F_α correctly indicates the flow regime. Thus, incorrect solutions of the energy equation can be accepted when the depth is near critical depth.

Compound-Channel Froude Number

Previous Investigations.—Previous investigations of the problems associated with defining the Froude number in compound channels are limited. Numerous laboratory investigations of compound-channel flow have been undertaken (8,11,15), but the focus of these experiments has been the quantification of changes in the boundary shear stress distribution resulting from momentum exchange between the main channel and floodplain. The Federal agencies which maintain and use water-surface profile programs recognize the Froude-number difficulties in compound channels as described in the previous section of this paper, and they examine these difficulties in their user's manuals. The Soil Conservation Service (16), e.g., warns of differences of as much as 2 ft between the critical depth determined by F (Eq. 1) and the critical depth determined by minimum specific energy.

The Corp of Engineers (5) presents an algorithm to solve for the depth corresponding to minimum specific energy when their water-surface profile program attempts to obtain a solution close to critical depth. The depth of minimum specific energy is compared with the profile depth to check the flow regime rather than using the Froude number as a check.

The United States Geological Survey (USGS) (12) proposes the use of an index Froude number based on the Froude number of the subsection carrying the greatest discharge. The index Froude number is thought by the USGS to better reflect the flow regime of the entire cross section, but it is also recognized as having limitations. The USGS does not consider the index Froude number to be a true Froude number, but rather a warning flag that identifies possible flow-regime problems. A later version of the USGS Water Surface Profile Program incorporates a routine to determine the depth of minimum specific energy.

Petryk and Grant (9) have proposed a discharge-weighted Froude number without experimental corroboration in order to eliminate the computational problems associated with the occurrence of two points of minimum specific energy in compound-channel flows. Although their proposed Froude number succeeds in doing this by identifying only one value of critical depth, it is nevertheless somewhat arbitrary and is divorced from the concept of minimum specific energy.

Clearly, the Froude number should be formulated to reflect the specific energy

curve under consideration and should indicate critical depth at the point (or points) of minimum specific energy. Such a Froude number would produce correct numerical solutions of the gradually varied flow equation (Eq. 3) and would eliminate the need for time-consuming routines used to solve for the depth of minimum specific energy in standard step water-surface profile computations.

Derivation and Formulation.—The specific energy, E, for a one-dimensional compound-channel flow is given by

$$E = y + \frac{\alpha Q^2}{2gA^2} \qquad (4)$$

in which y = the depth of flow. The kinetic energy flux correction coefficient, α, is defined as

$$\alpha = \frac{\int v^3 \, dA}{V^3 A} \qquad (5)$$

in which v = the velocity through the element of area, dA; and V = the mean cross-sectional velocity (3,6). Alpha is thus a measure of the nonuniformity of the velocity distribution. For computational purposes, flow is conventionally divided into channel and overbank subsections by appropriately located vertical lines which are assumed not to transmit shear stress from one section of flow to another, and which do not contribute to wetted perimeter. Wright and Carstens (15) have suggested that the wetted perimeter of the subsection dividing line be retained for the main channel, and that the shear stress applied by the main-channel flow section on the overbank section be considered. Regardless of the manner in which the main flow–flood-plain interaction is treated, the basic assumption in the computation of α, as previously mentioned, is that the contribution of the nonuniformity of the velocity distribution within each subsection is negligible in comparison to the variation in mean velocity between subsections. If Eq. 5 is applied with this assumption to a compound channel which has been divided into subsections, the kinetic energy flux correction coefficient becomes

$$\alpha = \frac{\sum_i \left(\frac{k_i^3}{a_i^2} \right)}{\frac{K^3}{A^2}} \qquad (6)$$

in which k_i = the conveyance of the ith subsection; a_i = the area of the ith subsection; and $K = \Sigma k_i$ = the conveyance of the total cross section (3,6). The subsection conveyance is computed from the Manning equation as follows:

$$k_i = \frac{1.49}{n_i} a_i r_i^{2/3} \qquad (7)$$

in which r_i $(= a_i/p_i)$ = the subsection hydraulic radius; p_i = the subsection wetted perimeter; and n_i = the subsection n value. In the SI system of units, the constant 1.49 is replaced by unity.

The point (or points) of minimum specific energy is obtained by differentiating Eq. 4 with respect to y and setting the derivative equal to zero. Because both α and area are functions of depth, the differentiation produces (14)

$$\frac{dE}{dy} = 1 - \frac{\alpha Q^2}{gA^3}\frac{dA}{dy} + \frac{Q^2}{2gA^2}\frac{d\alpha}{dy} = 0 \quad \ldots\ldots\ldots\ldots\ldots\ldots\ldots\ldots\ldots\ldots (8)$$

Noting that $dA/dy = T$, and that by rearranging terms, the following expression is obtained:

$$\frac{\alpha Q^2 T}{gA^3} - \frac{Q^2}{2gA^2}\frac{d\alpha}{dy} = 1 \quad \ldots\ldots\ldots\ldots\ldots\ldots\ldots\ldots\ldots\ldots\ldots\ldots (9)$$

The left-hand side of Eq. 9 is unity at the point of minimum specific energy; therefore, a compound-channel Froude number F_c can be defined from Eq. 9 as

$$\mathsf{F}_c = \left(\frac{\alpha Q^2 T}{gA^3} - \frac{Q^2}{2gA^2}\frac{d\alpha}{dy}\right)^{1/2} \quad \ldots\ldots\ldots\ldots\ldots\ldots\ldots\ldots\ldots\ldots (10)$$

At the point of minimum specific energy F_c will have a value of 1.

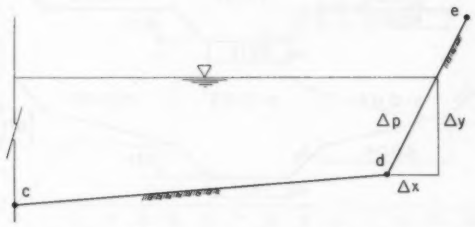

FIG. 1.—Definition Sketch for Evaluation of dp_i/dy

With the exception of $d\alpha/dy$, all of the terms on the right-hand side of Eq. 10 are routinely determined in water-surface profile computations. Evaluation of $d\alpha/dy$ can be achieved by differentiating Eq. 6 with respect to y. As shown in Appendix I, the derivative becomes

$$\frac{d\alpha}{dy} = \frac{A^2\sigma_1}{K^3} + \sigma_2\left(\frac{2AT}{K^3} - \frac{A^2\sigma_3}{K^4}\right) \quad \ldots\ldots\ldots\ldots\ldots\ldots\ldots\ldots\ldots\ldots (11)$$

$$\text{in which} \quad \sigma_1 = \sum_i \left[\left(\frac{k_i}{a_i}\right)^3 \left(3t_i - 2r_i\frac{dp_i}{dy}\right)\right] \quad \ldots\ldots\ldots\ldots\ldots\ldots\ldots\ldots (12)$$

$$\sigma_2 = \sum_i \left(\frac{k_i^3}{a_i^2}\right) \quad \ldots\ldots\ldots\ldots\ldots\ldots\ldots\ldots\ldots\ldots\ldots\ldots\ldots\ldots (13)$$

$$\sigma_3 = \sum_i \left[\left(\frac{k_i}{a_i}\right)\left(5t_i - 2r_i\frac{dp_i}{dy}\right)\right] \quad \ldots\ldots\ldots\ldots\ldots\ldots\ldots\ldots\ldots\ldots (14)$$

In Eqs. 12–14, t_i = the top width of the ith subsection; and dp_i/dy = the rate of change in wetted perimeter with respect to depth of flow in the ith subsection. Evaluation of dp_i/dy is simplified by the fact that the cross-section geometry of natural channels is defined by ground points connected with straight lines. The definition sketch in Fig. 1 (which is a portion of a right overbank subsection) shows the water surface intersecting the line segment $\overline{de}$. This line segment makes a contribution of Δp to the subsection wetted perimeter. The rate of change in wetted perimeter with respect to depth is a constant along $\overline{de}$, and therefore can be evaluated as

$$\frac{dp_i}{dy} = \frac{\Delta p}{\Delta y} \quad \ldots\ldots\ldots\ldots\ldots\ldots\ldots\ldots\ldots\ldots\ldots\ldots\ldots\ldots\ldots\ldots\ldots\ldots\ldots\ldots\ldots\ldots \quad (15)$$

The terms Δp and Δy are generally determined when computing the geometric properties of a cross section for use in a water-surface profile program. It should be noted that if the water surface is at point e, dp_i/dy should be evaluated for the line segment $\overline{de}$, but if the water surface is at point d, dp_i/dy should be evaluated for the line segment $\overline{cd}$. In situations where the water surface

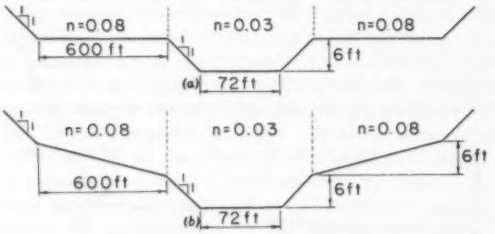

FIG. 2.—Channel Cross Sections for Evaluation of Specific Energy and Froude Numbers: (*a*) Cross Section A; (*b*) Cross Section B (1 ft = 0.3 m)

does not intersect the wetted perimeter of a subsection (e.g., the boundary between the main channel and overbank section above bankfull stage), dp_i/dy is zero. For a subsection where the water surface intersects both a left and right bank (e.g., the main channel below bankfull stage), dp_i/dy is the sum of $\Delta p/\Delta y$ for each of the banks.

The working equation for the compound-channel Froude number can be obtained by substituting Eq. 11 into Eq. 10 and simplifying:

$$F_c = \left[\frac{Q^2}{2gK^3}\left(\frac{\sigma_2\sigma_3}{K} - \sigma_1\right)\right]^{1/2} \quad \ldots\ldots\ldots\ldots\ldots\ldots\ldots\ldots\ldots\ldots\ldots\ldots\ldots\ldots\ldots\ldots\ldots\ldots \quad (16)$$

If the Manning's n value is considered to vary with depth of flow in any subsection, σ_1 and σ_3 can be written to reflect the variation:

$$\sigma_1 = \sum_i \left[\left(\frac{k_i}{a_i}\right)^3 \left(3t_i - 2r_i\frac{dp_i}{dy} - \frac{a_i}{n_i}\frac{dn_i}{dy}\right)\right] \quad \ldots\ldots\ldots\ldots\ldots\ldots\ldots\ldots\ldots\ldots\ldots\ldots\ldots\ldots \quad (17)$$

$$\sigma_3 = \sum_i \left[\left(\frac{k_i}{a_i} \right) \left(5t_i - 2r_i \frac{dp_i}{dy} - \frac{a_i}{n_i} \frac{dn_i}{dy} \right) \right] \quad \ldots \ldots \ldots \ldots \ldots \ldots \quad (18)$$

in which dn_i/dy = the rate of change in n_i with respect to depth of flow.

Evaluation.—The behavior of the compound-channel Froude number, F_c, may be evaluated by examining the specific-energy diagrams of two idealized, symmetric cross sections, each conveying 5,000 cfs (142 m^3/s). Cross section A [Fig. 2(*a*)] is from Petryk and Grant (9). In Fig. 3, the specific-energy curve for this cross section reveals two points of minimum specific energy at depths of flow of approx 6.8 ft (2.07 m) and 5.3 ft (1.62 m). These points are indicated by C1 and C2, respectively, in Fig. 3.

F_c (Eq. 16) for this cross section is plotted in Fig. 4 along with F (Eq. 1) and F_a (Eq. 2). As expected, all three equations produce the same curve below top of bank (simple channel situation), but only Eq. 16 for F_c correctly locates

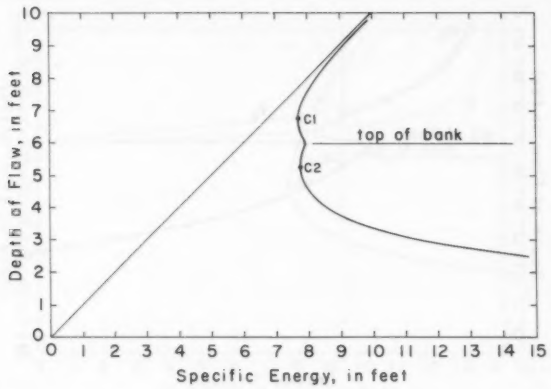

FIG. 3.—Specific Energy for Cross Section A Conveying 5,000 cfs (1 cfs = 0.028 m^3/s; 1 ft = 0.3 m)

C1, the upper depth of minimum specific energy (6.8 ft or 2.07 m), and connects with the lower curve at the top of bank depth.

The shape of the Froude number curve is independent of the discharge, and the fiducial point ($F_c = 1$) can be shifted left or right by varying the discharge. This means that once F_c is plotted for a particular cross section and discharge, points of minimum specific energy for other discharges may be determined without the necessity of constructing new specific-energy diagrams. In effect, the variable F_c/Q provides a universal horizontal scale for Fig. 4 which depends only on the conveyance and geometric properties of the particular cross section. Thus, for a given depth of flow, the critical discharge, Q_c, can be computed by taking the reciprocal of the corresponding value of F_c/Q, because F_c/Q for the given depth equals $1/Q_c$ for the critical condition.

Cross section B is presented in Fig. 2(*b*) and differs from cross section A only in that the flood plains have a 100:1 slope toward the channel. The

specific-energy diagram of cross section B (Fig. 5) reveals a single point of minimum specific energy below top of bank at the same depth of flow as for cross section A (point C2). The three Froude number curves shown in Fig. 6 for cross section B are again identical below top of bank, but F (Eq. 1) and F_α (Eq. 2) each indicate another point of minimum specific energy above top of bank at depths of flow of 6.5 ft (1.98 m) and 6.8 ft (2.07 m), respectively. The occurrence of these false points of minimum specific energy is a more serious deficiency of Eqs. 1 and 2 than the errors in critical depth shown in Fig. 4.

It is evident from these two examples that the Froude numbers generated by Eqs. 1 and 2 are not acceptable for use in the gradually varied flow equation (Eq. 3). Neither definition of Froude number faithfully reflects the specific-energy diagram in overbank flow situations, and either would produce divergence from a correct profile solution. It is equally evident that Eqs. 1 and 2 are not satisfactory

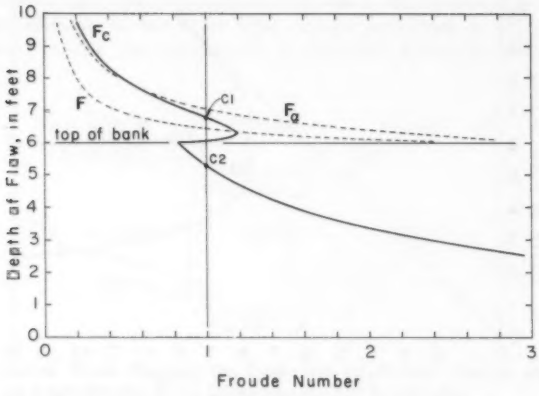

FIG. 4.—Froude Numbers for Cross Section A Conveying 5,000 cfs (1 cfs = 0.028 m^3/s; 1 ft = 0.3 m)

for checking the flow regime in the standard step method. Only F_c (Eq. 17) accurately reflects the specific-energy diagram and indicates the correct flow regime. The experimental investigation into the occurrence of two points of minimum specific energy in the following portion of this paper offers guidance for the interpretation of the flow regime between the two points of minimum specific energy, C1 and C2, in cross section A (Fig. 3).

Experimental Investigation

The experimental investigation consisted of measuring point velocities in a compound-channel cross section which was formed by constructing a single rectangular overbank section in a laboratory flume. Sufficient point velocity measurements were made at eight different depths of flow (at approximately the same discharge for each depth) to compute the discharge, mean velocity,

kinetic energy flux correction coefficient, and specific energy for each depth. Complete details of the experimental procedure are given by the first writer (2).

The experiments were conducted in a tilting steel flume 80 ft (24.38 m) long, 3.5 ft (1.07 m) wide, and 1.5 ft (0.46 m) deep. This flume was also used by Tracy and Lester (14) and details of its construction are given by them. The overbank section was constructed of 3/4-in. exterior plywood and two-by-six fir framing lumber, resulting in the channel dimensions shown in Fig. 7. All wood was coated with sanding sealer and exterior acrylic-latex paint. The overbank section was attached to the flume with silicon adhesive.

Point velocities were measured with a 0.072-in. (1.83-mm) outside diameter pitot-static tube operated in conjunction with a differential pressure transducer. Data collection, reduction, and analysis were accomplished with an HP9825A desktop computer controlling a digital voltmeter which measured the voltage

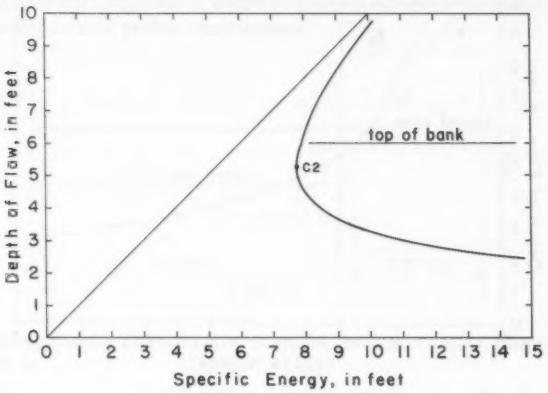

FIG. 5.—Specific Energy for Cross Section B Conveying 5,000 cfs (1 cfs = 0.028 m^3/s; 1 ft = 0.3 m)

output from the pressure transducer and preamplifier. Point velocity measurements were made at a station 65 ft (19.81 m) downstream of the flume entrance. Preliminary measurements were made at a station 60 ft (18.29 m) downstream. Comparison of dimensionless profiles of velocity between the two stations indicated that the flow was fully developed.

The preliminary experiments indicated that a discharge of 1.7 cfs (0.048 m^3/s) would produce a specific-energy curve with two points of minimum specific energy. An estimate of the error in setting the discharge to 1.7 cfs (0.048 m^3/s) included the calibration error of the Venturi meter used to measure the discharge and also included an estimate of the error introduced by observed fluctuations in the Venturi-meter manometer during the course of an experimental run. The estimated error in discharge was of the order of ±3%, which was the same range of error observed between individual discharges determined from the

Venturi meter and the discharges determined by integration of the point velocity measurements.

Establishing a truly uniform flow profile for the experimental runs proved impossible. Any discharge flowing near the depth corresponding to minimum specific energy, as these were, could be expected to be inherently unstable. The instability was exacerbated by the variations in the overbank surface, which were of the order of ±0.01 ft (0.3 cm). Standing waves in the overbank section and a cross-hatched water surface in the channel thwarted efforts to achieve a uniform water-surface profile. As a result, the adopted experimental procedure was to establish a profile as close to uniform as possible such that the desired depth of flow was obtained where the point velocities were to be measured. The maximum observed change in depth for overbank-flow runs was approx 0.05 ft (1.5 cm) between the channel entrance and the measuring station where the flow depth was 0.567 ft (17.3 cm). For larger depths of flow, the water-surface

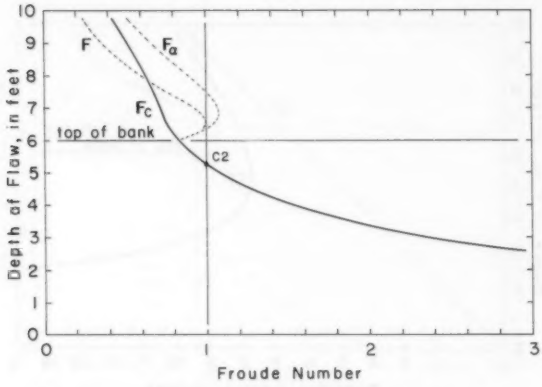

FIG. 6.—Froude Numbers for Cross Section B Conveying 5,000 cfs (1 cfs = 0.028 m^3/s; 1 ft = 0.3 m)

profiles tended to be more stable and more nearly uniform. A profile at a depth of flow of 0.7 ft (21.3 cm) was established to demonstrate that a uniform profile could be obtained in the downstream reach of the flume if the depth of flow was sufficiently greater than the depth corresponding to minimum specific energy.

Results

Table 1 presents the values of area, discharge, kinetic energy flux correction coefficient, and specific energy computed from experimental measurements for each of the eight reported runs. Runs 5 and 6 are not reported in the table because of operational difficulties during each run. It is apparent from the results presented in Table 1 that as the depth increased for those experimental runs with overbank flow, the proportion of the total discharge in the overbank

section increased. It should also be noted that the values of α for the main channel alone are measurably larger than 1.0 because of the narrowness of the main channel section.

Observations of the water surface for the four experimental runs with overbank flow indicated greater instability as the depth of flow decreased. The water-surface instability was manifested by standing waves in the overbank section and a choppy, cross-hatched water surface in the channel section. Beginning at the upper depth of minimum specific energy (run 2) and continuing with decreasing depth, the standing wave fronts in the overbank section were perpendicular to the mean flow direction and then were bent downstream into a cross-hatched pattern in the channel section characteristic of supercritical flow. The surface instability continued to increase for the experimental runs as depth decreased below top of bank. The fact that the water surface was unstable for experimental runs 7 and 8, the first two runs below top of bank in Table 1, suggests that the upper point of minimum specific energy could be considered the limit of subcritical flow for situations in which two points of minimum specific energy occur in water-surface profile computations.

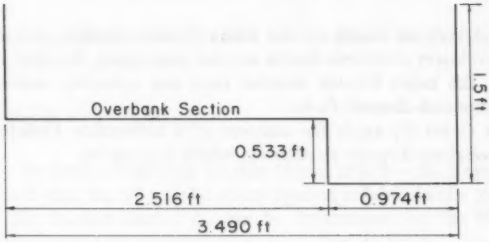

FIG. 7.—Cross Section of Flume and Overbank Section, Looking Downstream (1 ft = 0.3048 m)

The experimental specific-energy data in Table 1 are plotted in Fig. 8(*a*). Although the variation in discharge from run to run causes some scatter in the plot, there is evidence of two points of minimum specific energy. The experimental values of α plotted in Fig. 8(*b*) show little scatter and indicate that α is primarily a function of depth of flow. This observation suggests that a specific-energy diagram for a single value of discharge can be constructed by substituting the average discharge of eight runs (1.692 cfs or 0.048 m^3/s) into Eq. 4 while using the experimental data for all other variables. Fig. 9 presents the resulting average specific-energy diagram. The two points of minimum specific energy are more clearly apparent in this figure.

The concept of computing a Froude number for the flow in a subsection of a compound channel has already been mentioned with regard to the USGS index Froude number (12). The subsection Froude numbers (computed with Eqs. 1 and 2) for the experimental data of this investigation are presented in Table 2. The Froude number of the channel (Col. 3 or 4 of Table 2) is the index Froude number of these experimental runs because the channel is the subsection with the largest discharge. All four depths of flow above top

TABLE 1.—Experi

Run (1)	y, in feet (2)	S_0 (3)	E, in feet (4)	Channel: A, in square feet (5)	Channel: Q, in cubic feet per second (6)	Channel: α (7)
1	0.650	0.001018	0.718	0.633	1.363	1.084
4	0.625	0.001128	0.702	0.609	1.388	1.083
2	0.600	0.001485	0.700	0.584	1.496	1.082
3	0.567	0.002096	0.701	0.552	1.592	1.088
10	0.533	0.001903	0.704	0.519	1.648	1.093
7	0.500	0.002118	0.700	0.487	1.676	1.087
8	0.467	0.003300	0.690	0.455	1.645	1.096
9	0.433	0.004455	0.701	0.422	1.671	1.100

Note: 1 ft = 0.3048 m; 1 cfs = 0.028317 m^3/s.

of bank are subcritical based on the index Froude number, but as shown in Fig. 9, the two lower overbank depths are not subcritical. For this experimental investigation, the index Froude number does not correctly indicate the flow regime of compound-channel flow.

Petryk and Grant (9) apply the concept of a subsection Froude number to obtain their weighted Froude number F_r, which is given by

$$\mathsf{F}_r = \frac{\sum_i (q_i F_i)}{Q} \qquad (19)$$

in which q_i = the subsection discharge; and F_i = the subsection Froude number computed by Eq. 1. Values of F_r for the experimental data are presented in Col. 7 of Table 2. As in the case of the index Froude number, the weighted Froude number does not correctly indicate the flow regime.

Analysis

The proposed compound-channel Froude number cannot be directly determined from the experimental data. Attempts to use Eq. 10 fail because it is difficult to determine $d\alpha/dy$ from the limited number of experimental data points. Eq. 16 fails because the slope of the energy grade line is not precisely known, which means that the subsection resistance coefficient and thus the conveyance, k_i, cannot be determined from the experimental data. If it had been possible to establish a uniform flow condition for each run, the energy gradient would parallel the flume slope, and the conveyance for each subsection could be computed from the experimental data alone. The compound-channel Froude number can only be determined indirectly through an independent prediction of the experimental results.

Working in the same flume as used in the present investigation, Tracy and

mental Data

Overbank			Total		
A, in square feet (8)	Q, in cubic feet per second (9)	α (10)	A, in square feet (11)	Q, in cubic feet per second (12)	α (13)
0.294	0.411	1.108	0.927	1.774	1.192
0.231	0.326	1.132	0.840	1.714	1.198
0.169	0.230	1.169	0.753	1.726	1.224
0.083	0.087	1.340	0.635	1.680	1.238
			0.519	1.648	1.093
			0.487	1.676	1.087
			0.455	1.645	1.096
			0.422	1.671	1.100

Lester (14) experimentally determined a friction-factor relationship for smooth rectangular channels of the form

$$\frac{1}{\sqrt{f}} = 2.03 \log (\mathrm{R}\sqrt{f}) - 1.30 \quad \ldots \ldots \ldots \ldots \ldots \ldots \ldots \ldots \quad (20)$$

in which f = the Darcy-Weisbach friction factor; and R = the Reynolds number. If it is assumed that Eq. 20 is valid when applied independently to each channel subsection, the friction factor, f_i, can be determined for the ith subsection. The mean velocity in the ith subsection, v_i, is then given by

$$v_i = \left(\frac{8gr_iS_e}{f_i}\right)^{1/2} \quad \ldots \ldots \ldots \ldots \ldots \ldots \ldots \ldots \ldots \quad (21)$$

in which r_i = the hydraulic radius of the ith subsection; and S_e = the slope of the energy grade line. Because the values of f_i and v_i obtained from Eqs. 20 and 21 must be such that the subsection discharges sum to the average measured discharge, Q_m, of 1.692 cfs (0.048 m^3/s), the following equation must be satisfied:

$$S_e = \frac{Q_m^2}{\left[\sum_i \left(\frac{8g}{f_i} r_i a_i^2\right)^{1/2}\right]^2} \quad \ldots \ldots \ldots \ldots \ldots \ldots \ldots \quad (22)$$

It has been implicitly assumed that S_e is the same for all subsections. Eqs. 20, 21, and 22 can be solved iteratively for the friction factor and velocity in each subsection for a given total discharge and depth. The iterative solution procedure is given in detail by the first writer (2).

The velocities, v_i, were calculated by the procedure just described for the mean measured discharge of 1.692 cfs (0.048 m^3/s). It was assumed that the imaginary vertical boundary between the main channel and overbank section

made no contribution to wetted perimeter. Furthermore, the friction factors determined for each subsection were converted to Manning's n values because the formulation for the compound Froude number, F_c, is in terms of n. The n values so obtained exhibited a slight variation with depth; however, to facilitate the computations, constant n values of 0.009 and 0.010 were adopted for the channel and overbank sections, respectively. From the velocities and n values for each subsection, the specific energy and compound Froude number were computed for a series of depths within the range of measured depths. In the

TABLE 2.—Froude Numbers for Experimental Data

Run (1)	y, in feet (2)	Channel F (Eq. 1) (3)	Channel F_α (Eq. 2) (4)	Overbank F (Eq. 1) (5)	Overbank F_α (Eq. 2) (6)	Weighted F_r (Eq. 19) (7)
1	0.650	0.471	0.490	0.721	0.759	0.529
4	0.625	0.508	0.529	0.821	0.873	0.586
2	0.600	0.583	0.606	0.925	1.001	0.629
3	0.567	0.675	0.704	1.017	1.177	0.692

Note: 1 ft = 0.3048 m.

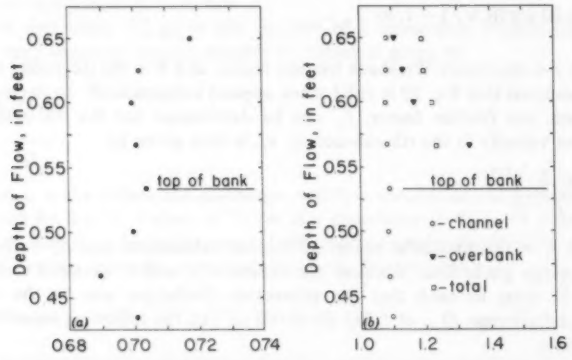

FIG. 8.—Specific Energy and Kinetic Energy Flux Correction Factor from Experimental Data (1 ft = 0.3 m): (*a*) Specific Energy, in feet; (*b*) Alpha

computation of the specific energy and F_c, it was assumed that α of each subsection had the value 1.0 rather than the measured value. In this way, the computational procedure remained independent of the measured data and was executed in the same manner as would be expected when determining F_c for a natural river channel in the course of a water-surface profile computation.

The predicted specific-energy diagram is shown in Fig. 10(*a*), and two depths of minimum specific energy are apparent, although each depth is approximately 2/100 ft smaller than the corresponding depths in Fig. 8(*a*) or Fig. 9. The

entire specific-energy curve in Fig. 10(*a*) is skewed slightly downward and to the left when compared with the measured curve in Fig. 8(*a*) or the average curve in Fig. 9. The predicted compound-channel Froude number curve in Fig. 10(*b*) exhibits the behavior typical for two points of minimum specific energy,

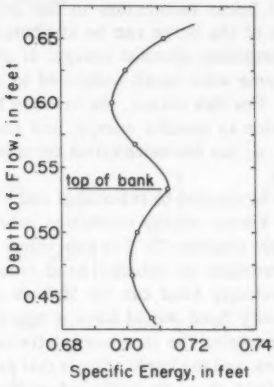

FIG. 9.—Experimental Specific Energy Curve for an Average Discharge of 1.692 cfs (1 cfs = 0.028 m^3/s; 1 ft = 0.3 m)

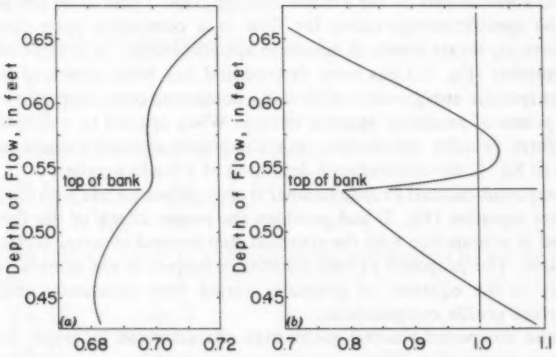

FIG. 10.—(*a*) Predicted Specific Energy in Experimental Flume for 1.692 cfs; (*b*) Compound Channel Froude Number for Fig. 10(*a*) (1 cfs = 0.028 m^3/s; 1 ft = 0.3 m)

and is in correspondence with the predicted specific-energy curve as expected.

To investigate the role that neglecting the transfer of linear momentum to the overbank section plays in the skew of the predicted specific-energy curve, the correction suggested by Wright and Carstens (15) was considered. Although

the correction improved the agreement between the measured and computed discharges in the overbank section, especially at the larger depths, the effect on the computed specific-energy curve was minimal because of the relatively small changes in α which resulted from the correction.

The skew in the specific-energy curve is most pronounced below top of bank depth where transfer of linear momentum to the overbank does not occur. The skew in this portion of the curve can be attributed to selecting subsection α values of unity in computing specific energy. It should be noted that the depths of flow in the flume were small compared to depths of flow normally found in field situations. For this reason, the velocity head in the flume makes a large relative contribution to specific energy, and any adjustment to velocity head (such as subsection α) has far more effect on specific energy in the flume than it would in the field.

The same analysis can be applied to subcritical and supercritical flow regimes in field situations where kinetic energy correction coefficients can be as much as 1.4 or more in the main channel (7). For subcritical flow where the velocity head is small, an α-adjustment to velocity head would be insignificant. For supercritical flow, the velocity head can be 50% or more of the depth, and an α-adjustment to velocity head would have a significant effect on specific energy. This reasoning explains the increasing leftward shift in Fig. 10(*a*) as the depth of flow decreases, and the implication is that predicted specific energies and Froude numbers in field channels under subcritical flow conditions would be closer to measured values.

Conclusions

Existing formulations of the Froude number (Eqs. 1 and 2) do not accurately reflect the specific-energy curve for flow in a compound open channel and do not correctly locate points of minimum specific energy. A compound-channel Froude number (Eq. 16) has been derived and has been shown to accurately reflect the specific-energy curve of flow in a compound open channel by correctly locating points of minimum specific energy. When applied to a simple channel with uniform velocity distribution, the compound channel Froude number is identical to Eq. 1, the conventional definition of Froude number.

The compound-channel Froude number is appropriate for use with the gradually varied flow equation (Eq. 3) and provides the proper check of the flow regime when used in conjunction with the standard step method of water-surface profile computation. The proposed Froude number is subject to the same assumptions that apply to the equation of gradually varied flow commonly employed in water-surface profile computations.

For some compound-channel geometries characterized by wide, level flood plains, two points of minimum specific energy can be computed for certain discharges. Laboratory investigation of a one-dimensional flow demonstrates that this phenomenon can in fact occur, and indicates that the upper point of minimum specific energy may be considered the proper limit of subcritical flow.

Acknowledgments

Financial support for the first writer was provided by the USGS during the experimental investigation. The School of Civil Engineering, Georgia Institute

of Technology, provided material support for the construction of the experimental apparatus and supplied the electronic instrumentation. The writers wish to express their appreciation to C. S. Martin, Georgia Institute of Technology, for his assistance with the instrumentation.

Appendix I.—Derivation of $d\alpha/dy$

Writing Eq. 6 as

$$\alpha = \frac{A^2}{K^3} \sum_i \left(\frac{k_i^3}{a_i^2} \right) \quad \ldots \ldots \ldots \ldots \ldots \ldots \ldots \ldots \ldots \ldots \ldots \ldots \quad (23)$$

and differentiating with respect to y produces

$$\frac{d\alpha}{dy} = \frac{A^2}{K^3} \sum_i \left[3 \left(\frac{k_i}{a_i} \right)^2 \frac{dk_i}{dy} - 2 \left(\frac{k_i}{a_i} \right)^3 \frac{da_i}{dy} \right]$$

$$+ \sum_i \left(\frac{k_i^3}{a_i^2} \right) \left[\frac{2A}{K^3} \frac{dA}{dy} - \frac{3A^2}{K^4} \frac{dK}{dy} \right] \quad \ldots \ldots \ldots \ldots \ldots \ldots \quad (24)$$

Noting that $da_i/dy = t_i$, $dA/dy = T$, and $dK/dy = \Sigma_i (dk_i/dy)$, the following is obtained:

$$\frac{d\alpha}{dy} = \frac{A^2}{K^3} \sum_i \left[3 \left(\frac{k_i}{a_i} \right)^2 \frac{dk_i}{dy} - 2t_i \left(\frac{k_i}{a_i} \right)^3 \right]$$

$$+ \sum_i \left(\frac{k_i^3}{a_i^2} \right) \left[\frac{2AT}{K^3} - \frac{3A^2}{K^4} \sum_i \left(\frac{dk_i}{dy} \right) \right] \quad \ldots \ldots \ldots \ldots \ldots \quad (25)$$

Evaluate dk_i/dy by writing Eq. 7 as

$$k_i = \left(\frac{1.49}{n_i} \right) \frac{a_i^{5/3}}{p_i^{2/3}} \quad \ldots \ldots \ldots \ldots \ldots \ldots \ldots \ldots \ldots \ldots \ldots \ldots \quad (26)$$

and differentiate with respect to y to obtain

$$\frac{dk_i}{dy} = \left(\frac{1.49}{n_i} \right) \left[\frac{5}{3} \left(\frac{a_i}{p_i} \right)^{2/3} \frac{da_i}{dy} - \frac{2}{3} \left(\frac{a_i}{p_i} \right)^{5/3} \frac{dp_i}{dy} \right] \quad \ldots \ldots \ldots \ldots \quad (27)$$

Again noting that $da_i/dy = t_i$, and multiplying and dividing by a_i, the following is obtained:

$$\frac{dk_i}{dy} = \frac{1}{3} \left(\frac{k_i}{a_i} \right) \left[5t_i - 2r_i \frac{dp_i}{dy} \right] \quad \ldots \ldots \ldots \ldots \ldots \ldots \ldots \quad (28)$$

Substituting Eq. 28 into Eq. 25 and simplifying, results in Eq. 11.

Appendix II.—References

1. Bakhmeteff, B. A., *Hydraulics of Open Channels*, McGraw-Hill Book Co., Inc., New York, N.Y., 1932.
2. Blalock, M. E., "Minimum Specific Energy in Open Channels of Compound Section," thesis presented to the Georgia Institute of Technology at Atlanta Ga., in June, 1980,

in partial fulfillment of the requirements for the degree of Master of Science in Civil Engineering.
3. Chow, V. T., *Open Channel Hydraulics*, McGraw-Hill Book Co., Inc., New York, N.Y., 1959.
4. Eichert, B. S., "Critical Water Surface by Minimum Specific Energy Using the Parabolic Method," United States Army Corps of Engineers, Hydrologic Engineering Center, Sacramento, Calif.
5. "HEC-2: Water Surface Profile Users Manual with Supplement," United States Army Corps of Engineers, Hydrologic Engineering Center, Davis, Calif., Nov., 1976.
6. Henderson, F. M., *Open Channel Flow*, The Macmillan Co., New York, N.Y., 1969.
7. Hulsing, H., Smith, W., and Cobb, E. D., "Velocity Head Coefficients in Open Channels," *U.S. Geological Survey Water Supply Paper 1869-C*, USGS, Washington, D.C., 1966.
8. Myers, B. C., and Elsawy, E. M., "Boundary Shear in Channel With Flood Plain," *Journal of the Hydraulics Division*, ASCE, Vol. 101, No. HY7, Proc. Paper 11452, July, 1975, pp. 933–946.
9. Petryk, S., and Grant, E. U., "Critical Flow in Rivers with Flood Plains," *Journal of the Hydraulics Division*, ASCE, Vol. 104, No. HY5, Proc. Paper 13733, May, 1978, pp. 583–594.
10. Prasad, R., "Numerical Method of Computing Flow Profiles," *Journal of the Hydraulics Division*, ASCE, Vol. 96, No. HY1, Proc. Paper 7005, Jan., 1970, pp. 75–86.
11. Rajaratnam, N., and Ahmadi, R. M., "Interaction Between Main Channel and Flood Plain Flows," *Journal of the Hydraulics Division*, ASCE, Vol. 105, No. HY5, Proc. Paper 14591, May, 1979, pp. 573–588.
12. Shearman, J. O., "Computer Applications for Step-Backwater and Floodway Analysis," *U.S. Geological Survey Open File Report 76-499*, USGS, Washington, D.C., 1976. 1976.
13. Thomas, W. A., "Water Surface Profiles," *Hydrologic Engineering Methods for Water Resources Development*, Vol. 6, United States Army Corps of Engineers, Hydrologic Engineering Center, Davis, Calif., July, 1975.
14. Tracy, H. J., and Lester, C. M., "Resistance Coefficients and Velocity Distribution, Smooth Rectangular Channel," *U.S. Geological Survey Water Supply Paper 1592-A*, USGS, Washington, D.C., 1961.
15. Wright, R. R., and Carstens, M. R., "Linear Momentum Flux to Overbank Sections," *Journal of the Hydraulics Division*, ASCE, Vol. 96, No. HY9, Proc. Paper 7517, Sept., 1970, pp. 1781–1793.
16. "WSP-2 Computer Program," *Technical Release No. 61*, Engineering Division, Soil Conservation Service, Washington, D.C., May, 1976.
17. Yen, B. C., "Open-Channel Flow Equations Revisited," *Journal of the Engineering Mechanics Division*, ASCE, Vol. 99, No. EM5, Proc. Paper 10073, Oct., 1973, pp. 979–1009.

Appendix III.—Notation

The following symbols are used in this paper:

A = total cross-section area;
a_i = subsection area;
E = specific energy;
F = Froude number;
F_c = compound-channel Froude number;
F_i = subsection Froude number;
F_r = weighted Froude number;
F_α = Froude number with kinetic energy flux correction;
f = Darcy-Weisbach friction factor;
f_i = subsection friction factors;

g = acceleration of gravity;
K = total cross-section conveyance;
k_i = subsection conveyance;
n = Manning's n value;
n_i = subsection n value;
p_i = subsection wetted perimeter;
Q = total cross-section discharge;
Q_m = average measured discharge;
q_i = subsection discharge;
R = Reynolds number;
r_i = subsection hydraulic radius;
S_e = slope of energy grade line;
S_0 = bed slope of channel or flume;
T = total cross-section top width;
t_i = subsection top width;
V = total cross-section mean velocity;
v = mean velocity associated with incremental area, dA;
v_i = subsection mean velocity;
x = distance along channel;
y = depth of flow;
α = kinetic energy flux correction coefficient;
Δp = increment of wetted perimeter;
Δy = increment of depth; and
$\sigma_1, \sigma_2, \sigma_3$ = subsection parameters of compound-channel Froude number.

DIFFUSION-WAVE FLOOD ROUTING IN CHANNEL NETWORKS

By Ali Osman Akan[1] and Ben Chie Yen,[2] F. ASCE

INTRODUCTION

For subcritical flow in an open-channel network, mutual backwater effects exist among the channel branches joining at a junction. Therefore, the branches cannot be treated individually when a dynamic wave model (4,10) is adopted to route floods in an open-channel network. Ideally, the entire network should be considered as a single unit and the flow in all the channels and junctions should be solved simultaneously. However, for a network consisting of more than a few channels, this approach requires an excessive amount of computer storage and expense.

In the sequential type models (3,6) traditionally employed for routing floods through a channel network, the difficulty caused by the mutual backwater effect of channels does not arise because the backwater effect from downstream is ignored. The routing starts from the most upstream channels and is carried towards downstream, channel by channel in sequence, satisfying the flow continuity requirement at junctions. The downstream boundary condition of a channel required in the computations is treated somewhat casually since it actually is unknown at the time of seeking a solution. However, Sevük and the second writer (8), and the writers (11) have shown that sequential models give unrealistic solutions when the downstream backwater effect is significant.

In order to reduce the high computer cost and storage requirements in solving large network problems, a successive decomposition technique called the overlapping-segment scheme has been employed in routing floods through channel networks (7,11). An example is given in Fig. 1. Solution is sought separately and successively for each individual segment which consists of one junction and the channels joining it. Consequently, the computer storage requirement is substantially decreased. When the Saint Venant equations, together with the junction continuity and dynamic equations are employed to describe the flow, the coefficient matrix involved in the solution process is not banded and therefore the matrix solution technique is not most efficient.

[1]Asst. Prof. of Civ. Engrg., Middle East Technical Univ., Ankara, Turkey.
[2]Prof. of Civ. Engrg., Univ. of Illinois at Urbana-Champaign, Urbana, Ill. 61801.

Note.—Discussion open until November 1, 1981. To extend the closing date one month, a written request must be filed with the Manager of Technical and Professional Publications, ASCE. Manuscript was submitted for review for possible publication on July 22, 1980. This paper is part of the Journal of the Hydraulics Division, Proceedings of the American Society of Civil Engineers, ©ASCE, Vol. 107, No. HY6, June, 1981. ISSN 0044-796X/81/0006-0719/$01.00.

Another avenue to reduce the computational costs in flow routing is to use an approximation to the Saint-Venant equations (dynamic wave) instead of the complete equations. It is well-known that only approximations of the level of diffusion wave model or higher can account for the downstream backwater effect whereas the kinematic wave models cannot (10). Ponce, et al. (5) investigated the conditions under which the diffusion wave can be a good approximation of the dynamic wave model.

In this paper, a nonlinear diffusion wave model to simulate the unsteady flow in a dentritic network accounting for the downstream backwater effect is presented. The overlapping-segment technique is applied to the diffusion wave equations which are written in finite differences. The resulting set of nonlinear algebraic equations for each segment is solved by using the Newton iteration method. The coefficient matrices obtained in the solution process are banded and, therefore, the matrix equations are solved by a very efficient numerical

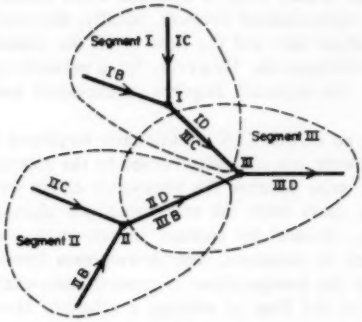

FIG. 1.—Overlapping Segments

technique. The results of the proposed model compare favorably to those of a complete dynamic wave and of a kinematic wave model.

Unsteady Flow Equations

Gradually varied unsteady flow in open channels is mathematically described by a set of one-dimensional shallow water equations commonly known as the Saint-Venant equations. In a gravity-oriented coordinate system, these equations are written as (9,10)

$$\frac{\partial A}{\partial t} + \frac{\partial Q}{\partial x} = 0 \quad \ldots\ldots\ldots\ldots\ldots\ldots\ldots\ldots\ldots\ldots\ldots\ldots\ldots\ldots\ldots\ldots (1)$$

$$\frac{\partial Q}{\partial t} + \frac{\partial}{\partial x}\left(\beta \frac{Q^2}{A}\right) + gA\left(\frac{\partial h}{\partial x} + S_f\right) = 0 \quad \ldots\ldots\ldots\ldots\ldots\ldots\ldots\ldots\ldots\ldots (2)$$

in which x = distance measured horizontally along the channel; A = flow cross-sectional area measured normal to x; Q = discharge through A; h = water surface elevation measured vertically from a horizontal datum; β =

momentum correction coefficient; g = gravitational acceleration; S_f = friction slope; and t = time. For practical purposes, β is usually taken as unity. The friction slope S_f for turbulent flow can be estimated by using Manning's formula

$$S_f = \frac{n^2 Q|Q|}{K^2 A^2 R^{4/3}} \quad \text{(3)}$$

in which n = the Manning roughness factor; R = hydraulic radius; and the constant K = 1 for *SI* units and 1.486 for U.S. Customary units. Alternatively, other friction formulas such as Darcy-Weisbach's or Chezy's may also be used.

Hydraulic conditions at a junction may be described by the continuity equation

$$\Sigma Q_k = Q_o + \frac{ds}{dt} \quad \text{(4)}$$

and the dynamic equation

$$h_k + \frac{V_k^2}{2g} - H_k = h_o + \frac{V_o^2}{2g} \quad \text{(5)}$$

in which s = the storage within the junction; H = head loss through the junction; and V = flow velocity. The subscript k stands for any one of the in-flowing channels and o represents the out-flowing channel. Other symbols are as previously defined.

Junctions have small storage volumes in most open-channel networks for which the term ds/dt in Eq. 4 is negligible. Thus, one can write

$$\Sigma Q_k = Q_o \quad \text{(6)}$$

Also, when the flows in all the branches joining at a junction are subcritical, Eq. 5 can be approximated by a kinematic compatibility condition as

$$h_k = h_o \quad \text{(7)}$$

Description of Proposed Diffusion-Wave Model

Diffusion Wave Equations.—In the diffusion wave approximation of the Saint-Venant equations, the local and convective acceleration terms in the momentum equation (i.e., the first two terms in Eq. 2) are neglected (10). Thus, Eq. 2 is simplified as

$$S_f = -\frac{\partial h}{\partial x} \quad \text{(8)}$$

Combining Eqs. 3 and 8 yields

$$Q = \frac{K}{n} A R^{2/3} \frac{-\dfrac{\partial h}{\partial x}}{\left|\dfrac{\partial h}{\partial x}\right|^{1/2}} \quad \text{(9)}$$

which may account for flows in both positive and negative x directions.

Finite Difference Equations.—Consider a Y-segment shown in Fig. 2 as an example. At the Y-junction, B and C are the two incoming channels and D is the outflowing channel. These channels are subdivided by M, L, and N cross sections, respectively, for the branches B, C, and D, into $M - 1$, $L - 1$, and $N - 1$ computational reaches. Numerical solutions are sought at the flow cross sections. Although the reach length, Δx, is allowed to vary in the model, it is treated here as a constant for a channel for simplicity.

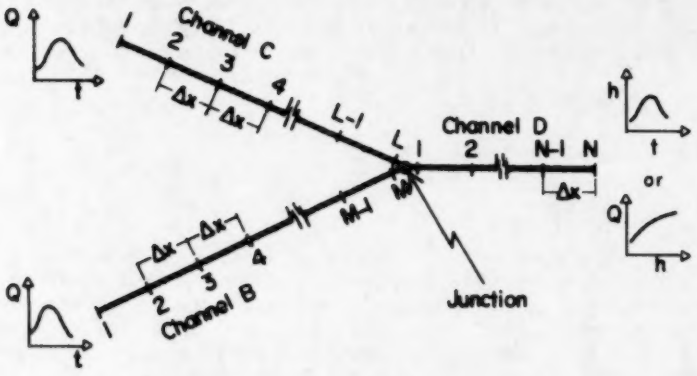

FIG. 2.—Discretization of a Y-Segment

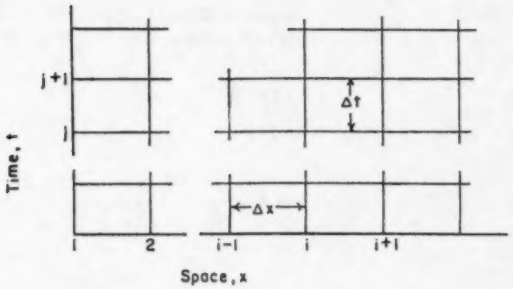

FIG. 3.—Computational Grid

Inflow discharge hydrographs at the upstream end of channels B and C are given as the upstream boundary conditions. In other words, $Q_{B,1}$ and $Q_{C,1}$ are prescribed functions of time where the first subscript denotes the channel and the second subscript stands for the flow section considered. A downstream boundary condition for channel D must also be known. This condition can be prescribed as a stage hydrograph or a stage-discharge relationship.

With reference to Fig. 3, Eq. 1 is written in finite difference quotients for a reach in Channel B as

$$\frac{A^{j+1}_{B,i+1} + A^{j+1}_{B,i} - A^{j}_{B,i+1} - A^{j}_{B,i}}{2\Delta t} + \frac{Q^{j+1}_{B,i+1} - Q^{j+1}_{B,i}}{\Delta x} = 0. \quad \ldots\ldots\ldots\ldots \quad (10)$$

in which $i = 1, 2, \ldots, M - 1$. In Eq. 10, the superscript $j + 1$ = the time stage at which solutions are sought; and j = the previous time stage at which solutions are already known. The time increment between the two stages is denoted by Δt. The unknown terms in Eq. 10 are those containing the superscript $j + 1$ except for $Q^{j+1}_{B,1}$ which is specified as the upstream boundary condition. The discharge, Q, at an interior flow section is computed by using Eq. 9 which is written in finite difference form as

$$Q^{j+1}_{B,i+1} = \frac{K}{n_{B,i+1}} A^{j+1}_{B,i+1} (R^{j+1}_{B,i+1})^{2/3} \frac{\dfrac{h^{j+1}_{B,i+1} - h^{j+1}_{B,i}}{\Delta x}}{\left| \dfrac{h^{j+1}_{B,i+1} - h^{j+1}_{B,i}}{\Delta x} \right|^{1/2}} \quad \ldots\ldots\ldots\ldots \quad (11)$$

Since the flow area A and the hydraulic radius R are known functions of the water surface elevation h, substituting Eq. 11 into Eq. 10 for $i = 1, 2, \ldots, M - 1$, yields a set of $M - 1$ equations with M unknowns in the form of

$$f_{B,i}(h^{j+1}_{B,i-1}, h^{j+1}_{B,i}, h^{j+1}_{B,i+1}) = 0; \quad i = 1, 2, \ldots, \mathrm{M} - 1 \quad \ldots\ldots\ldots\ldots \quad (12)$$

in which $h^{j+1}_{B,i}$ for $i = 1, 2, \ldots, M$ are the unknowns.

Similarly, for channel C, a set of $L - 1$ equations with L unknowns are obtained as

$$f_{C,i}(h^{j+1}_{C,i-1}, h^{j+1}_{C,i}, h^{j+1}_{C,i+1}) = 0; \quad i = 1, 2, \ldots, L - 1 \quad \ldots\ldots\ldots\ldots \quad (13)$$

For channel D a set of N $-$ 2 finite difference equations with N unknowns for the interior flow sections is

$$f_{D,i}(h^{j+1}_{D,i-1}, h^{j+1}_{D,i}, h^{j+1}_{D,i+1}) = 0; \quad i = 2, 3, \ldots, N - 1 \quad \ldots\ldots\ldots\ldots \quad (14)$$

The downstream boundary condition for channel D is expressed as

$$f_{D,N}(h^{j+1}_{D,N}) = 0 \quad \ldots\ldots\ldots\ldots \quad (15)$$

Eqs. 12–15 together provide a total of $M + N + L - 3$ equations with $M + N + L$ unknowns. Additional three equations are obtained from the junction conditions. For the Y-junction being considered, Eq. 6 becomes

$$Q^{j+1}_{D,1} = Q^{j+1}_{B,M} + Q^{j+1}_{C,L} \quad \ldots\ldots\ldots\ldots \quad (16)$$

Also, Eq. 7 written separately for branches B and C yields

$$h^{j+1}_{B,M} = h^{j+1}_{D,1} \quad \ldots\ldots\ldots\ldots \quad (17)$$

$$h^{j+1}_{C,L} = h^{j+1}_{D,1} \quad \ldots\ldots\ldots\ldots \quad (18)$$

Making use of Eq. 11 and the cross-sectional geometry of the channels, Eqs. 16–18 are expressed as

$$f_{D,1}(h^{j+1}_{D,1}, h^{j+1}_{B,M}, h^{j+1}_{C,L}) = 0 \quad \ldots\ldots\ldots\ldots \quad (19)$$

$$f_{B,M}(h^{j+1}_{D,1}, h^{j+1}_{B,M}) = 0 \quad \ldots\ldots\ldots\ldots \quad (20)$$

$$f_{C,L}(h^{j+1}_{D,1}, h^{j+1}_{C,L}) = 0 \quad \ldots\ldots\ldots\ldots \quad (21)$$

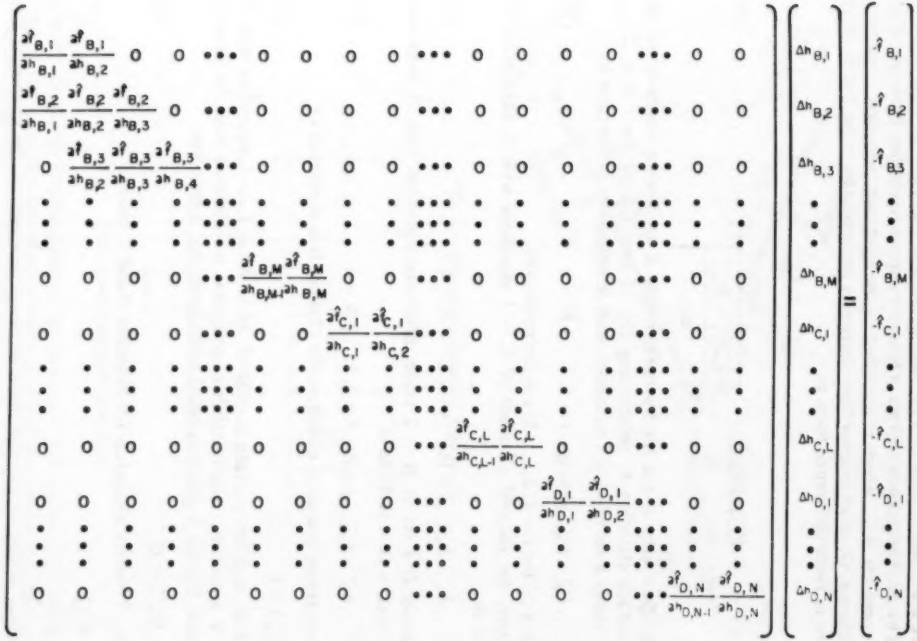

FIG. 4.—Matrix Equation Solved in Each Iteration Cycle

Solution Technique for Finite Difference Equations.—The Newton iteration method is employed for the solution of the simultaneous nonlinear finite difference equations. The procedure can be summarized as follows:

1. A set of trial values, $\hat{h}^{j+1}$, are assigned to the unknowns h^{j+1}.
2. Substituting $\hat{h}^{j+1}$ into Eqs. 12–15 and Eqs. 19–21, $\hat{f}$ values are computed.
3. Partial derivatives of the functions f appearing in Eqs. 12–15 and Eqs. 19–21 with respect to h^{j+1} are taken and evaluated by using $\hat{h}^{j+1}$ to yield $\partial \hat{f} / \partial h^{j+1}$.
4. The matrix equation shown in Fig. 4 is obtained using the values of $\hat{f}$ and $\partial \hat{f} / \partial h^{j+1}$. The superscripts $j + 1$ are not shown in Fig. 4 for the sake of clarity. It should be noted that the variables, $h'^{j+1}_{B,M}$ and $h'^{j+1}_{C,L}$, in Eq. 19, and the variable, $h'^{j+1}_{D,1}$, in Eqs. 20 and 21 are treated as constants assuming their values as obtained at the previous iteration cycle while computing the partial derivatives of the functions $f_{D,1}$, $f_{B,M}$, and $f_{C,L}$. Only with this approximation can a banded coefficient matrix be obtained in Fig. 4.
5. The matrix equation of Fig. 4 is solved for the corrections Δh. If the magnitudes of these corrections are within tolerable limits for all the flow sections, the trial values $\hat{h}$ are accepted. Otherwise, the trial values are improved as $\hat{h} = \hat{h} + \Delta h$ for all the flow sections, and a new iteration cycle is initiated.

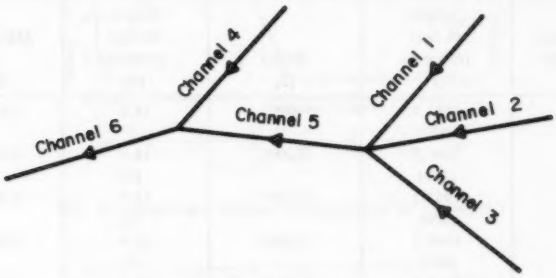

FIG. 5.—Hypothetical Network Used in Examples I and II

It should be noted that the coefficient matrix in Fig. 4 is banded with at most three nonzero elements on the diagonal. This allows a very efficient solution procedure which has been described elsewhere (1) in detail and will not be repeated here.

Overlapping-Segment Approach.—When flow in a channel network containing more than one junction is to be simulated, the proposed model employs an overlapping-segment technique as mentioned in the "Introduction." As shown in Fig. 1, the network is assumed to be composed of a number of segments each containing only one junction. The outflowing channel of a segment is also an in-flowing channel of the immediate following segment. For instance, in Fig. 1 the out-flowing channel ID of segment I serves also as the inflowing channel IIIC for segment III.

Each segment is treated as a separate unit in the computation. Computations

start from upstream segments and progress towards downstream. For example, in Fig. 1, first, segments I and II are considered separately with the downstream boundary conditions for channels ID and IID assumed to be approaching the normal flow for a long channel. Finite difference equations for each of these two segments are obtained and solved respectively in a manner similar to those previously described for the simple Y-segment of Fig. 2. The only exception is that Eq. 15 is replaced by a uniform flow equation corresponding to the assumed downstream boundary condition. Solutions obtained are assumed valid for channels IB, IC, IIB, and IIC. However, solutions for flow in channels ID and IID are discarded and then recomputed as channels IIIC and IIIB in segment III. Naturally, the algebraic sum of outflows from channels IB and IC at each time level constitutes the upstream inflow for channel ID (IIIC). Similarly, the sum of outflows from IIB and IIC gives the upstream boundary condition for IID (IIIB). Knowing the upstream inflows for channels IIIC and IIIB, computations are performed for segment III.

TABLE 1.—Properties of Example Open-Channel Network

Channel number (1)	Length, in feet (meters) (2)	Slope (3)	Width, in feet (meters) (4)	Manning n (5)
1	1968.5 (600)	0.0005	16.4 (5)	0.0138
2	1968.5 (600)	0.0005	16.4 (5)	0.0207
3	1968.5 (600)	0.0005	16.4 (5)	0.0207
4	1968.5 (600)	0.0005	16.4 (5)	0.0138
5	1968.5 (600)	0.0010	26.2 (8)	0.0141
6	1968.5 (600)	0.0010	32.8 (10)	0.0125

The single overlapping scheme just described may not be sufficiently accurate if the downstream backwater effect is serious and significant backwater propagates beyond one upstream channel. In this case a double overlapping scheme may be adopted.

Comparison with Other Methods

In order to test the validity of the proposed diffusion wave model for simulation of flow in open-channel networks, comparisons with two other methods, namely, a dynamic wave and a kinematic wave models, have been made. The two models are briefly described as follows.

Implicit Nonlinear Dynamic Wave Model.—A four-point fully implicit scheme which is adopted in this study for dynamic-wave routing is a modified version of that proposed by Baltzer and Lai (2) to incorporate the simultaneous solutions

of the Saint-Venant and the junction equations. In this scheme, the finite difference quotients for a reach between flow sections i and $i + 1$ are written as

$$F_{i+0.5} \approx \frac{1}{2}(F_i^{j+1} + F_{i+1}^{j+1}) \quad \text{(22)}$$

$$\left(\frac{\partial F}{\partial x}\right)_{i+0.5} \approx \frac{1}{\Delta x}(F_{i+1}^{j+1} - F_i^{j+1}) \quad \text{(23)}$$

$$\left(\frac{\partial F}{\partial t}\right)_{i+0.5} \approx \frac{1}{2\Delta t}(F_{i+1}^{j+1} + F_i^{j+1} - F_{i+1}^{j} - F_i^{j}) \quad \text{(24)}$$

in which F = any reach function. The set of finite difference equations obtained

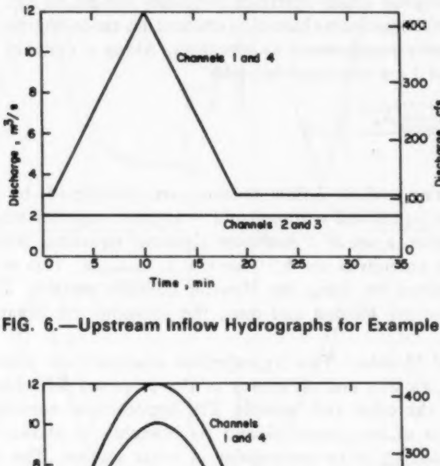

FIG. 6.—Upstream Inflow Hydrographs for Example I

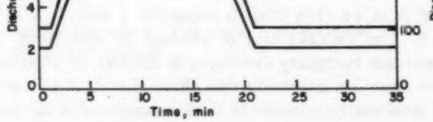

FIG. 7.—Upstream Inflow Hydrographs for Example II

by substituting Eqs. 22–24 into Eqs. 1 and 2 contains two unknowns, namely h_i^{j+1} and Q_i^{j+1}, for each flow section i along a channel. When a simple channel network composed of three junctions and seven branches as shown in Fig. 1 is considered, at each time step, the finite difference forms of Eqs. 1 and 2 provide 14(J − 1) nonlinear equations with $14J$ unknowns if the number

of flow sections selected along each channel is J. The additional 14 equations necessary for solving the problem are provided by four upstream boundary conditions for channels IB, IC, IIB, and IIC, one downstream boundary condition for channel IIID, and nine junction equations, namely, Eqs. 6 and 7 applied to junctions I, II, and III. The solution is obtained by using the Newton iteration technique. The coefficient matrix obtained in each iteration cycle has a rank of $14J \times 14J$, and it is not banded. This makes the solution difficult and costly for small networks like that in Fig. 1 and unmanageable for larger systems.

Nonlinear Kinematic Wave Model.—In the kinematic-wave approximation, the inertia as well as pressure terms of the momentum equation (Eq. 2) are neglected and thus, the friction slope, S_f, is approximated by the bottom slope, S_b, of the channel (10). The downstream backwater effects of channels are neglected and each channel is treated individually. Computations start from the most upstream channels for which upstream boundary conditions are specified, and progress towards downstream channel by channel in a cascading manner, satisfying the flow continuity requirement at junctions. Along a channel reach with $S_f = S_b$, Eqs. 1 and 3 are combined to yield

$$\frac{\partial A}{\partial t} + \frac{\partial}{\partial x}\left(K A R^{2/3} \frac{S_b^{1/2}}{n}\right) = 0 \quad \ldots \ldots \ldots \ldots \ldots \ldots \ldots \ldots \ldots \ldots \quad (25)$$

For a channel along which J flow sections are considered, by applying Eqs. 22, 23, and 24 to Eq. 25 and writing for $(J - 1)$ grids, together with an upstream boundary condition, a set of J nonlinear algebraic equations with J unknowns is obtained. The unknowns are h_i^{t+1} for $i = 1, 2, \ldots, J$. This set of nonlinear equations are solved by using the Newton iteration method. The coefficient matrices involved are banded and thus, the solutions are obtained in a very efficient manner.

Comparison of Models.—Two hypothetical examples are presented here to demonstrate the validity and efficiency of the proposed diffusion wave model as compared to the other two models. The hypothetical network used in the examples consists of two junctions and six branches as shown in Fig. 5. All branches are assumed to be rectangular in cross section. The dimensions of the channels are listed in Table 1. The hypothetical floods that are routed through the network in the two examples are shown in Figs. 6 and 7, respectively. The initial condition for both examples is a steady flow condition corresponding to a discharge of 3 m^3/s (106 cfs) in channels 1 and 4, 2 m^3/s (71 cfs) in channels 2 and 3, 7 m^3/s (247 cfs) in channel 5, and 10 m^3/s (353 cfs) in channel 6. Downstream boundary condition at the exit of channel 6 is specified as a uniform flow equation assuming this channel is hydraulically long. A time increment of $\Delta t = 60$ sec is selected in both examples for all the three models. A constant reach length of $\Delta x = 60$ m (196.9 ft) is adopted for the diffusion and dynamic-wave models. The reach length is reduced to $\Delta x = 30$ m (98.4 ft) in the kinematic-wave model since numerical convergence could not be achieved with $\Delta x = 60$ m (196.9 ft).

The computed discharge hydrographs using the three models are shown in Figs. 8 and 9, respectively, for Examples I and II. As can be observed from these figures, the results of the proposed diffusion-wave model are in good agreement with those of the dynamic wave model. Conversely, the kinematic

wave solutions are not as reliable. The outflow hydrographs computed for channels 2 and 3 in Example I and shown in Fig. 8(*b*) clearly demonstrate the downstream backwater effects. In Example I, a constant upstream inflow of 2 m^3/s (71 cfs) equal to the base flow rate is adopted for channels 2 and 3 as shown in Fig. 6. Thus, a steady flow condition would prevail in both channels 2 and 3 if the time variant backwater effects of the other channels in the network did not exist. Indeed, the kinematic wave method which ignores the backwater effects from downstream predicts a steady flow in these two branches as shown

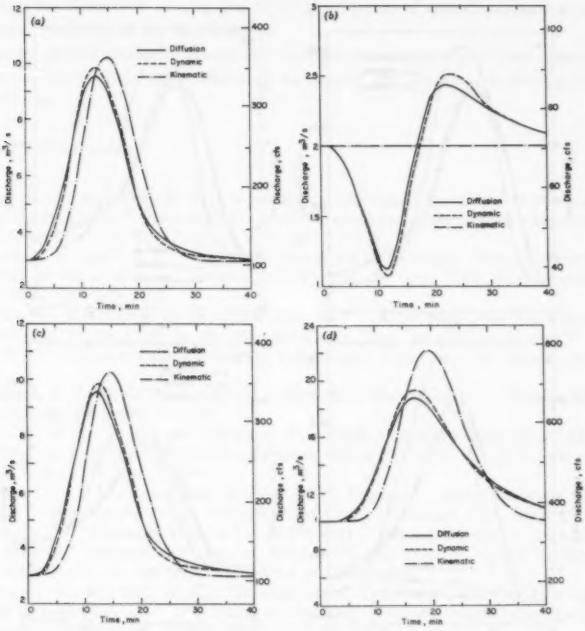

FIG. 8.—Comparison of Results of Example I: (*a*) Channel 1; (*b*) Channels 2 and 3; (*c*) Channel 4; and (*d*) Channel 6

in Fig. 8(*b*). However, in actuality, the flood wave travelling through channel 1 raises the water surface at the junction where branches 1, 2, and 3 join. This decreases the hydraulic gradient in channels 2 and 3 causing discharges lower than the constant upstream inflow and base flow rate. Naturally, from continuity requirements, the channel storage is increased during the period of low discharges. As the downstream backwater recedes with time, the excess water is released from the channel storage, and discharges higher than the constant inflow rate occur until steady state condition is again reached asymptotically. As shown in Fig. 8(*b*), this phenomena is satisfactorily simulated by both the

dynamic wave and proposed diffusion wave models but ignored completely in the kinematic wave model.

The computations for the two examples presented here was performed on an IBM 370/145 computer at the Middle East Technical University. For each one of the examples, the execution time was approx 90 sec, 150 sec, and 480 sec, respectively, for the diffusion, kinematic, and dynamic wave models. These values are presented merely as a reference. The noticeably different execution times for the kinematic and the diffusion wave models are partly due to a smaller computation grid adopted in the former, and partly due to faster

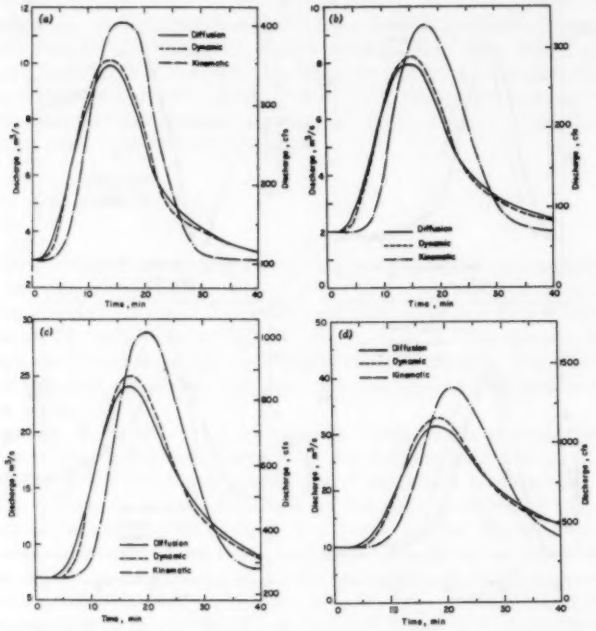

FIG. 9.—Comparison of Results of Example II: (*a*) Channel 1; (*b*) Channels 2 and 3; (*c*) Channel 5; and (*d*) Channel 6

convergence of numerical results in the latter model. The difference in computer execution times for these two models is smaller for other examples (not reported here) having identical grid sizes and numerical schemes which show consistently shorter execution time for the proposed diffusion wave model than the nonlinear kinematic wave model. The difference in the execution times for the diffusion and the dynamic wave models arises from faster convergence of the former and the difference in the structures of the two models and is expected to increase exponentially with increasing size of the network considered.

Conclusions

A nonlinear diffusion wave model for flood routing in dentritic-type open-channel networks is developed and presented in this study. Comparison of this model with dynamic wave and nonlinear kinematic wave models leads to the following conclusions:

1. The proposed diffusion-wave model can satisfactorily simulate the mutual backwater effects of channels joining at a junction.
2. The proposed model is nearly as accurate as the dynamic wave model which may be classified among the most sophisticated one-dimensional routing techniques available in the literature.
3. The proposed model is faster and cheaper in computation than a kinematic wave model which may be considered as one of the simplest hydraulic routing models known.

Appendix I.—References

1. Akan, A. O., and Yen, B. C., "A Nonlinear Diffusion-Wave Model for Unsteady Open-channel Flow," *Proceedings of the 17th Congress*, International Association for Hydraulic Research, Vol. 2, Aug., 1977, pp. 181–190.
2. Baltzer, R. A., and Lai, C., "Computer Simulation of Unsteady Flows in Waterways," *Journal of the Hydraulics Division*, ASCE, Vol. 94, No. HY4, Proc. Paper 6048, July, 1968, pp. 1083–1117.
3. Bowers, C. E., Harris, G. S., and Pabst, A. F., "The Real-Time Computation of Runoff and Storm Flow in the Minneapolis-St. Paul Interceptor Sewers," *Memo. M-118*, St. Anthony Falls Hydraulics Laboratory, University, of Minnesota, Dec., 1968.
4. Dronkers, J. J., *Tidal Hydraulics*, North-Holland Publishing Co., Amsterdam, The Netherlands, 1964, pp. 203–204.
5. Ponce, V. M., Li, R.-M., and Simons, D. B., "Applicability of Kinematic and Diffusion Models," *Journal of the Hydraulics Division*, ASCE, Vol. 104, No. HY3, Proc. Paper 13635, Mar., 1978, pp. 353–360.
6. Schaake, J. C., Jr., "Synthesis of the Inlet Hydrograph," *Storm Drainage Research Project Technology Report 3*, Johns Hopkins Univ., Baltimore, Md., June, 1965.
7. Sevük, A. S., "Unsteady Flow in Sewer Network," thesis presented to the University of Illinois at Urbana-Champaign, at Urbana, Ill., in 1973, in partial fulfillment of the requirements for the degree of Doctor of Philosophy.
8. Sevük, A. S., and Yen, B. C., "Comparison of Four Approaches in Routing Flood Wave through Junction," *Proceeding of the 15-th Congress*, International Association for Hydraulic Research, Vol. 5, Sept., 1973, pp. 169–172.
9. Yen, B. C., "Further Study on Open-Channel Flow Equations," *Sonderforschungsbereich 80 Publication No. SFB 80/T/49*, University of Karlsruhe, Karlsruhe, West Germany, Apr., 1975.
10. Yen, B. C., "Unsteady Flow Mathematical Modeling Techniques," *Modeling of Rivers*, H. W. Shen, ed., Chapter 13, Wiley-Interscience, Inc., New York, N.Y., 1979.
11. Yen, B. C., and Akan, A. O., "Flood Routing Through River Junctions," *Rivers '76*, Vol. I, ASCE, 1976, pp. 212–231.

Appendix II.—Notation

The following symbols are used in this paper:

A = flow cross-sectional area;
B = incoming channel;

C = incoming channel;
D = out-flowing channel;
F = any reach function;
f = function of flow parameters;
$\hat{f}$ = residual of function f;
g = gravitational acceleration;
H = head loss through junction;
h = water surface elevation;
$\hat{h}$ = initial guess for h;
$\hat{\hat{h}}$ = improved guess for h;
i = index for flow sections;
J = number of flow sections in a channel in dynamic- and kinematic-wave models;
j = index for time stage;
K = constant;
k = index for incoming channels;
L = number of flow cross sections along channel C;
M = number of flow cross sections along channel B;
N = number of flow cross sections along channel D;
n = Manning's roughness factor;
o = index for out-flowing channels;
Q = discharge;
R = hydraulic radius;
S_b = channel bottom slope;
S_f = friction slope;
s = storage in junction;
t = time;
V = cross-sectional averaged flow velocity;
x = horizontal distance;
Δh = correction on h;
Δt = time increment;
Δx = reach length; and
β = momentum correction coefficient.

STOCHASTIC MODELS OF SUSPENDED-SEDIMENT DISPERSION

By Carlos V. Alonso,[1] M. ASCE

INTRODUCTION

Considerable progress has been made in recent years in the analysis of dispersion of dissolved substances in turbulent streams (68), and of dispersion of discrete sediment particles moving slowly as bed load by rolling or sliding along the stream bed (71).

Between these two transport modes is the class of transport typified by the movement of discrete sediment particles carried mainly in suspension. Suspended particles follow the movement of the dispersive fluid, except that they tend to lag behind and settle under the influence of their own inertia and the gravitational pull. A sizable part of the sediment transported by natural streams is frequently carried in suspension and when in suspension moves at a rate quite close to the stream velocity. An accurate prediction of this suspended load is of utmost importance in many instances. This paper is solely concerned with the movement of sediment particles while carried in suspension.

Sediment particles being transported by a streamflow are suspended by turbulent fluctuations and further dispersed by mean-velocity gradients. In addition, the mean flow exhibits random characteristics due to the irregularities of the stream boundaries and the daily variations in the stream discharge. This behavior is reflected in the variability of the suspended load distribution (9). Therefore, the transport of suspended sediment can justifiably be regarded as an intrinsically random process. The conventional theories of suspended transport are, however, exclusively deterministic (33) and largely restricted to the condition of steady, uniform flow. This limitation prompted a number of investigators to use probabilistic methods in order to derive time and space distributions of suspended particles under more general conditions. Two distinct approaches developed independently over the years. One is based on the theories of turbulent diffusion by continuous movements, whereas, the other arose from the random walk theory of stochastic processes. Review of these theories' development and applications is the main objective of this paper.

[1]Research Hydr. Engr., U.S. Dept. of Agric. Science and Education Administration, Sedimentation Lab., P.O. Box 1157, Oxford, Miss. 38655.

Note.—Discussion open until November 1, 1981. To extend the closing date one month, a written request must be filed with the Manager of Technical and Professional Publications, ASCE. Manuscript was submitted for review for possible publication on September 5, 1980. This paper is part of the Journal of the Hydraulics Division, Proceedings of the American Society of Civil Engineers, ©ASCE, Vol. 107, No. HY6, June, 1981. ISSN 0044-796X/81/0006-0733/$01.00.

Evolution of Probabilistic Theories.—The theory of diffusion by continuous movements was originated by Taylor (79), who considered the Lagrangian history of a single fluid particle in a homogeneous isotropic turbulent flow. Subsequently, Richardson (65), Batchelor (4,5,6), Taylor (80), and others (29) evolved the original ideas into a more complete theory. Tchen (81) used this approach to study the diffusion of a rigid particle carried by a turbulent flow. In so doing he extended the equation of motion of submerged rigid particles developed by Basset (3), Boussinesq (10), and Oseen (58) (BBO equation). Corrsin and Lumley (22), among others, further developed Tchen's formulation. Because of the nonlinear nature of this equation, a solution is not readily obtainable. This led to many linearizing assumptions in subsequent efforts to solve the BBO equation (35,36,46,72,81). All these studies have introduced strong simplifications that rendered the solutions inapplicable. In other words, all these solutions suggest a diffusivity of the suspended particles equal to the diffusivity of the surrounding fluid, which is experimentally incorrect (41,75). Subsequent analyses by Friedlander (30), Csanady (23), and Peskin (61) introduced more realistic approximations and were able to show that the difference in diffusivities stems from the fact that, in general, the Lagrangian correlation of turbulent fluid velocities and the correlation of velocities experienced by the particles do not coincide. Peskin (61) went on to derive conditions under which the fluid and particle diffusivities may be taken to be the same. This criterion is significant in the experimental determination of sediment diffusion from measurements of turbulence characteristics (57).

The random walk concept was introduced by Pearson (60), although Rayleigh earlier considered a formally identical problem while studying the composition of vibrations of unit amplitude with phases distributed at random (64). This concept became the object of many investigations, which were later reviewed by Chandrasekhar (14) and Kac (39) among others. The random walk theory has been applied to the solution of diffusion problems in two distinct manners. The classical approach consisted in obtaining the solution of complex differential equations as the limiting solution of an equivalent discrete probabilistic process. The classical example is the solution of the Fokker-Planck diffusion equation, which is formally equivalent to the "second Kolmogorov equation" of the theory of random functions (31). The other approach is a direct simulation of the physical process by imitating the behavior of representative discrete particles through computer simulation. The effectiveness of this method was demonstrated by Bugliarello and Jackson (12,13), Sullivan (77), Chiu (16), Bayazit (8), Sumer (78), and Li and Shen (48).

This paper was written at the instance of the ASCE Task Committee on the State of the Art of Stochastic Hydraulics. It is intended as a review of some of the more significant findings that evolved from the above analyses, and presents some suggestions regarding their extension to complex problems of practical interest. The underlying theories are only briefly outlined. A detailed presentation can be found in the treatise by Monin and Yaglom (56).

Diffusion by Continuous Movements

Diffusion in Stationary Homogeneous Turbulent Flows.—Consider a set of discrete rigid particles diffusing in a statistically steady homogeneous turbulent

field without mean shear. The particles are all supposed to have the same settling velocity w and fill the volume V at time $t_0 = 0$ and at all subsequent times $t > t_0$ (Fig. 1). Assuming that the particles are initially distributed with a uniform concentration C_0, the problem is to find their concentration distribution at subsequent times. This problem is equivalent to determining the probability $P(\mathbf{x}, t)$ that a particle x lies within the space of volume $V(t)$, given that $P(\mathbf{x}_0, t_0)$ is the initial probability of the particle being within V at t_0 (4).

Assume that each particle is not influenced by the neighboring particles, that is, the distribution of its displacement is independent of the other particle

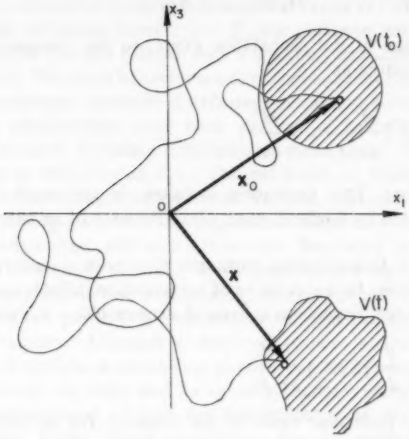

FIG. 1.—Motion of Suspended Particle

trajectories. If Q is the conditional probability of a particle displacement $\mathbf{x} - \mathbf{x}_0$ given its initial position at $\mathbf{x}_0$, then

$$P(\mathbf{x}, t) = \int_{-\infty}^{\infty}\int\int\int P(\mathbf{x}_0, t_0)\, Q(\mathbf{x} - \mathbf{x}_0 | \mathbf{x}_0)\, d\mathbf{x}_0 \quad \ldots\ldots\ldots\ldots\ldots\ldots (1)$$

in which the integration is over all space. This equation can also be written as the convolution

$$P(\mathbf{x}, t) = P(\mathbf{x}_0, t_0) * Q(\mathbf{x} - \mathbf{x}_0 | \mathbf{x}_0) \quad \ldots\ldots\ldots\ldots\ldots\ldots\ldots\ldots (2)$$

The Fourier transform of this convolution yields the following characteristic function of $P(\mathbf{x}, t)$:

$$C_x(\xi) = C_{x_0}(\xi) \cdot C_{x-x_0}(\xi) \quad \ldots\ldots\ldots\ldots\ldots\ldots\ldots\ldots\ldots (3)$$

Assume further that the probability distribution of the particle displacements is Gaussian with a nonzero mean given by $\mathbf{w}(t - t_0)$. The characteristic function for the displacement is then

$$C_{\mathbf{x}-\mathbf{x}_0}(\xi) = \exp\left\{ j\xi_3 \mathbf{w}t \frac{\xi_i \xi_j}{2} [X_i X_j] \right\} \quad \ldots\ldots\ldots\ldots\ldots\ldots\ldots\ldots (4)$$

in which $j = (-1)^{1/2}$, X_k is the kth component of the displacement $\mathbf{X} = \mathbf{x} - \mathbf{x}_0$, and $[\cdot]$ denotes an average over the ensemble of all particles. Eq. 4 is substituted into Eq. 3 and, after computing the inverse transform, the result is differentiated with respect to time. This yields

$$\frac{\partial}{\partial t} P(\mathbf{x}, t) = \frac{1}{2} \frac{d}{dt} [X_i X_j] \frac{\partial^2 P(\mathbf{x}, t)}{\partial x_i \partial x_j} + \mathbf{w} \frac{\partial}{\partial x_3} P(\mathbf{x}, t) \quad \ldots\ldots\ldots\ldots\ldots (5)$$

Noting the relation of the probability $P(\mathbf{x}, t)$ to the concentration at point $\mathbf{x}$, Eq. 5 can be rewritten as

$$\frac{\partial C}{\partial t} = \frac{1}{2} \frac{d}{dt} [X_i X_j] \frac{\partial^2 C}{\partial x_i x_j} + w \frac{\partial C}{\partial x_3} \quad \ldots\ldots\ldots\ldots\ldots\ldots\ldots\ldots (6)$$

in which $w = |\mathbf{w}|$. This derivation is based on the work of Batchelor (3), which was extended by Barfield, et al. (2) to the case of an external gravitational field.

Consider now a homogeneous turbulent flow with a uniform mean velocity U in the x_1 direction. In the absence of a gravitational field, a similar derivation assuming a Gaussian displacement around a mean $U(t - t_0)$ gives

$$\frac{\partial C}{\partial t} + U \frac{\partial C}{\partial x_1} = \frac{1}{2} \frac{d}{dt} [X_i X_j] \frac{\partial^2 C}{\partial x_i \partial x_j} \quad \ldots\ldots\ldots\ldots\ldots\ldots\ldots\ldots (7)$$

Eqs. 6 and 7 are particular cases of the equation for diffusion of suspended sediment that can be derived from the conservation of mass principle (70).

The time rate of change of the displacement covariance matrix appearing in Eqs. 6 and 7 can be written as (4,6)

$$\frac{d}{dt} [X_i X_j] = [X_i v_j] + [v_i X_j] = \int_0^t [v_i(\tau)\, v_j(t)]\, d\tau + \int_0^t [v_i(t)\, v_j(\tau)]\, d\tau$$

$$= [v_i^2 v_j^2]^{1/2} \int_0^t [R_{ij}(\tau) + R_{ji}(\tau)]\, d\tau \quad \ldots\ldots\ldots\ldots\ldots\ldots\ldots\ldots (8)$$

in which v = the instantaneous Lagrangian particle velocity; and $R_{ij}(\tau)$ = the particle Lagrangian velocity correlation tensor. Experience has shown that the Lagrangian correlation function of isotropic turbulent velocities has a shape similar to the Eulerian correlation function (35). Assuming that this holds true for the solid particle correlation and considering the turbulent motion to be isotropic, $R_{ij} = R_{ji} = R_{ii}$. In addition, $R_{ii} \cong 1$ for small diffusion times. Thus, integrating Eq. 8 twice results in the displacement variance

$$\sigma_X^2 = [X_i^2] = [v_i^2]\, t^2 \quad \ldots\ldots\ldots\ldots\ldots\ldots\ldots\ldots\ldots\ldots\ldots\ldots (9)$$

As the diffusion time increases, the integral in Eq. 8 approaches asymptotically the Lagrangian time integral scale

$$T_L = 2\int_0^\infty R_{ii}(\tau)\,d\tau \quad \ldots\ldots\ldots\ldots\ldots\ldots\ldots\ldots\ldots\ldots\ldots\ldots\ldots\ldots\ldots\ldots\ldots\ldots \quad (10)$$

and Eq. 8 yields in the limit

$$\sigma_X^2 = [X_i^2] = 2\,[v_i^2]\,T_L t \quad \ldots\ldots\ldots\ldots\ldots\ldots\ldots\ldots\ldots\ldots\ldots\ldots\ldots\ldots\ldots\ldots\ldots\ldots \quad (11)$$

$$\text{or} \quad \frac{[X_i^2]}{2D_P T_L} = \frac{t}{T_L} \quad \ldots\ldots\ldots\ldots\ldots\ldots\ldots\ldots\ldots\ldots\ldots\ldots\ldots\ldots\ldots\ldots\ldots\ldots \quad (12)$$

in which $D_P = [v_i^2]\,T_L$ is interpreted as a constant diffusion coefficient. Consequently, the variance of particle displacement varies as t^2 for small diffusion times, whereas for diffusion times $t >> T_L$ the variance varies linearly with time and the diffusion process follows Fick's law (i.e., diffusion with a constant transfer coefficient). The latter behavior is a direct consequence of having assumed the particle displacements normally distributed around the convective mean.

The preceding relationships have been derived to describe diffusion in a stationary, homogeneous turbulent field without mean shear. Thus, they would seem inapplicable to diffusion in open channel flows of finite cross sections. Moreover, in these cases the longitudinal differential convection combined with lateral turbulent mixing gives rise to longitudinal dispersion (27), usually more important than longitudinal diffusion. However, Batchelor and Townsend (7) pointed out that in steady, uniform flows confined by rigid boundaries the turbulence is homogeneous and nondecaying in the streamwise direction, and the velocity of a fluid particle is a stationary random function of time about the mean flow velocity. Although a confined stream is nonhomogeneous in the cross-stream direction, a wandering particle moves randomly towards one wall and then towards the other and its velocity becomes statistically stationary after a long enough period of time for the influence of the particle's initial position to vanish. Under these conditions, Eq. 12 applies to longitudinal dispersion in uniform shear flows. Taylor (80) observed that far enough downstream from the source the concentration gradients associated with the velocity shear would be balanced by the tendency of the lateral turbulent mixing to decrease those concentration gradients. He found that the spread of the cross-sectional mean value of concentration, relative to a coordinate system moving with the mean flow velocity, produces indeed an apparent Fickian diffusion along the channel axis. Elder (25) extended Taylor's asymptotic analysis to dispersion in an infinitely wide open channel. More recently Fischer (27) gave a method for applying Taylor's analysis to natural streams. Also, Fischer (28) noted that as far as Taylor's theory is concerned, stream curvature and nonuniformity can be tolerated if the reach is long enough, and provided that the nonuniformity is random in such a way that the Lagrangian velocity remains statistically stationary. The preceding observations support the applicability of Fickian diffusion theory in open channels for large dispersion times. This conclusion has been confirmed by a number of experimental investigations (26,57,70). They all restricted their measurements to the principal components of the diffusivity tensor which do not depend on the assumption of local isotropy. Some of the results of these investigations are summarized below.

Sayre and Chang (70) measured the longitudinal dispersion of suspended 15 μ–30 μ silt particles in a wide open-channel flow having an average velocity

of 0.35 m/s and a depth of 0.24 m. Concentration-versus-time distributions were measured at several dispersion distances by collecting samples in rapid succession as the dispersant passed a sampling station. The distributions measured at mid-depth do not differ significantly from the distributions measured at 1/4 and 3/4 of the flow depth because no appreciable settling occurred over the range of dispersion distances. As the diffusion time increases the concentration distributions approach a Gaussian shape, suggesting that the fine silt diffuses in accordance to the normality hypothesis. The time variances of these distributions, σ_t^2, are plotted against the travel distance, x_1, in Fig. 2. Although there is considerable scatter, the data tend to follow the linear relationship between σ_t^2 and x_1 derived by Yotsukura (Ref. 83; see also Eq. 11, Ref. 70) for one-dimensional Fickian diffusion in turbulent open channel flows:

$$\sigma_t^2 = \frac{2K_1x_1}{U^3} + \frac{8K_1^2}{U^4} \qquad (13)$$

Here K_1 ($\equiv D_p$) is a constant diffusion coefficient. The value of K_1 used in Fig. 3 was determined by Sayre and Chang (70) from dye dispersion experiments for the same flow conditions used in the silt dispersion studies.

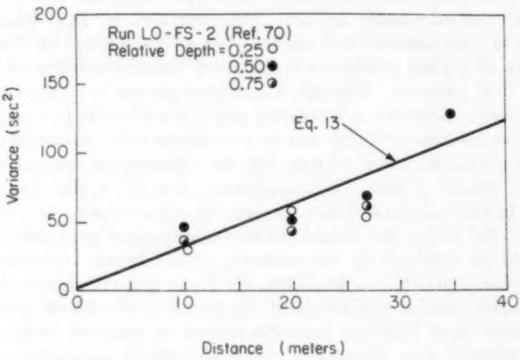

FIG. 2.—Time Variance as Function of Travel Distance (After Ref. 70)

Engelund (26) conducted dispersion experiments where he tracked the motion of discrete particles in a wide rectangular open channel flow 0.055 m deep with an average velocity of 0.30 m/s. Buoyant spheres 9 mm in diam were released on the free surface and their longitudinal, X_1, and lateral, X_2, displacements were measured at subsequent diffusion times. After repeating the experiments many times, he determined the variances of those displacements. The corresponding rms velocities and time integral scales were obtained from a set of turbulence measurements. The results, shown in Fig. 3 corroborate Eq. 12. The surface turbulence was found to be anisotropic, the longitudinal diffusion coefficient being nearly twice the lateral coefficient.

Eq. 12 describes the turbulent diffusion in terms of Lagrangian characteristics of a particle moving along its path. In practice, the Lagrangian characteristics are not easily obtainable and most of the information available consists of Eulerian descriptions. Thus, it is important to relate these two types of information in order to express the Eulerian results in Lagrangian form. In homogeneous, steady, turbulent flows, the Eulerian time-averaged turbulent velocity, $\overline{u^2}$, is commonly assumed to be equal to $[u^2]$. That is, sampling many different particles as they pass a fixed point is taken as equal to an instantaneous ensemble average of many point velocity traces. Lumley (50) presents formal arguments which validate the equivalence of these measurements under the restrictions of homogeneous, isotropic, and stationary turbulence.

The problem of estimating turbulent diffusivities from point measurements, therefore, becomes how to approximate the Lagrangian autocorrelation function

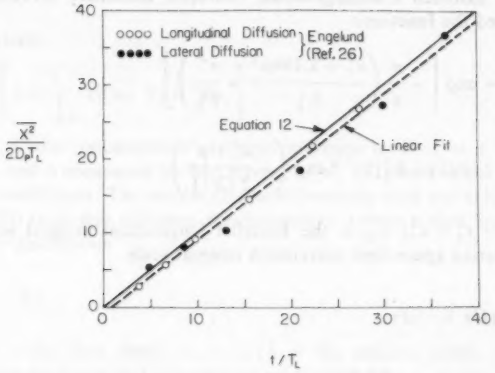

FIG. 3.—Displacement Variance as Function of Travel Time (After Ref. 26)

and its integral scale. Hay and Pasquill (34) proposed that the Eulerian autocorrelation might be transformed into the Lagrangian autocorrelation. That is:

$$R_E(0,0,0,\delta t) \cong R_L(t) \quad \ldots \ldots \ldots \ldots \ldots \ldots \ldots \ldots \ldots \ldots \ldots \quad (14)$$

Here δ is a dimensionless constant related to the time integral scale ratio

$$\delta = \frac{T_L}{T_E} \quad \ldots \ldots \ldots \ldots \ldots \ldots \ldots \ldots \ldots \ldots \ldots \ldots \ldots \quad (15)$$

in which T_E = the Eulerian time integral scale. Although subsequent work tended to support this approximation (73), it became apparent that δ was dependent on other turbulent characteristics (1), invalidating the empirical constant value, $\delta = 4$, proposed by Hay and Pasquill (34). Because of the convenience afforded by Eq. 15 a number of studies sought to clarify the functional properties of δ, most notably that of Philip (62). This analysis was based on the "independence" hypothesis proposed by Corrsin (19,20). The Lagrangian autocorrelation function

is formed from an ensemble average of the time-lagged product of single-particle velocities having a common origin. According to Corrsin's hypothesis this function can be estimated from the general Eulerian space-time correlation function relative to a coordinate system moving with the mean flow velocity, by properly sampling (or weighting) the Eulerian data to account for the particle distribution in space and time. Then

$$R_L(\tau) = \int_{-\infty}^{\infty}\int\int\int \gamma(\mathbf{x};\tau) R_E(\mathbf{x};\tau)\, d\mathbf{x} \quad \ldots\ldots\ldots\ldots\ldots\ldots\ldots\ldots \quad (16)$$

in which γ = the probability of finding a particle released at $\tau = 0$ in the interval $(\mathbf{x}, \mathbf{x} + d\mathbf{x})$ at time τ, and the origin of $\mathbf{x}$ is coincident with the mean convective frame of reference.

Philip (62) assumed a homogeneous, isotropic, stationary turbulent motion, and introduced the functions

$$R_E(x_1, \rho, \tau) = \exp\left[-\frac{\pi}{4}\left(\frac{x_1^2 + 3.138\rho^2}{L_E^2} + \frac{\tau^2}{T_S^2}\right)\right] \quad \ldots\ldots\ldots\ldots \quad (17)$$

$$\gamma(x_1, \rho, \tau) = 2\pi\rho(2\pi[X_1^2])^{-3/2} \exp\left(-\frac{x_1^2 + \rho^2}{2[X_1^2]}\right) \quad \ldots\ldots\ldots\ldots \quad (18)$$

in which $\rho^2 = x_2^2 + x_3^2$; L_E = the Eulerian longitudinal integral length scale; T_S = the Eulerian space-time correlation integral scale

$$T_S = \int_0^{\infty} R_E(U\tau, 0, \tau)\, d\tau \quad \ldots\ldots\ldots\ldots\ldots\ldots\ldots\ldots\ldots\ldots \quad (19)$$

and $$[X_1^2(\tau)] = 2[u_1^2] \int_0^{\tau}\int_0^{\tau_1} R_L(\tau)\, d\tau\, d\tau_1 \quad \ldots\ldots\ldots\ldots\ldots\ldots \quad (20)$$

which results from integration of Eq. 8. Combining Eqs. 16, 17, 18, and 20, Philip obtained an integral equation for $R_L(\tau)$ that he solved by iteration for various values of the Eulerian diffusivity parameter $\alpha_E = T_S(\overline{u_1^2})^{1/2}/L_E$. Introducing the results in Eq. 10 yielded, after numerical integration, the Lagrangian-to-Eulerian space-time scale ratio

$$\frac{T_L}{T_S} = \int_0^{\infty} R_L(t_*)\, dt_* = F(\alpha_E); \quad t_* = \frac{\tau}{T_S} \quad \ldots\ldots\ldots\ldots\ldots\ldots \quad (21)$$

in which F turned out to be a decaying function of α_E, that is borne out by data reported by Baldwin and Mickelsen (1). The behavior of this function is such that $T_L \to T_S$ as the Eulerian parameter α_E approaches zero, while $F(\alpha_E)$ becomes approximately inversely proportional to α_E for $\alpha_E \geq 2$. To express the results in terms of δ, Philip (62) employed Taylor's hypothesis over the entire time span, namely:

$$R_E(0, 0, \tau) = R_E(U\tau, 0, \tau); \quad \tau > T_S \quad \ldots\ldots\ldots\ldots\ldots\ldots\ldots\ldots \quad (22)$$

His result is $$\delta = \frac{T_L}{T_E} = \left[1 + \left(\frac{\alpha_E^2}{I_u^2}\right)\right]^{1/2} F(\alpha_E) \quad \ldots \quad (23)$$

in which $I_u = (\overline{u_1^2})^{1/2}/U$ = the Eulerian intensity of turbulence. This expression is supported by available atmospheric and laboratory data (see Fig. 3, Ref. 62). Clearly, Eq. 23 does not predict a unique dependence of δ on turbulent intensity.

Knowledge of the time integral scale ratio δ permits the evaluation of the Fickian diffusion rate from Eq. 12 using Eulerian measurements. Nordin and McQuivey (57) used this approach to compute the vertical distribution of mean sediment concentration in a two-dimensional steady uniform flow. In this case, Eqs. 6, 12, and 15 yield

$$\delta \overline{u_3^2}\, T_E \frac{\partial C}{\partial x_3} + wC = 0 \quad \ldots \quad (24)$$

Integrating yields

$$C = C_a \exp\left[-w \int_0^{x_3} (\delta \overline{u_3^2}\, T_E)^{-1} dx_3\right] \quad \ldots \quad (25)$$

in which C_a = the concentration at some reference level $x_3 = a$. The values of $\overline{u_3^2}$, T_E, and δ measured by McQuivey, et al. (53) were used to evaluate the transfer coefficient. The results compare favorably with the values obtained by Jobson (37) from dye diffusion measurements. Jobson's data follow closely the parabolic distribution

$$\epsilon_S = \frac{\epsilon_0}{h}\eta(1-\eta) \quad \ldots \quad (26)$$

in which h = the flow depth; $\eta = x_3/h$ = the relative depth; and ϵ_0 = a constant. It can be shown that this constant takes the value κu_* in two-dimensional turbulent flows, where κ is the von Karman's constant and u_* is the bed shear velocity. Substituting ϵ_S for $\delta\, \overline{u_3^2}\, T_E$ in Eq. 25 and integrating gives

$$\frac{C}{C_a} = \left[\frac{1-\eta}{\eta}\frac{a}{h-a}\right]^z \quad \ldots \quad (27)$$

in which $z = w/\kappa u_*$. This equation was first introduced by Rouse (66) and has been the base for many deterministic studies of suspended sediment load (33).

The preceding example illustrates the combination of probabilistic and deterministic methods to obtain practical solutions. The probabilistic theories permit point estimates of local diffusion rates, while solutions to the mass transfer equation incorporate the appropriate boundary conditions as well as the sediment settling. Other illustrations of this combined approach are discussed by Sayre (67,69).

Relative Diffusivity of Solid and Fluid Particles.—The foregoing results assume that the solid particles follow exactly the motion of the surrounding fluid. As shown in the following, this leads to the experimentally incorrect conclusion that the particle diffusivity is identical, in general, to the fluid diffusivity. It

is thus important to investigate the conditions under which the foregoing assumption is valid.

The problem of relative diffusivity was first considered by Tchen (81). His analysis, and subsequent clarifications by others (22,35) extended the BBO equation to the case of a spherical particle moving in a turbulent flow. The particle Reynolds number is taken to be small enough so that the particle drag can be described by Stokes' law. The particle is regarded as part of a sparse cloud diffusing in a turbulent domain of infinite extent, in order to neglect the effect of boundaries and particle interaction. After assuming that the particle encounters a "locally uniform" flow along its trajectory, and by neglecting all nonlinear resistance, Tchen (81) obtained the following first-order linear equation

$$\frac{dv_{pi}}{dt} + \alpha\beta\, v_{pi} = \alpha\beta\, u_{fi} + \beta \frac{du_{fi}}{dt} + \beta \left(\frac{3d}{2\pi}\right)^{1/2} \int_{t_0}^{t} \frac{\dfrac{d}{d\tau}(u_{fi} - v_{pi})}{(t-\tau)^{1/2}} + f_i \quad \ldots \quad (28)$$

In this equation $\alpha = 12\nu/d^2$; $\beta = 3/(2S - 1)$; v_{pi} = the ith component of the solid particle velocity along its trajectory; u_{fi} = the ith velocity component of the "locally uniform" flow; d = the solid particle diameter; S = the specific gravity of the particle relative to the fluid; ν = the fluid kinematic viscosity; t_0 = the time at the beginning of the particle trajectory; and f_i = the ith component of the gravitational field force. Tchen (81) used Eq. 28 to obtain the particle diffusivity in terms of the stationary ($t_0 = -\infty$) Lagrangian energy-spectrum function. Chao (15) further generalized Tchen's analysis and related studies (23,30,74) by treating Eq. 28 as a stochastic equation subject to a Fourier transformation. He dropped the deterministic external force f_i, and introduced expressions defining the Fourier transform of the fluid and solid particle velocities and of the corresponding energy-spectrum density functions, F_f and F_p. Using the Wiener-Khintchine theorem, the stationary autocorrelation coefficients for the fluid and solid particle velocities were expressed as Fourier cosine transforms of the energy-spectrum densities. Following Tchen (81), Chao (15) assumed that small solid particles would tend to follow the fluid motion and that the Lagrangian correlation would thus serve as a good approximation of the particle correlation function. This is also the case for which the assumption of Stokesian motion of the particle is most likely to hold. Introducing the Lagrangian correlation functions in Eq. 8, Chao (15) formulated the ratio of the solid particle, D_p, to fluid, D_f, diffusivities as

$$\frac{D_p}{D_f} = \frac{\overline{v_{pi}^2} \displaystyle\int_0^t R_{Lp}(\tau)\, d\tau}{\overline{u_{fi}^2} \displaystyle\int_0^t R_{Lf}(\tau)\, d\tau} = \frac{\overline{v_{pi}^2} \displaystyle\int_0^\infty \frac{\sin \omega t}{\omega} F_p(\omega)\, d\omega}{\overline{u_{fi}^2} \displaystyle\int_0^\infty \frac{\sin \omega t}{\omega} F_f(\omega)\, d\omega} \quad \ldots \quad (29)$$

in which ω defines the harmonic frequency component. This ratio was shown by Chao to approach unity at large diffusion times, regardless of the particle inertial properties and the structural features of the flow. This result, also obtained by Tchen (81), is not supported by available experimental evidence (41,75).

This disagreement stems from the assumption that the solid particle always "sees" the same fluid elements in its neighborhood. However, the particle is made to follow the irregular path of the fluid by accelerations induced by drag forces exerted by the fluid itself. These drag forces can only exist at the expense of a relative velocity between the particle and the fluid. One effect of this relative motion is that the particle is forced to continuously change its fluid neighborhood and therefore to lose its velocity correlation more rapidly than the fluid. This has been termed the "effect of crossing trajectories" by Yudine (84). Consequently, a better definition of solid particle diffusivity should contain some measure of the time-space correlation between the particle and fluid velocities. A significant step in this direction was taken by Peskin (61).

Considering a heavy particle, Eq. 28 may be approximated as

$$\frac{d^2 y_i}{dt^2} + \sigma \frac{dy_i}{dt} = \sigma u_i(y_i, t) \quad \ldots \ldots \ldots \ldots \ldots \ldots \ldots \ldots \quad (30)$$

in which y_i = the ith component of the particle displacement, y; $\sigma = 18\nu/d^2 S$; and $u_i(y_i, t)$ = the ith component of the Eulerian fluid velocity, **u**, encountered

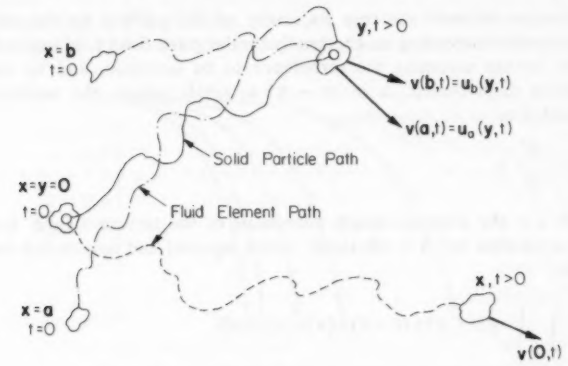

FIG. 4.—Effect of Crossing Trajectories

by the particle. The turbulent velocity **u** will be considered a random function with zero mean relative to some uniform mean flow velocity. Integrating Eq. 30 gives (49)

$$y_i = \int_0^t \{1 - \exp[\sigma(t-\tau)]\} u_i(y_i, \tau) d\tau \quad \ldots \ldots \ldots \ldots \ldots \quad (31)$$

in which the initial particle position has been omitted for convenience. This is a nonlinear stochastic equation since the velocity **u** is a random function of the random particle displacement. Peskin (61) solved it indirectly in a statistical sense, by considering the most probable fluid velocity encountered by the particle at a given position.

Fig. 4 shows the trajectories of solid and fluid particles coinciding at t = 0. Because of particle-fluid slip occurrence, the particles' Lagrangian displace-

ments **y** and **x**, are not necessarily the same at a later time t. While the fluid element has a Lagrangian velocity $\mathbf{v}(0,t)$ at **x**, the fluid velocity encountered by the solid particle at **y** will be one of many possible velocities associated with fluid particles having positions **a**, **b**, **c**, ..., at $t = 0$. Estimation of particle diffusivity requires relating the velocity encountered by the solid at time t, to the velocity of the fluid element coinciding with the solid particle at $t = 0$. This relation is obtained by computing the most probable fluid velocity encountered by the particle at **y** given a certain fixed Lagrangian fluid process. Mathematically, this probable velocity is expressed as the conditional expectation of $\mathbf{u}(\mathbf{y},t)$ given $\mathbf{v}(0,t)$ at **x**. Assuming, for simplicity, that $\mathbf{u}(\mathbf{y},t)$ and $\mathbf{v}(0,t)$ are distributed according to a joint Gaussian distribution with Eulerian correlation $R_E(\mathbf{y},\mathbf{x})$ gives

$$E[\mathbf{u}(\mathbf{y},t)|\mathbf{v}(0,t)] = \mathbf{v}(0,t)R_E(\mathbf{y},\mathbf{x}) \quad \ldots\ldots\ldots\ldots\ldots\ldots\ldots\ldots \quad (32)$$

The equation of motion (Eq. 31) can now be written as

$$y_i(t) = \int_0^t \{1 - \exp[-\sigma(t-\tau)]\} v_i(0,\tau) R_{E_{ii}} d\tau \quad \ldots\ldots\ldots\ldots\ldots \quad (33)$$

This equation replaces the true trajectory of the particle by the path of an average particle depending stochastically on the given fluid Lagrangian information. By further assuming the turbulence to be isotropic, and by restricting the relative displacement $\Delta = |\mathbf{y} - \mathbf{x}|$ to small values, the correlation can be expanded as

$$R_E \cong 1 - \frac{\Delta^2}{\lambda^2} + \ldots \quad \ldots\ldots\ldots\ldots\ldots\ldots\ldots\ldots\ldots\ldots\ldots \quad (34)$$

in which λ = the Eulerian length microscale of the turbulent field. Using Eq. 33, an expression for Δ is obtained, which squared and substituted back into 33 yields

$$y^2(t) = \int_0^t \int_0^t g(t-\tau)g(t-s)v(\tau)v(s)\,d\tau\,ds$$

$$+ \frac{1}{\lambda^2}\int_0^t \int_0^t g(t-\tau)g(t-s)v(\tau)v(s)\left\{\int_0^s \int_0^s \exp[-\sigma(s-m)\right.$$

$$\left. - \sigma(s-n)]\, v(m)v(n)\,dn\,dm\right\} ds\,d\tau + \ldots \quad \ldots\ldots\ldots\ldots\ldots\ldots \quad (35)$$

in which the subscripts have been dropped; $g(t-\xi) = 1 - \exp[-\sigma(t-\xi)]$; and $v(\zeta) = v(0,\zeta)$. The mean square value of the particle displacement is obtained by integration over the joint probability density of the Lagrangian fluid velocities $v(\tau)$, $v(s)$, etc. This results in an integral equation requiring information on the fourth-order fluid-velocity moments. A closure assumption is introduced by taking a quasinormal form for the fourth-order moment, and by using the following form of the velocity Lagrangian correlation (42)

$$\overline{v(\tau)v(s)} = (\overline{v^2})^{1/2} \exp\left(-\frac{|\tau - s|}{T_L}\right) \quad \ldots\ldots\ldots\ldots\ldots\ldots\ldots \quad (36)$$

The final expression for the mean square displacement at large times is (61)

$$\lim_{t\to\infty} \overline{y^2} = 2tT_L\,\overline{v^2} - \frac{(\overline{v^2})^2}{\sigma}\frac{T_L^2}{\lambda^2}\frac{6t}{\sigma T_L + 1} + \ldots \quad (37)$$

and from Eq. 8:

$$D_P = \frac{1}{2}\frac{d\overline{y^2}}{dt} = T_L\,\overline{v^2} - \frac{(\overline{v^2})^2}{\sigma}\frac{T_L^2}{\lambda^2}\frac{3}{\sigma T_L + 1} \quad (38)$$

Introducing now the Lagrangian length integral scale $L_L = (\overline{v^2})^{1/2} T_L$ (79), and dividing Eq. 38 by the turbulent fluid diffusivity, $D_f = \overline{v^2}\, T_L$, yields the following diffusivity ratio:

$$\frac{D_P}{D_f} = 1 - \frac{1}{2}\frac{L_L^2}{\lambda^2}\left(\frac{3K^2}{K+2}\right) \quad (39)$$

in which $$K = \frac{2}{\sigma T_L} = \frac{S}{9}\frac{d(\overline{v^2})^{1/2}}{\nu}\frac{d}{L_L} \quad (40)$$

Eq. 39 is plotted in Fig. 5 along with data measured by Kennedy (41) and later corrected by Peskin (61). Both the inertial parameter K and the turbulence

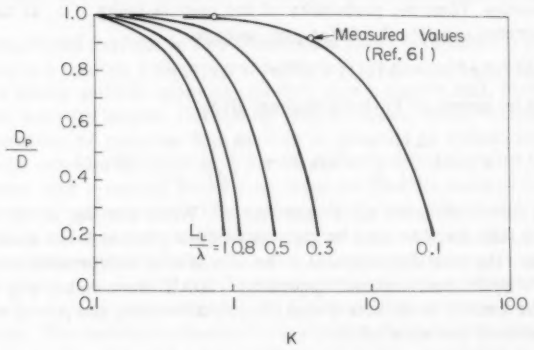

FIG. 5.—Rate of Particle Diffusivity to Fluid Diffusivity (After Ref. 61)

scales have a significant influence on the relative diffusivity of solid particles. A physical interpretation of this relationship is not difficult. When a flow is highly correlated (i.e., $L_L/\lambda << 1$) the fluid particles in the neighborhood of the solid particle all have similar velocities. Consequently, the correlation of fluid velocities encountered by the particle will be similar to the Lagrangian fluid correlation and the diffusivity ratio will approach unity. On the contrary, as L_L becomes larger than λ the particle will "see" almost random fluid velocities and its diffusivity will decrease relative to the fluid.

In most turbulent flows the length scale L_L is comparable to the lateral Eulerian integral scale l. This scale is associated with large-scale eddies; thus its magnitude

may be taken equal to the flow depth in two-dimensional flows. The ratio $L_L/\lambda \cong l/\lambda$ can be approximated by (82)

$$\frac{l}{\lambda} = C_1 \mathsf{R}_l^{1/2} \quad \ldots \ldots \ldots \ldots \ldots \ldots \ldots \ldots \ldots \ldots \ldots \ldots \ldots \quad (41)$$

in which $C_1 = 0(1)$; and $\mathsf{R}_l = (\overline{v^2})^{1/2} l/\nu$. Because $\mathsf{R}_l >> 1$ in all cases, the microscale λ is always much larger than the integral scale l. Therefore, one must have $\mathsf{K} << 1$ for the diffusivity ratio to be close to unity. Introducing $l \cong h$, and $(\overline{v^2})^{1/2} \cong 0.02U$, Eq. 40 yields for sand particles diffusing in water

$$\mathsf{K} \cong 10^{-2} \mathsf{R}_e (d/h)^2 << 1 \quad \ldots \ldots \ldots \ldots \ldots \ldots \ldots \ldots \ldots \ldots \quad (42)$$

in which $\mathsf{R}_e = hU/\nu$ is the flow Reynolds number. It is obvious that this condition is satisfied in the experiments of Engelund (26) and of Sayre and Chang (70).

Random Walk Models

Consider a discrete particle undergoing a sequence of random independent displacements of magnitude Δx_1 in the x_1 direction. Let p denote the probability of one-step transition in the positive direction, and q the probability of one-step transition in the opposite direction. Further assume that the process is stationary and Markovian. Then the probability of the particle being at x_1 at time t after n displacements satisfies the difference equation

$$P(x_1, t + \Delta t) = pP(x_1 - \Delta x_1, t) + qP(x_1 + \Delta x_1, t) \quad \ldots \ldots \ldots \ldots \quad (43)$$

Expanding by means of Taylor's theorem gives

$$\frac{\partial}{\partial t} P(x_1, t) = (q - p) \frac{\Delta x_1}{\Delta t} \frac{\partial}{\partial x_1} P(x_1, t) + \frac{(\Delta x_1)^2}{2\Delta t} \frac{\partial^2}{\partial x_1^2} P(x_1, t) \quad \ldots \ldots \ldots \quad (44)$$

neglecting terms of order $(\Delta t)^2$ and $(\Delta x_1)^3$. When passing to the limit, an appropriate ratio $\Delta x_1/\Delta t$ must be maintained if the process is not to degenerate. During time t the total displacement is the sum of $t/\Delta t$ independent steps having mean $(p - q)\Delta x_1$ and variance $4pqt(\Delta x_1)^2/\Delta t$. If these values are to remain finite in the limit, it is necessary that $(\Delta x_1)^2/\Delta t = 0(1)$ and $p - q = 0(\Delta x_1)$. These conditions are satisfied if

$$\frac{(\Delta x_1)^2}{2\Delta t} = d; \quad (p - q) \frac{d}{\Delta x_1} = c \quad \ldots \ldots \ldots \ldots \ldots \ldots \quad (45)$$

in which c and d = suitable constants. The mean and variance of the net displacement at time t are now given by $2ct$ and $2dt$, respectively. If c and d are interpreted as the mean convective velocity, U, and the turbulent diffusion coefficient, K_1, respectively, Eq. 44 becomes

$$\frac{\partial P}{\partial t} + U \frac{\partial P}{\partial x_1} = K_1 \frac{\partial^2 P}{\partial x_1^2} \quad \ldots \ldots \ldots \ldots \ldots \ldots \ldots \ldots \ldots \quad (46)$$

which is known as the Fokker-Planck equation. This result has been generalized by Kolmogorow to a multidimensional equation with variable coefficients (31).

If the simulation is applied to the dispersion of a large number of particles the probability $P(\mathbf{x},t)$ multiplied by the total number of realizations gives the particle concentration at a point $\mathbf{x}$ at time t.

Eq. 46 shows that a random walk simulation replaces, in the limit, the solution of the Fickian diffusion equation. Taylor (79) recognized this in introducing the Lagrangian integral time scale. This integral can be regarded as a measure of the interval over which the particle velocity retains a correlation with its initial value. If the duration of the random walk steps are selected such that $\Delta t \geqq T_L$, then the particle displacement at time t may be represented as a sum of small displacements that are weakly dependent random variables. Therefore, according to the central limit theorem, the probability distribution of the sum will approach the normal form as the number of steps becomes very large. Furthermore, Goldstein (32) has shown that a random walk model embodying the behavior of turbulent diffusion at small and large times leads to the so-called "telegraph equation." For small times this equation reduces to the wave-propagation equation; for large times it becomes a diffusive equation. Corrsin (21) has shown that this dual behavior is analogous to the asymptotic behavior of turbulent diffusion (Eqs. 9 and 11). These observations serve to illustrate the fact that the random walk and the continuous movements theories are basically equivalent.

Examples of some typical applications of the random walk technique in its more basic form, direct simulation, to the study of suspended-sediment dispersion follow.

Settlement of Solid Particles in Two-Dimensional Flows.—Bayazit (8) developed a model akin to a random walk process to simulate the motion of a solid particle settling in a steady uniform open-channel flow over a smooth bed. Incorporated in the model are path lengths, fluctuating velocity scales, mean velocities, etc., that are functions of position. The particle is assumed to follow exactly the motion of the surrounding fluid as it moves downwards through the statistical field variables with a settling velocity w. Once the particle reaches the stream bed, the motion is terminated. This occurrence defines the settling length L of the particle. Many such realizations are used to compile the probability distribution of the settling lengths.

Because of the lack of available Lagrangian information, an attempt is made to simulate the process using the available Eulerian information in a pseudo-Lagrangian way. The turbulent velocity fluctuations in the longitudinal and lateral directions are neglected, and the vertical fluctuations are assumed to be normally distributed around a zero mean. That is

$$f(u_3) = (2\pi\,\overline{u_3^2})^{-1/2} \exp\left(\frac{-u_3^2}{2\,\overline{u_3^2}}\right) \quad \ldots\ldots\ldots\ldots\ldots\ldots\ldots\ldots\ldots\ldots (47)$$

in which the rms of u_3 is obtained from experimental data analyzed by Partheniades and Blinco (59). The vertical fluctuation is assigned a certain value at each time level by means of a random number generator. During each time step the particle experiences a horizontal convection displacement $\Delta x_1 = \bar{u}_1(x_3,t)\Delta t$ followed by a randomly directed vertical displacement $\Delta x_3 = (u_3 - w)\Delta t$, where $\bar{u}_1$ is the local mean velocity. The time step is selected so as to render Δx_3 equal to the turbulence Eulerian microscale estimated from the data collected by Raichlen (63) and McQuivey and Richardson (54).

This model was later on extended by Li and Shen (47), who introduced several refinements. They computed the local mean velocity from the velocity-defect law, which is valid over a larger depth range than the law of the wall used by Bayazit (8). They further assumed that the streamwise fluctuations are not negligible and normally distributed, such that

$$f(u_1) = (2\pi\,\overline{u_1^2})^{-1/2} \exp\left(\frac{-u_1^2}{2\,\overline{u_1^2}}\right) \quad \ldots\ldots\ldots\ldots\ldots\ldots\ldots\ldots \quad (48)$$

The rms of u_1 is computed from

$$\overline{u_1^2} = \frac{\overline{u_1 u_3}}{\rho c} \quad \ldots\ldots\ldots\ldots\ldots\ldots\ldots\ldots\ldots\ldots\ldots\ldots \quad (49)$$

in which the covariance $\overline{u_1 u_3}$ is obtained from a simplified form of the Reynolds equations governing the two-dimensional mean flow; ρ = a correlation coefficient derived from available experimental data (43,54); and c defines the ratio (54)

$$c = \left(\frac{\overline{u_3^2}}{\overline{u_1^2}}\right)^{1/2} \quad \ldots\ldots\ldots\ldots\ldots\ldots\ldots\ldots\ldots\ldots\ldots\ldots \quad (50)$$

In the light of Eqs. 47 and 48, Li and Shen assumed u_1 and u_3 to have a bivariate normal joint distribution. Thus, they obtained

$$f(u_1|u_3) = [2\pi(1-\rho^2)\,\overline{u_1^2}\,]^{-1/2} \exp\left[\frac{-\left(u_1 - \dfrac{\rho u_3}{c}\right)^2}{2(1-\rho^2)(\overline{u_1^2})}\right] \quad \ldots\ldots\ldots \quad (51)$$

At each time step the rms of u_1 and u_3 are computed from Eqs. 49 and 50; then u_1 and u_3 are randomly generated using 47 and 51. The time step and vertical displacement are computed following Bayazit (8), and the convective displacement is obtained from $\Delta x_1 = (\bar{u}_1 + u_1)\,\Delta t$. However, contrary to Bayazit, Δt is not treated as a random quantity, but as a local mean convective time increment chosen so that the expected value of $|\Delta x_3|$ is equal to the local Eulerian length scale.

The random walk model was simulated on a computer for various flow conditions and particle characteristics. In each case the random walk was realized more than 100 times, and the mean value and standard deviation of the settling length distribution were computed. The computed values compare favorably with the measurements of Bayazit (8) and Lean (45), as shown in Fig. 6. The frequency histograms of the simulated settling length distributions for sediment mixtures agree with the experimental results obtained by Jobson and Sayre (38).

In the preceding models the solid particles move between a reflecting boundary at the free surface, and an absorbing boundary at the channel bed. A similar model using reflecting barriers at both the bed and free surface was developed by Sumer (78). This model was basically patterned after those of Sullivan (77) and Bayazit (8).

Dispersion of Sediment in Three-Dimensional Turbulent Flows.—Chiu (16) was the first to formulate a random walk simulation of solid particles dispersing

in a three-dimensional turbulent flow. His analysis leads to a three-dimensional analog of Eq. 44. As in the preceding examples, the random walk step is considered to be the resultant of a convective component (which incorporates the particle settling), and a random diffusive component. Because of the lack of information on the distribution of turbulence characteristics in three-dimensional flows, Chiu represented the diffusive step by a random vector. The model also assumes that there is no particle-fluid slip, and that interactions between particles do not exist. The time increment is determined by equating the diffusion coefficient to a momentum transfer coefficient based on a von Karman mixing length model.

Chiu and Chen (17) applied this model to simulate the dispersion of 100-μ

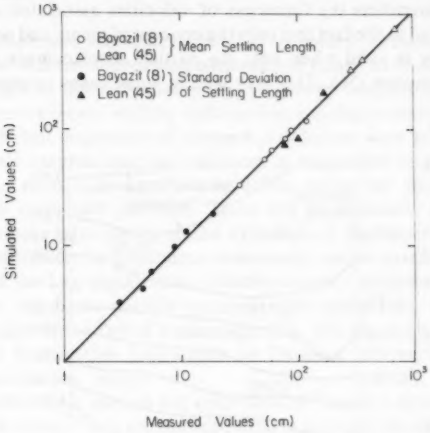

FIG. 6.—Comparison of Simulated and Measured Settling Lengths (After Ref. 48)

sand particles in a steady, uniform open channel flow. Measurements conducted in a 0.60-m deep flow with an average velocity of 1.10 m/s yielded information on the distribution of longitudinal mean velocity and sediment concentration at a cross section located in the established flow region (18). The sediment distribution over the cross section was computed by continuously releasing sand particles from a hypothetical point source. This source was located upstream near a lower corner of the channel, where the presence of the side wall and the corner eddies render the mean flow three-dimensional. The transversal mean velocity components were computed from the measured velocity distribution using the method developed by Ligget, et al. (48). The simulation consisted of releasing a large number of particles, one at a time, and tracking their trajectories. This is equivalent to releasing all the particles simultaneously because of the stationarity of the flow. At some distance from the source the influence of the source location will cease to be felt by the particles. Thus, the concentration will approach the same steady distribution independent of whether the particles are being released from a point or a distributed source. Fig. 7 presents the simulated steady state concentration distribution, in the form of lines of equal

concentration, along with the measured values. In this figure the concentration values are normalized by the total amount of sediment in the entire cross section. Although the data are quite limited, they compare well with the simulated values. The simulation reflects the effects of gravity, resulting in an increase of concentration towards the channel bed.

The preceding experimental verifications tend to substantiate the random walk simulations reviewed in this paper. However, there is a need for additional refinements to make this technique adaptable to more general situations. Some aspects susceptible to further development are now considered.

The parabolic character of Eq. 46 implies that sediment particles introduced in a fluid stream will spread instantaneously throughout the length of the stream. This clearly contradicts the finiteness of velocities associated with actual fluid flows. It is related to the fact that only the concept of mean, and not instantaneous, particle velocity is valid when only the particle displacement is interpreted as a Markovian function (56). This may lead in some cases to unacceptable errors

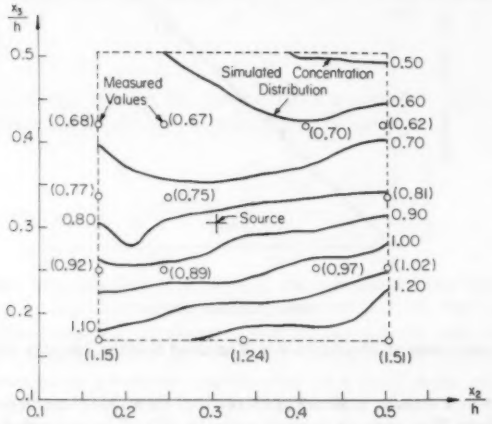

FIG. 7.—Comparison of Simulated and Measured Steady-State Distribution of Suspended Sediment (After Ref. 17)

close to the edges of the dispersing cloud. Therefore, it is desirable to have models based on a more general theory in which the boundedness of the particle velocity would be taken into account. Monin (55) proposed one such theory were not the particle displacement but the two-dimensional random function formed by the particle position and velocity is Markovian.

There is also a need for more general dispersion models capable of handling strongly nonstationary flow fields. They will find application in instances where the interest is focussed in the dispersion of sediment in relatively short channel reaches of irregular geometry. These models should be free of the approximations made in the existing models regarding the turbulence structure, and should take into consideration the dependence of solid-particle diffusivity on the turbulent flow features as well as on particle inertia. A promising approach was presented

by Kau and Peskin (40). They used an improved version of Deardorff's Navier-Stokes solver (24) to investigate the Eulerian structure of a three-dimensional turbulent flow. Mean flow characteristics and Eulerian statistics were obtained from the solution. An approximate form of Eq. 28 was integrated to obtain Lagrangian information on the motion of solid particles released in the streamflow. Lagrangian statistics describing the particle diffusivities were obtained from the simulated particle trajectories. This study is another good illustration of an effectual combination of probabilistic and deterministic techniques.

Summary and Conclusions

Prediction of suspended-sediment dispersion in natural streams is important in the evaluation of sediment deposition patterns and transport of sediment-borne pollutants. Starting with the early theory of diffusion by continuous movements, and proceeding to more recent random walk models, existing probabilistic methods for predicting turbulent dispersion of suspended sediment were reviewed.

All these models assume that the sediment is suspended in concentrations that are not large enough to significantly affect either the fluid velocity or the motion of the suspended particles. These are all kinematic models in the sense that they require information on the dynamics of the dispersive medium.

The theory of diffusion by continuous movement can be extended to natural channels provided the Lagrangian mean velocity remains statistically stationary. In those cases in which the particle properties and turbulence characteristics result in a small value of the Peskin's parameter (Eq. 40), the sediment diffusivity may be obtained from either Lagrangian or Eulerian information about the turbulence characteristics.

Markovian random walk models are equivalent to Taylor's theory in the limit of large dispersion times. They are not restricted in principle to stationary flows, but impose probability-distribution restrictions which are not present in the continuous movements technique. The random walk simulations depend for accuracy on knowledge of the turbulent flow characteristics. These data are very limited and mostly restricted to two-dimensional flows. This obstacle may be surmounted, however, by using Navier-Stokes solvers when no experimental information is available. These solvers have already been introduced in turbulent boundary-layer computations, and workers in this field are extending them to include complex three-dimensional flows (11,44,76). The dispersion models considered in this paper assume that discrete particles follow exactly the turbulent fluctuations. This assumption usually limits the permissible particle size range to silts and fine sands. Nevertheless, this constraint can be relaxed by coupling the flow models to a suitable form of the BBO equation.

The ultimate evolution of probabilistic methods into formulations of general applicability may still lie ahead. There is still a large gap between the models that have been developed so far and the practical solution of complex hydraulic problems associated with the transport of suspended sediments. For the present, the combination of probabilistic and deterministic solutions seems to be the most efficient approach to practical applications, where the strengths of both methods are used while their individual weaknesses are complemented. Nevertheless, large-scale simulation of sediment dispersion using a probabilistic-de-

terministic approach cannot be regarded as practical even with today's largest digital computers. However, such an approach can be used in a reduced scale to complement the fully deterministic models derived from continuous theory. The weakest part of these deterministic models is the lack of accurate procedures for predicting the effect of channel curvature and irregularities along short reaches, on the spatial variation of mass transfer coefficients. This information could be obtained by simulating the dispersion of suspended particles in a fashion similar to those propounded by Chiu and Chen (17), and by Kau and Peskin (40).

Acknowledgments

This study was supported by a reimbursable agreement with the U.S. Army Corps of Engineers, Vicksburg District, Miss. The writer is sincerely grateful to Richard L. Peskin and William W. Sayre for making many helpful comments on a draft of this paper.

Appendix I.—References

1. Baldwin, L. V., and Mickelsen, W. R., "Turbulent Diffusion and Anemometer Measurements," *Transactions*, ASCE, Vol. 128, Part I, Paper No. 3507, 1963, pp. 1595–1627.
2. Barfield, B. J., Smerdon, E. T., and Hiler, E. A., "Prediction of Sediment Profiles in Open Channel Flow by Turbulent Diffusion Theory," *Water Resources Research*, Vol. 5, No. 1, 1969, pp. 291–299.
3. Bassett, A. B., *A Treatise on Hydrodynamics*, Vol. 2, Chapter 5, Deighton, Bell, and Co., Cambridge, England, 1888.
4. Batchelor, G. K., "Diffusion in a Field of Homogeneous Turbulence, I, Eulerian Analysis," *Australian Journal of Scientific Research*, Vol. 2, No. 4, 1949, pp. 437–450.
5. Batchelor, G. K., "Diffusion in a Field of Homogeneous Turbulence, II, The Relative Motion of Particles," *Proceedings of the Cambridge Philosophical Society*, Vol. 48, 1952, pp. 345–362.
6. Batchelor, G. K., "Diffusion in Free Turbulent Shear Flow," *Journal of Fluid Mechanics*, Vol. 3, Part 1, 1957, pp. 67–80.
7. Batchelor, G. K., and Townsend, A. A., "Turbulent Diffusion," *Surveys in Mechanics*, G. K. Batchelor and R. M. Davies, eds., Cambridge University Press, London, England, 1956, pp. 352–399.
8. Bayazit, M., "Random Walk Model for Motion of a Solid Particle in Turbulent Open-Channel Flow," *Journal of Hydraulic Research*, Vol. 10, No. 1, 1972, pp. 1–14.
9. Bennett, J. P., and Nordin, C. F., "Suspended-Sediment Sampling Variability," *Environmental Impact on Rivers*, H. W. Shen, ed., Water Resources Publications, Littleton, Colo., Chapter 17, 1973.
10. Boussinesq, J., *Theories Analytique de la Chaleur*, Vol. 2, Gauthier-Villars, Paris, France, 1903.
11. Bradshaw, P., "Calculation of Three-Dimensional Turbulent Boundary Layers," *Journal of Fluid Mechanics*, Vol. 46, Part 3, 1971, pp. 417–445.
12. Bugliarello, G., and Jackson, E. D., III, "Random Walk Study of Convective Diffusion," *Journal of the Engineering Mechanics Division*, ASCE, Vol. 90, No. EM4, Proc. Paper 4003, Aug., 1964, pp. 49–77.
13. Bugliarello, G., and Jackson, E. D., III, "A Stochastic Model of Convective Diffusion from a Continuous Source," *Journal of Hydraulic Research*, Vol. 7, No. 2, 1969, pp. 177–204.
14. Chandrasekhar, S., "Stochastic Problems in Physics and Astronomy," *Reviews of Modern Physics*, Vol. 15, No. 1, 1943, pp. 1–89.
15. Chao, B. T., "Turbulent Transport Behaviour of Small Particles in Dilute Suspension," *Osterreichisches Ingenieur-Archiv*, Vol. 18, Part 1/2, 1964, pp. 7–21.

16. Chiu, C. L., "Stochastic Model of Motion of Solid Particles," *Journal of the Hydraulics Division*, ASCE, Vol. 93, No. HY5, Proc. Paper 5445, Sept., 1967, pp. 203–218.
17. Chiu, C. L., and Chen, K. C., "Stochastic Hydrodynamics of Sediment Transport," *Journal of the Engineering Mechanics Division*, ASCE, Vol. 95, No. EM5, Proc. Paper 6858, Oct., 1969, pp. 1215–1230.
18. Chiu, C. L., and McSparran, J. E., "Effect of Secondary Flow in Sediment Transport," *Journal of the Hydraulics Division*, ASCE, Vol. 92, No. HY5, Proc. Paper 4905, Sept., 1966, pp. 57–70.
19. Corrsin, S., "Progress Report on Some Turbulent Diffusion Research," *Advances in Geophysics*, Vol. 6, 1959, pp. 161–164.
20. Corrsin, S., "Theories of Turbulent Dispersion," *Proceedings of the International Colloquium on Turbulence (Marseille, 1961)*, Centre National de la Recherche Scientifique, Paris, 1962, pp. 27–52.
21. Corrsin, S., "Limitations of Gradient Transport Models in Random Walks and in Turbulence," *Turbulent Diffusion in Environmental Pollution*, F. N. Frenkiel and R. E. Munn, eds., Academic Press, New York, N.Y., 1974, pp. 25–60.
22. Corrsin, S., and Lumley, J. L., "On the Equation of Motion for a Particle in Turbulent Fluid," *Applied Scientific Research, Section A*, Vol. 6, 1956, pp. 114–116.
23. Csanady, G. T., "Turbulent Diffusion of Heavy Particles in the Atmosphere," *Journal of the Atmospheric Sciences*, Vol. 20, 1963, pp. 201–208.
24. Deardorff, J. W., "A Numerical Study of Three-Dimensional Turbulent Channel Flow at Large Reynolds Number," *Journal of Fluid Mechanics*, Vol. 41, Part 2, 1970, pp. 453–480.
25. Elder, J. W., "The Dispersion of Marked Fluid in Turbulent Shear Flow," *Journal of Fluid Mechanics*, Vol. 5, Part 4, 1959, pp. 544–560.
26. Engelund, F., "Dispersion of Floating Particles in Uniform Channel Flow," *Journal of the Hydraulics Division*, ASCE, Vol. 95, No. HY4, Proc. Paper 6659, July, 1969, pp. 1149–1162.
27. Fischer, H. B., "Longitudinal Dispersion in Laboratory and Natural Streams," *Report No. KH-R-12*, W. M. Keck Laboratory of Hydraulics and Water Resources, California Institute of Technology, Pasadena, Calif., 1966.
28. Fischer, H. B., "Longitudinal Dispersion and Turbulent Mixing in Open-Channel Flow," *Annual Review of Fluid Mechanics*, Vol. 5, 1973, pp. 59–78.
29. Frenkiel, F. N., and Munn, R. E., eds., *Turbulent Diffusion in Environmental Pollution*, Academic Press, New York, N.Y., 1974.
30. Friedlander, S. K., "Behaviour of Suspended Particles in a Turbulent Fluid," *Journal of the American Institute of Chemical Engineers*, Vol. 3, 1957, pp. 381–385.
31. Gnedenko, B. V., *Theory of Probability*, Chelsea Publishing Co., New York, N.Y., 1968.
32. Goldstein, S., "On Diffusion by Discontinuous Movements, and on the Telegraph Equation," *Quarterly Journal of Mechanics and Applied Mathematics*, Vol. 4, 1951, pp. 129–156.
33. Graf, W. H., *Hydraulics of Sediment Transport*, McGraw-Hill Book Co., New York, N.Y., 1971.
34. Hay, J. S., and Pasquill, F., "Diffusion from a Fixed Source at a Height of a Few Hundred Feet in the Atmosphere," *Journal of Fluid Mechanics*, Vol. 2, Part 3, 1957, pp. 299–310.
35. Hinze, J. O., *Turbulence*, McGraw-Hill Book Co., New York, N.Y., 1959.
36. Hjelmfelt, A. T., Jr., and Mockros, L. F., "Motion of Discrete Particles in a Turbulent Fluid," *Applied Scientific Research*, Vol. 16, 1966, pp. 149–161.
37. Jobson, H. E., "Vertical Mass Transfer in Open Channel Flow," *Open File Report*, U.S. Geological Survey, Fort Collins, Colo., Sept., 1968.
38. Jobson, H. E., and Sayre, W. W., "Vertical Transfer in Open Channel Flow," *Journal of the Hydraulics Division*, ASCE, Vol. 96, No. HY3, Proc. Paper 7148, Mar., 1970, pp. 703–724.
39. Kac, M., "Random Walk and the Theory of Brownian Motion," *American Mathematical Monthly*, Vol. 54, 1947, pp. 369–391.
40. Kau, C. J., and Peskin, R. L., "Numerical Simulation of Turbulence and Diffusion in Three-Dimensional Flow," *Technical Report 101*, Geophysical Fluid Dynamics Program, 1972.

41. Kennedy, D. A., "Some Measurements of the Dispersion of Spheres in a Turbulent Flow," thesis presented to The John Hopkins University, at Baltimore, Md., in 1965, in partial fulfillment of the requirements for the degree of Doctor of Philosophy.
42. Krasnoff, E. L., "Dynamical Description of Diffusion in Hydrodynamic Turbulence," thesis presented to Rutgers University, at New Brunswick, N.J., in 1970, in partial fulfillment of the requirements for the degree of Doctor of Philosophy.
43. Laufer, J., "The Structure of Turbulence in Fully Developed Pipe Flow," *Report No. 1174*, National Advisory Committee for Aeronautics, 1954.
44. Launder, B. E., Reece, G. J., and Rodi, W., "Progress in the Development of a Reynolds-Stress Turbulence Closure," *Journal of Fluid Mechanics*, Vol. 68, Part 3, 1975, pp. 537–566.
45. Lean, G. H., "The Settling Velocity of Particles in Channel Flow," *International Symposium on Stochastic Hydraulics*, C. L. Chiu, ed., University of Pittsburgh, 1971, pp. 339–351.
46. Levich, V. G., and Kuchanov, S. I., "Motion of Particles Suspended in Turbulent Flow," *Soviet Physics Doklady*, Vol. 12, No. 6, 1967, pp. 546–548.
47. Li, R. M., and Shen, H. W., "Solid Particle Settlement in Open-Channel Flow," *Journal of the Hydraulics Division*, ASCE, Vol. 101, No. HY7, Proc. Paper 11460, July, 1975, pp. 917–931.
48. Liggett, J. A., Chiu, C. L., and Miao, L. S., "Secondary Currents in a Corner," *Journal of the Hydraulics Division*, ASCE, Vol. 91, No. HY6, Proc. Paper 4538, Nov., 1965, pp. 99–117.
49. Lumley, J. L., "Some Problems Connected with the Motion of Small Particles in Turbulent Fluid," thesis presented to The John Hopkins University, at Baltimore, Md., in 1957, in partial fulfillment of the requirements for the degree of Doctor of Philosophy.
50. Lumley, J. L., "An Approach to the Eulerian-Lagrangian Problem," *Journal of Mathematical Physics*, Vol. 3, 1962, pp. 309–312.
51. McQuivey, R. S., "Turbulence in a Hydrodynamically Rough and Smooth Open Channel Flow," *Open File Report*, U.S. Geological Survey, Fort Collins, Colo., 1967.
52. McQuivey, R. S., "Summary of Turbulence Data from Rivers, Conveyance Channels and Laboratory Flumes," *Open File Report*, U.S. Geological Survey, Bay St. Louis, Miss., 1972.
53. McQuivey, R. S., Keefer, T. N., and Shirazi, M. A., "Turbulent Spread of Heat and Matter," *Open File Report*, U.S. Geological Survey, Fort Collins, Colo., 1971.
54. McQuivey, R. S., and Richardson, E. V., "Some Turbulence Measurements in Open-Channel Flow," *Journal of the Hydraulics Division*, ASCE, Vol. 95, No. HY1, Proc. Paper 6349, Jan., 1969, pp. 209–223.
55. Monin, A. S., "Diffusion with Finite Velocity," *Izvestiya Akademii Nauk SSSR, Seriya Geofizicheskaya*, No. 3, 1955, 234–248.
56. Monin, A. S., and Yaglom, A. M., *Statistical Fluid Mechanics: Mechanics of Turbulence*, Vol. 1, The MIT Press, Cambridge, Mass., 1971.
57. Nordin, C. F., and McQuivey, R. S., "Suspended Load," *River Mechanics*, H. W. Shen, ed., Vol. I, Fort Collins, Colo., 1971, Chap. 12.
58. Oseen, G. W., *Hydrodynamik*, Leipzig, Germany, 1927.
59. Partheniades, E., and Blinco, P. H., discussion of "Some Turbulence Measurements in Open Channel Flow," by R. S. McQuivey and E. V. Richardson, *Journal of the Hydraulics Division*, ASCE, Vol. 96, No. HY1, Proc. Paper 6988, Jan., 1970, pp. 272–275.
60. Pearson, K., "The Problem of the Random Walk," *Nature*, Vol. 72, No. 1865, 1905.
61. Peskin, R. L., "Stochastic Estimation Applications to Turbulent Diffusion," *International Symposium on Stochastic Hydraulics*, C. L. Chiu, ed., University of Pittsburgh, Pittsburgh, Pa., 1971, pp. 251–267.
62. Philip, J. R., "Relation between Eulerian and Lagrangian Statistics," *The Physics of Fluids Supplement*, Vol. 10, Part II, 1967, pp. 569–571.
63. Raichlen, F., "Somz Turbulence Measurements in Water," *Journal of the Engineering Mechanics Division*, ASCE, Vol. 93, No. EM2, Proc. Paper 5195, Apr., 1967, pp. 73–97.
64. Rayleigh, Lord, "On the Resultant of a Large Number of Vibrations of the Same Pitch and of Arbitrary Phase," *Philosophical Magazine*, Vol. X, 1880, pp. 73–78.

65. Richardson, L. F., "Atmospheric Diffusion Shown on a Distance-Neighbour Graph," *Proceedings of the Royal Society*, Series A, Vol. 110, 1926, pp. 709–737.
66. Rouse, H., "Modern Conceptions of the Mechanics of Turbulence," *Transactions*, ASCE, Vol. 102, Paper No. 1965, 1937, pp. 463–505.
67. Sayre, W. W., "Dispersion of Mass in Open-Channel Flow," *Hydraulics Paper No. 3*, Colorado State University, Fort Collins, Colo., 1968.
68. Sayre, W. W., "Natural Mixing Processes in Rivers," *Environmental Impact on Rivers*, H. W. Shen, ed., Water Resources Publications, Littleton, Colo., 1973, Chap. 6.
69. Sayre, W. W., "Transport and Dispersion of Fluvial Sediments: Some Mathematical Models and Their Verification by Tracer Methods," *Technical Report Series No. 145*, Tracer Techniques in Sediment Transport, International Atomic Energy Agency, Vienna, Austria, 1973, pp. 49–68.
70. Sayre, W. W., and Chang, F. M., "A Laboratory Investigation of Open-Channel Dispersion Processes for Dissolved, Suspended, and Floating Dispersants," *Professional Paper 433-E*, U.S. Geological Survey, Washington, D.C., 1968.
71. Shen, H. W., and Cheong, H. F., "Dispersion of Contaminants Attached to Sediment Bed Load," *Environmental Impact in Rivers*, H. W. Shen, ed., Fort Collins, Colo., 1973, Chap. 13.
72. Shirazi, M. A., "On the Motion of Small Particles in a Turbulent Field," thesis presented to the University of Illinois, at Urbana, Ill., in 1967, in partial fulfillment of the requirements for the degree of Doctor of Philosophy.
73. Snyder, W. H., and Lumley, J. L., "Some Measurements of Particle Velocity Autocorrelation Functions in a Turbulent Flow," *Journal of Fluid Mechanics*, Vol. 48, Part 1, 1971, pp. 41–71.
74. Soo, S. L., "Statistical Properties of Momentum Transfer in Two-Phase Flow," *Chemical Engineering Science*, Vol. 5, 1956, pp. 57–63.
75. Soo, S. L., Ihrig, H. K., and El Kouh, A. L., "Experimental Determination of Statistical Properties of Two-Phase Turbulent Motion," *Journal of Basic Engineering*, ASME, 82D(3), 1960, pp. 609–621.
76. Spalding, D. B., "Mathematical Modeling of Rivers," *Report HTS/74/4*, Department of Mechanical Engineering, Imperial College, London, 1974.
77. Sullivan, P. J., "Longitudinal Dispersion within a Two-Dimensional Turbulent Shear Flow," *Journal of Fluid Mechanics*, Vol. 49, Part 3, 1971, pp. 551–576.
78. Sumer, B. M., "Simulation of Dispersion of Suspended Particles," *Journal of the Hydraulics Division*, ASCE, Vol. 99, No. HY10, Proc. Paper 10070, Oct., 1973, pp. 1705–1726.
79. Taylor, G. I., "Diffusion by Continuous Movements," *Proceedings of the London Mathematical Society*, Vol. 20, Series 2, 1921, pp. 196–212.
80. Taylor, G. I., "The Dispersion of Matter in Turbulent Flow Through a Pipe," *Proceedings of the Royal Society London*, Series A, Vol. 223, 1954, pp. 446–468.
81. Tchen, C. M., "Mean Value and Correlation Problems Connected with the Motion of Small Particles Suspended in a Turbulent Fluid," *Publication 51*, Laboratory for Aero- and Hydrodynamics, Technical University, Delft, 1947.
82. Tennekes, H., and Lumley, J. L., *A First Course in Turbulence*, The MIT Press, Cambridge, Mass., 1972.
83. Yotsukura, N., "Turbulent Dispersion of Miscible Materials in Open Channels," *Transport of Radionuclides in Fresh Water Systems*, USACE TID-7664, 1963, pp. 311–326.
84. Yudine, M. I., "Physical Considerations on Heavy-Particle Diffusion," *Atmospheric Diffusion and Air Pollution, Advances in Geophysics*, Vol. 6, 1959, pp. 185–191.

Appendix II.—Notation

The following symbols are used in this paper:

C = concentration of discrete solid particles;
C_x = probability characteristic function;

c = ratio of rms of transverse velocity fluctuations to that of streamwise velocity fluctuations;
D_f = turbulent fluid diffusivity;
D_p = solid particle diffusivity;
d = solid particle size;
$F_f(\omega), F_p(\omega)$ = energy spectrum density functions;
$f(\cdot)$ = probability density function;
f_i = scalar component of gravitational field force;
h = flow depth;
I_u = Eulerian intensity of turbulence;
K = Peskin's parameter;
K_1 = Fickian diffusion coefficient;
l = lateral Eulerian integral scale;
L_E = Eulerian length integral scale;
L_L = Lagrangian length integral scale;
p, P, q, Q = probabilities;
R_e = flow Reynolds number;
R_E = Eulerian velocity correlation;
R_t = macroeddy Reynolds number;
R, R_L = Lagrangian velocity correlation;
S = specific gravity of solid particles;
T_E = Eulerian time integral scale;
T_L = Lagrangian time integral scale;
T_S = Eulerian space-time correlation integral scale;
t = time;
U = cross-sectional average velocity;
$\bar{u}$ = local mean velocity;
$\underline{\mathbf{u}}$ = Eulerian velocity fluctuation;
$\overline{u^2}$ = mean-square of Eulerian velocity fluctuation;
u_f = scalar component of Eulerian fluid velocity;
u_p = scalar component of Eulerian particle velocity;
u_* = bed shear velocity;
V = volume;
$\mathbf{v}$ = Lagrangian fluid velocity;
v_p = scalar component of Lagrangian particle velocity;
$\mathbf{w}$ = solid particle settling velocity;
X = relative displacement;
$\mathbf{x}, \mathbf{y}$ = vector positions;
z = $|\mathbf{w}|/\kappa u_*$;
α, β = coefficients of the BBO equation;
α_E = Eulerian parameter;
γ = probability distribution of particle displacements;
Δ = fluid-solid particle relative displacement;
Δt = time increment;
Δx = displacement increment;
δ = time integral scale ratio;
ϵ = mass transfer coefficient;
η = relative depth;
κ = von Karman turbulence coefficient;

λ = Eulerian length microscale;
ν = fluid kinematic viscosity;
ξ = wave number vector;
ρ = correlation coefficient;
σ = constant derived from Stokes drag law;
σ_t^2 = time variance;
σ_x^2 = displacement variance;
ω = harmonic frequency component; and
$[\cdot]$ = denotes average over the ensemble of all marked particles.

RUN HYDROGRAPHS FOR PREDICTION OF FLOOD HYDROGRAPHS

By Lourens A. V. Hiemstra,[1] M. ASCE and David M. Francis[2]

INTRODUCTION

For most practical applications, a flood is sufficiently defined if the complete flood hydrograph and its exceedance probability is known. Important elements of the flood hydrograph are its instantaneous peak discharge rate, its total flood volume, and its shape. The flood peak and its exceedance probability give enough information for many practical problems, e.g., in the sizing of storm drainage pipes, some culvert sizes etc., where storage is unimportant. There are many methods which can be used to estimate the peaks and their exceedance probabilities. All these methods are explicitly or tacitly based on the marginal probability distribution of flood peaks. Flood volumes can be treated in a similar way. Flood volumes are important in problems where storage plays an important part, e.g., in the sizing of spillways for dams, in the calculation of flood damage, and in flood routing. Flood volume analysis is very seldom done in isolation because actual data on flood volumes is scarce and relatively difficult to process. Flood volumes alone also have a limited value because they do not supply information on depth or duration of inundation. Therefore, the complete flood hydrograph is needed. The only general method which is widely used, and purports to supply the complete hydrograph, is the unit hydrograph method and its derivatives. The unit hydrograph technique, however, suffers two important limitations. Firstly, many observed floods are composite floods and are therefore not easily described by unit hydrograph methods. It is, of course, possible to combine design hydrographs, derived by the unit hydrograph method, into one composite flood hydrograph, but this illustrates the second limitation—the return period of this composite hydrograph is unknown! Indeed, any design hydrograph derived through a standard unit hydrograph technique, or by conceptual modeling, has an unknown return period. This comes from the combination of a peak and a volume whose cross correlation is not unity. This is a serious limitation because most analyses of floods and designs involving floods require

[1]Prof., Dept. of Civ. Engrg., Univ. of Stellenbosch, Stellenbosch 7600, South Africa.
[2]Engr., Dept. of Water Affairs, Pretoria.

Note.—Discussion open until November 1, 1981. To extend the closing date one month, a written request must be filed with the Manager of Technical and Professional Publications, ASCE. Manuscript was submitted for review for possible publication on July 22, 1980. This paper is part of the Journal of the Hydraulics Division, Proceedings of the American Society of Civil Engineers, ©ASCE, Vol. 107, No. HY6, June, 1981. ISSN 0044-796X/81/0006-0759/$01.00.

that the return periods of the floods be known. The importance of relating flood peaks and flood volumes was also expressly stated in Ref. 10. The few efforts towards extracting the composite flood hydrographs with the desired return period (5,7), were not very satisfactory, which highlights the limitations in the unit hydrograph technique.

The problem addressed in this paper, therefore, involves two related variables, namely flood peaks and their associated volumes. It is immediately apparent that more than one combination of flood peak and flood volume may have exactly the same probability of being jointly exceeded. For example, a relatively large flood peak combined with a small volume may have the same return period as an equally large volume combined with a small peak. (Here, and in what follows, "return period" means the reciprocal of the probability of joint exceedance of peak and associated volume.) This means that for each catchment there exists a possible family of hydrographs for any selected return period. The design hydrograph obtained by unit hydrograph technique may be only one member of one of the families.

A method which demonstrates the extraction of such families of hydrographs from the flow record of a river was described in a previous paper (7). In this paper, the authors assumed a fixed shape for all the hydrographs and they described the return periods for the hydrographs in terms of a bivariate lognormal probability distribution in peaks and surplus run lengths at a selected base value. The volume of flood runoff, although not directly modeled, follows from the assumed shape of the hydrograph. This method was not entirely satisfactory because the assumed hydrograph shape looked unnatural and the method resulted in a general underprediction of flood volumes. The direct identification of the flood volume as one variable in the bivariate description, instead of indirectly, should improve the method.

This paper reports on the results obtained during the analysis of the instantaneous continuous streamflow records of 43 selected South African catchments. Altogether 1,172 individual flood hydrographs were analyzed, from catchment sizes ranging from 10 sq mile–41,730 sq mile (26 km^2–108,081 km^2).

Theoretical Basis

Bivariate Lognormal Probability Distribution.—The bivariate lognormal probability distribution function was selected as a possible suitable descriptor for the flood peaks and their associated volumes. This function is relatively easy to manipulate, and experience has shown that the univariate lognormal often satisfactorily describes the probability distribution of flood peaks. Use of the standardized form of the bivariate normal function on the natural logarithms of the flood peaks and volumes makes comparisons across many catchments possible. This function in standardized form (7) is

$$f_{xy}(x, y) = \frac{1}{2\pi\sqrt{1-\rho_{uv}^2}} \exp\left[\left(\frac{-1}{2(1-\rho_{uv}^2)}\right)(x^2 - 2\rho_{uv}xy + y^2)\right] \quad \ldots\ldots (1)$$

in which $x = (u - \mu_u)/\sigma_u$ and $y = (v - \mu_u)/\sigma_v$ = the standardized values of the two variables u and v, respectively. In this application, u represents the natural logarithm of the flood peaks; v represents the natural logarithm

of the associated flood volumes; μ_u and μ_v represent the means; σ_u and σ_v represents the standard deviations of the variables u and v, respectively; and ρ_{uv} represents the cross correlation coefficients for the variables.

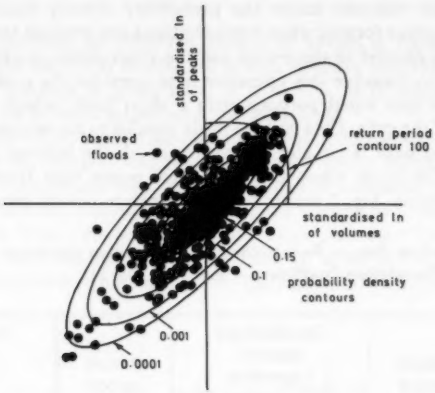

FIG. 1.—Contours of Standardized Bivariate Normal Function with Observed Floods Shown and Cross Correlation = 0.85

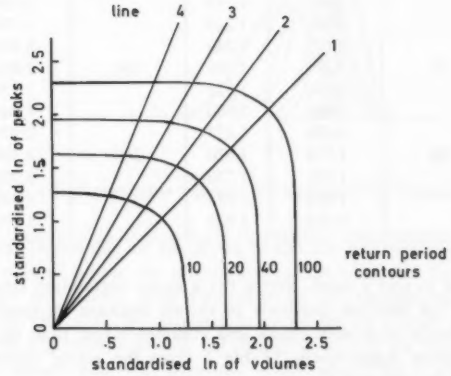

FIG. 2.—Bivariate Return Period Contours in Positive Quadrant of Standardized cdf with Cross Correlation = 0.85

Fig. 1 shows the bivariate normal density function for a cross correlation coefficient of 0.85 in the form of equal probability contour lines. On this figure, the standardized flood peaks, x, and their associated standardized volumes, y, for the 43 selected catchments are shown. (Note that data of several catchments with different ρ are shown; thus the return period contours are only valid for those catchments with $\rho = 0.85$.)

For practical applications it is useful to present results in terms of return periods. Lines of equal return periods can be obtained through volume integration under relevant parts of the probability density function. An integration method as described by Tihansky (12) was used. This method seeks points which define stipulated equal volumes under the probability density function within the north-easterly space formed when vertical planes are dropped through this point, with one plane parallel to the y-axis and the other plane parallel to the x-axis. (An easy way to visualize this operation is to consider the problem of dividing part of a cake into equal portions with a short knife which does not reach to the center of the cake. Cuts must be made parallel to the rectangular coordinate axes, and if the cake is circular and symmetrical, the leftover part must again be circular.) The locus which connects these points then forms a contour of equal return period. Fig. 2 shows such equal return period lines in the positive

TABLE 1.—Bivariate Return Period Contours in Positive Quadrant of Standardized cdf with Cross Correlation Coefficient = 0.85 (See Fig. 2)

Line (1)	Return period contour (2)	Standardized Natural Logarithm		Return period contour (5)	Standardized Natural Logarithm	
		Volume (3)	Peak (4)		Volume (6)	Peak (7)
1	10	1.040	1.040	50	1.790	1.790
2		0.880	1.142		1.500	1.954
3		0.700	1.210		1.170	2.024
4		0.520	1.246		0.850	2.046
1	20	1.390	1.390	100	2.050	2.050
2		1.180	1.522		1.720	2.236
3		0.930	1.600		1.340	2.304
4		0.680	1.627		0.970	2.322
1	30	1.570	1.570	200	2.300	2.300
2		1.330	1.720		1.920	2.494
3		1.040	1.795		1.480	2.560
4		0.760	1.822		1.070	2.573

quadrant of the x- and y-axes system for a cross correlation coefficient equal to 0.85. Only the positive quadrant is shown because engineers are mostly interested in floods with both peaks and volumes larger than the mean of the peaks and volumes respectively. (Table 1 gives the actual values on the line crossings with the contours.)

If the lognormal bivariate probability distribution function is found suitable for the description of the joint occurrences of flood peaks and volumes, then Fig. 2 and similar figures for different cross correlation coefficients can be used for practical applications, as demonstrated later in this paper. The chi-square test was used as a criterion for the goodness of fit. The chi-square test is sensitive to the number of class intervals (CI) selected, but a guide to the number of CI to be used is given by Sturgess (11) as

$$CI = 3.3 \log_{10} k + 1 \quad \text{. . . . . (2)}$$

in which k represents the number of events under consideration. The chi-square value is given by

$$\chi^2 = \sum_{i=1}^{k} \frac{(O_i - E_i)^2}{E_i} \quad \ldots\ldots\ldots\ldots\ldots\ldots\ldots\ldots\ldots\ldots\ldots\ldots\ldots\ldots\ldots\ldots (3)$$

in which O_i represents the observed number of events in class interval i; and E_i represents the expected number of events in class interval i. The number of degrees of freedom is given by $\gamma = k - 1 - m$ in which m represents the number of parameters estimated from the sample.

The magnitude of the base value (the level used to decide which floods should be admitted to the sample) was found to have a strong influence on the way the data fitted the bivariate lognormal distribution as measured by the chi-square test. By trial and error, a suitable base value can usually be found which ensures a reasonable fit. Fig. 3 shows this trial and error procedure for the Vaal River at Standerton, with catchment area of 3,187 sq miles (8,254 km^2). The test was applied at the 95% significance level. The figure shows the density functions

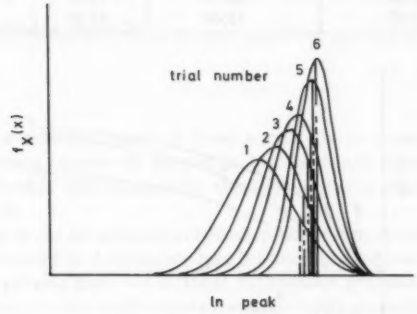

FIG. 3.—Trial and Error Solution for Suitable Truncation Level

for the natural logarithms of the flood peaks for various base values; Table 2 gives information about the chi-square values obtained for each trial and the percentage truncation. (The estimation of the parameters of the density functions from the truncated samples is explained in a later paragraph.) The base value which gives the lowest chi-square value for the bivariate lognormal function was usually selected, provided it was above the 1.5-yr return period peak, gave a reasonable chi-square fit for the peaks and was not unrealistically high. For the example shown on Fig. 3, trial number 6 was selected which truncates 44.7% of the probability density function. (The 1.5-yr return period for peaks was selected as a lower truncation limit to ensure independence between successive hydrographs in the streamflow record.)

Out of the 43 selected catchments, only one catchment could not satisfy the chi-square test for peaks, and only 2 stations could not satisfy the chi-square test for the bivariate lognormal distribution. The flood volumes did not fit so well, but the overall fit was considered satisfactory. The cross correlation

coefficients for the logarithms of peaks and their associated volumes for each of the 43 selected stations varied from a value of 0.4–0.9 with a mean of 0.78 and a standard deviation of 0.12.

Base Value.—It is desirable to use as much information in the streamflow record as possible. This means using a partial duration series of flood events

TABLE 2.—Iteration Procedure to Find Best Truncation Level (See Fig. 3)

Trial number (1)	χ^2 for natural logarithm peaks (2)	χ^2 for natural logarithm volumes (3)	Bivariate χ^2 (4)	Truncation, as a percentage (5)
1	7.01	1,698.48	218.64	88.2
2	5.91	1,080.60	113.28	81.9
3	6.06	93.98	113.61	76.1
4	3.43	176.39	61.68	70.0
5	6.59	74.79	23.71	52.3
6	4.16	38.75	14.39	44.7
7	2.97	73.64	33.16	61.5

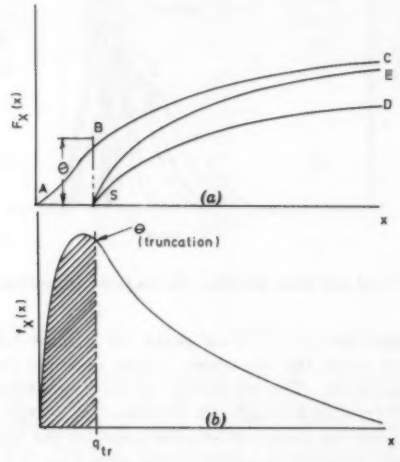

FIG. 4.—Relations between Distributions of Total Populations and Truncated Populations

with a relatively low base value instead of an annual series of floods. This also implies that the return period, in years, is not simply equal to the reciprocal of the exceedance probability. Using a partial duration series of floods results in truncation of the population probability density function, with the truncation given by the level below which the flood events are ignored. Fig. 4(*b*) shows this truncated probability density function. Integration of the truncated density

function results in the cumulative distribution function (cdf) shown in Fig. 4(*a*) by curve SD, whereas the integration of the full (untruncated) density function results in line ABC as the cdf.

The curve SE is the conditional cdf formed by normalization. Note that for very big floods the cumulative probabilities for both the partial duration series (given by SE) and the annual series (given by ABC) approximately coincide.

It is fairly easy to correct the partial duration series return periods so that the return periods are given in years. By assuming that the arrival of flood events, which exceed the truncation level, is a Poisson process, it can be shown (4) that

$$F_j(x) = \exp\{-\lambda[1 - F_s(x)]\} \quad \ldots\ldots\ldots\ldots\ldots\ldots\ldots\ldots\ldots\ldots (4)$$

in which $F_j(x)$ represents the cdf of the annual series of events; $F_s(x)$ represents the cdf derived from the associated partial duration series of events; and λ represents the mean number of events which arrive per year in the partial duration series. The exceedance probability is given by the survival function

$$G_j(x) = 1 - F_j(x) \quad \ldots\ldots\ldots\ldots\ldots\ldots\ldots\ldots\ldots\ldots\ldots\ldots\ldots (5)$$

and the return period in years by

$$T_R(x) = \frac{1}{G_j(x)} \quad \ldots\ldots\ldots\ldots\ldots\ldots\ldots\ldots\ldots\ldots\ldots\ldots\ldots\ldots (6)$$

The assumption that the arrival of flood events above a suitable base value is a Poisson process, seems to be acceptable for South African catchments (5) and in fact, further confirmation for this assumption is provided by Cramer and Leadbetter (3).

For application to the bivariate exceedance probabilities consider Fig. 4. Note that the shaded area of Fig. 4 corresponds to the univariate exceedance probability for variable x. Applying Eqs. 4–6 to these exceedance probabilities is therefore all that is necessary to relate the bivariate partial duration exceedance probabilities to the annual exceedance probabilities and thus to the return periods, in years. This becomes more clear in a later section of the paper when the application of the theory is demonstrated on an actual catchment.

The truncation of the streamflow records also complicates the parameter estimation for the bivariate normal probability distribution. The problem is, namely, to estimate the untruncated population parameters from a truncated sample. (The writers are of the opinion that this complication is well worth the effort because a more realistic fit of the large events to the selected probability distribution function usually results. This means a slight emphasis of the large events by truncation of the small events.)

Parameter Estimation.—The necessary parameters for the standardized bivariate normal distribution function are the means and standard deviations of the natural logarithms of the flood peaks and their associated volumes, respectively, as well as their cross correlation coefficient. To relate the partial duration series return periods to the annual return periods we need, in addition, the mean number of flood events per year as well as the percentage truncation. This brings the number of parameters to be estimated from the data to a total of 7 for each catchment.

It is desirable to select the base value in such a way that successive hydrographs are independent from each other. Serial independence greatly simplifies inferences about probabilities of occurrences of hydrographs. It was found by the senior writer (5) that consecutive surplus run lengths on horizontal truncation levels tend to become less serially dependent with higher truncation level. At a base value of about 1.5-yr return period peak, these surplus run lengths are already serially uncorrelated. With this as a guide, and the desire to get a reasonable fit of the data to the bivariate lognormal distribution, base values can be selected. In other words, for each catchment a base value can be selected which ensures that the hydrographs which protrude through it are almost serially independent while at the same time giving a reasonable good fit to the bivariate lognormal distribution in peaks and volumes. This level is called $\hat{q}_{tr}$ and its logarithm $\hat{u}_{tr}$. (This juggling of base values merely to satisfy the chi-square test, is perhaps not justified, due to the small size of the samples generally available. A base value can be fixed at, e.g., the 1.5-yr return period peak value for all the catchments under study.)

With the base value selected, it follows that a flood hydrograph can be defined as the locus described by the discharge rate between an up crossing and a down crossing on this base value. This locus is then extended from the base value to the zero flow level. The hydrograph peak is the highest point on this curve. The area under this curve gives the volume of the flood. No effort was made to separate the baseflow from the hydrograph, because the baseflow forms part of the flood and must be included. Furthermore, at this stage it was not envisaged to predict run hydrograph families from the causative rainfall and the inclusion of baseflow therefore does not present a problem. For the calculation of the total flood volume, both the rising limb and the recession limb of the hydrograph had to be extended from the truncation level to zero flow level. Various methods were tried and eventually a satisfactory method was adopted. For this method, weighted average slopes were calculated for the rising and recession limb of the hydrograph, respectively. Slopes were weighted in accordance with the lengths of portions of the limb, above the truncation level, which exhibits more or less the same slope. The rising limb was then extrapolated downwards at its weighted slope from the first point below the truncation level where a reversal in slope occurs. The recession limb was likewise extrapolated. For most of the flood hydrographs analyzed, the base value was at a relatively low discharge rate, compared to its peak, so that this rather arbitrary extension of the hydrograph limbs to zero flow level could not have a large effect on the total flood volume. It was thus possible to extract all the peaks and volumes for all the hydrographs exceeding q_{tr} in an objective manner by automatic computation.

The peaks, q_o, and the volumes, w, for the truncated streamflow record for each catchment are therefore available. From this data, parameters must be estimated for the untruncated population. Aitchison and Brown (1) explained how the maximum likelihood estimates of these parameters can be obtained with the help of specially constructed tables. They also referred to an iterative procedure, based on the Newton-Raphson method, which can accomplish the same objective without the use of tables.

Assume that there are n pairs of observations, u_i, v_i, with $i = 1, 2, \ldots n$, in which $u_i > u_{tr}$ = the sequence of logs of flood peaks exceeding the

log of the truncation level; and v_i = the logs of the associated volumes. The estimation procedure is summarized as follows, following Cohen (2):

$$\text{Define} \quad \Phi(t) = (\sqrt{2\pi})^{-1} \exp\left(\frac{-t^2}{2}\right) \quad \ldots\ldots\ldots\ldots\ldots\ldots\ldots\ldots (7)$$

the standard normal density function and

$$G(\xi) = \int_{\xi}^{\infty} \Phi(t)\, dt \quad \ldots\ldots\ldots\ldots\ldots\ldots\ldots\ldots\ldots\ldots\ldots\ldots\ldots\ldots (8)$$

the normal survivor function. In terms of these functions

$$Z(\xi) = \frac{\Phi(\xi)}{G(\xi)} \quad \ldots\ldots\ldots\ldots\ldots\ldots\ldots\ldots\ldots\ldots\ldots\ldots\ldots\ldots\ldots (9)$$

From the data calculate

$$v_k = \sum_{i=1}^{n} \frac{(u_i - u_{tr})^k}{n}, \quad k = 1, 2 \quad \ldots\ldots\ldots\ldots\ldots\ldots\ldots\ldots\ldots\ldots (10)$$

and then estimate $\hat{\xi}$ from the implicit formula

$$\frac{1 - \xi(Z - \xi)}{(Z - \xi)^2} - \frac{v_2}{v_1^2} = 0 \quad \ldots\ldots\ldots\ldots\ldots\ldots\ldots\ldots\ldots\ldots\ldots\ldots (11)$$

which can be achieved by any convenient root-finding technique such as bisection.

Then calculate directly

$$\hat{\sigma}_u = \frac{v_1}{Z - \hat{\xi}}$$

$$\hat{\mu}_u = \hat{u}_{tr} - \hat{\sigma}_{tr}\hat{\xi} \quad \ldots\ldots\ldots\ldots\ldots\ldots\ldots\ldots\ldots\ldots\ldots\ldots\ldots\ldots (13)$$

giving estimations of the population parameters of the logs of the peaks. However, to get the joint distribution of peaks and volumes the following is necessary.

Calculate the sample statistics

$$\bar{u} = \sum_{i=1}^{n} \frac{u_i}{n} \quad \ldots\ldots\ldots\ldots\ldots\ldots\ldots\ldots\ldots\ldots\ldots\ldots\ldots\ldots\ldots (14)$$

$$\bar{v} = \sum_{i=1}^{n} \frac{v_i}{n} \quad \ldots\ldots\ldots\ldots\ldots\ldots\ldots\ldots\ldots\ldots\ldots\ldots\ldots\ldots\ldots (15)$$

$$\bar{s}_u^2 = \sum_{i=1}^{n} \frac{(u_i - \bar{u})^2}{n} \quad \ldots\ldots\ldots\ldots\ldots\ldots\ldots\ldots\ldots\ldots\ldots\ldots\ldots\ldots (16)$$

$$\bar{s}_v^2 = \sum_{i=1}^{n} \frac{(v_i - \bar{v})^2}{n} \quad \ldots\ldots\ldots\ldots\ldots\ldots\ldots\ldots\ldots\ldots\ldots\ldots\ldots\ldots (17)$$

$$\bar{r} = \sum_{i=1}^{n} \frac{(u_i - \bar{u})(v_i - \bar{v})}{(n\bar{S}_u - \bar{S}_v)} \quad \ldots\ldots\ldots\ldots\ldots\ldots\ldots\ldots\ldots\ldots\ldots\ldots\ldots (18)$$

Then, defining

$$\hat{\alpha} = \bar{v} \quad \ldots \quad (19)$$

$$\hat{\beta} = \frac{\bar{r}\,\bar{s}_v}{\bar{s}_u} \quad \ldots \quad (20)$$

and $$\hat{\sigma} = \bar{s}_v \sqrt{1 - \bar{r}^2} \quad \ldots \quad (21)$$

the estimates of the remaining population parameters can be computed from

$$\hat{\mu}_v = \hat{\alpha} + \hat{\beta}(\hat{\mu} - \bar{u}) \quad \ldots \quad (22)$$

$$\hat{\sigma}_v = (\hat{\sigma}^2 + \hat{\sigma}_u^2 \hat{\beta}^2)^{1/2} \quad \ldots \quad (23)$$

$$\hat{\rho} = \frac{\hat{\sigma}_u \hat{\beta}}{\hat{\sigma}_v} \quad \ldots \quad (24)$$

The five parameters for the untruncated population which follows the bivariate lognormal probability distribution can therefore be estimated from a truncated sample.

The remaining parameter, namely the average number of events which occur per year in the truncated sample, is easily obtained by counting. Note that $\hat{q}_{tr}$ is found by iteration, in the sense that the best fit of the bivariate lognormal distribution, as defined by the chi-square test, fixes the optimum $\hat{q}_{tr}$.

With the flood peaks and their associated flood volumes satisfactorily described by a probability distribution function, it only remains to describe the time distribution of runoff rates for each pair.

The Pearson Type III function, with which engineers are familiar, has a shape that resembles the average flood hydrograph shape. This function is also more flexible than two parameter functions and it was previously used to describe hydrographs by Yevjevich (13) and Reich (9). For the purpose of this paper, it was decided to follow Reich closely. To fit hydrograph shapes, the Pearson Type III function can be expressed as

$$q = q_o e^{-t/G} \left(1 + \frac{t}{m}\right)^{m/G} \quad \ldots \quad (25)$$

in which q represents the flow rate at any time t_i; q_o represents the peak discharge rate; m represents the time from the beginning of the hydrograph to the peak; and G represents the time from the peak to the centroid of the hydrograph. Fig. 5 shows equation 25 and its parameters. Integration of Eq. 25 results in the flood volume as

$$w = q_o e^{m/G} \left(\frac{G}{m}\right)^{m/G} G\,\Gamma\left(1 + \frac{m}{G}\right) \quad \ldots \quad (26)$$

in which $\Gamma(\cdot)$ = the gamma function. According to Eq. 26, when for a particular flood, the volume, w, and the peak, q_o, are known, then G and m are uniquely related. Consequently, only one extra parameter besides q_o and w is necessary to describe a hydrograph uniquely, namely either m or G. The parameter G is expected to be a function of w and q_o, and also of some catchment properties. To this end, various forms of linear and nonlinear regressions were performed,

without much success. Eventually, it was decided to simply regress G on w and q_o and to ignore catchment properties. This means that the original three-parameter function selected to describe the hydrograph shape, degenerates to a two-parameter function, but considerable simplification in applications results. The final equation was

$$\ln G = -18.1129 + 8.336 \ln (\ln w - \ln q_o) \quad \ldots \ldots \ldots \ldots \ldots \ldots \quad (27)$$

with $R^2 = 0.72$.

Here, w is in cubic meters, q_o in cubic meters per second, and G is in hours ($1\ m^3 = 35.31$ cu ft). This equation is based on 1,112 hydrographs with positive G. A few hydrographs with negative G were excluded from this part of the analysis.

For properly-gaged catchments, all the necessary parameters can therefore be estimated. With q_o, w, and thus, G chosen for a desired hydrograph, it

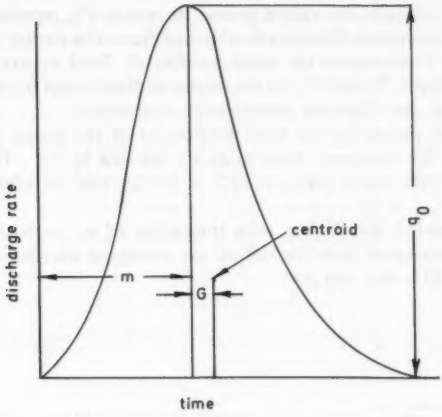

FIG. 5.—Hydrograph Shapes Defined

is possible to find the time to peak, m, from Eq. 26. Proceed as follows following Reich (9).

Eq. 26 can be rewritten as

$$\alpha' = \frac{\left(\frac{w}{q_o}\right)}{G} \quad \ldots \ldots \ldots \ldots \ldots \ldots \ldots \ldots \ldots \ldots \ldots \quad (28)$$

$$\text{in which} \quad \alpha' = e^{m/G} \left(\frac{G}{m}\right)^{m/G} \Gamma\left(1 + \frac{m}{G}\right) \quad \ldots \ldots \ldots \ldots \ldots \quad (29)$$

Thus, given q_o and w, find G from Eq. 27 and then compute α' from Eq. 28. The ratio m/G is then found from Eq. 29 or by using Fig. 6. The hydrograph shape follows from Eq. 25.

Application

For a fully-gaged catchment, all the necessary parameters can be estimated as described and the application is straightforward. If a partial duration series of floods is used to obtain the parameters, then the return period contours of Fig. 2, which also appears in Table 1, do not necessarily give the return period in years. To get the desired return period in years, T_R, the selection of the correct return period contours, T_{R1}^{II}, to use information from Table 1, can be obtained through the relationship given as Eq. 4. For convenience, Eqs. 4 and 6 can be rewritten as

$$T_R = \frac{1}{1 - \exp\left[-\lambda\left(\frac{1}{T_R^I}\right)\right]} \quad \ldots\ldots\ldots\ldots\ldots\ldots\ldots\ldots\ldots\ldots \quad (30)$$

in which T_R represents the return period, in years; T_R^I represents the return period for the truncated distribution obtained from the partial duration series of floods; and λ represents the mean number of flood events per annum in the truncated sample. To find T_R^I for the truncated distribution from the underlying total distribution, the following manipulation is necessary.

Let the return period for the total distribution of the partial duration series estimated from the truncated distribution be denoted by T_R^{II}. The exceedance probability for this return period is $G_s^{II} = 1/T_R^{II}$, and therefore, $F_s^{II} = 1 - G_s^{II}$.

For the truncated distribution with truncation of q_{tr} such that $F^{II}(q_{tr}) = \hat{\Theta}$ is the area truncated then the cdf of the truncated distribution is given by $F_s^I = (F_s^{II} - \hat{\Theta})(1 - \hat{\Theta})$, and thus

$$T_R^I = \frac{1}{(1 - F_s^I)}$$

$$T_R^I = \frac{1}{1 - \left(\frac{F_s^{II} - \hat{\Theta}}{1 - \hat{\Theta}}\right)} \quad \ldots\ldots\ldots\ldots\ldots\ldots\ldots\ldots\ldots\ldots \quad (31)$$

Use of Eqs. 30 and 31 in a trial and error procedure will then allow the calculation of the correct return period contour which must be selected from Table 1 in order to produce the family of run hydrographs with the desired return period.

An approximate way to obtain the desired return period contour comes from simply assuming that the number of events below the truncation level is proportional to those counted above the truncation level. That means the number of events expected per year over the full (untruncated) sample will be

$$\hat{\lambda}^I = \frac{\hat{\lambda}}{(1 - \hat{\Theta})} \quad \ldots\ldots\ldots\ldots\ldots\ldots\ldots\ldots\ldots\ldots\ldots\ldots \quad (32)$$

An approximation to T_R^{II} which will result in the desired T_R is now simply

$$T_R'' = \hat{\lambda}' T_R = \frac{T_R \hat{\lambda}}{(1 - \Theta)} \quad \text{(33)}$$

or, accurately

$$T_R'' = \frac{\hat{\lambda}}{(1 - \hat{\Theta}) \ln \left(1 - \frac{1}{T_R} \right)} \quad \text{(34)}$$

so that given $\hat{\lambda}$ and $\hat{\Theta}$, from the data, and the desired T_{R1}, then T_R'' is the curve to use. The following example should clarify the ideas.

Example.—Assume that a T_R = 50-yr return period family of hydrographs is desired for the Vaal River at Standerton. From the streamflow record, the following information is known: (1) Mean of ln peaks, $\hat{\mu}_u = 6.162$; (2) standard deviation of ln peaks, $\hat{\sigma}_u = 0.678$; (3) mean of ln volumes, $\hat{\mu}_v = 10.158$; (4) standard deviation of ln volumes, $\hat{\sigma}_v = 0.907$; (5) cross correlation coefficient, $\hat{\rho}_{uv} = 0.847$; (6) area of truncation, $\hat{\Theta} = 0.447$; (7) number of events in the

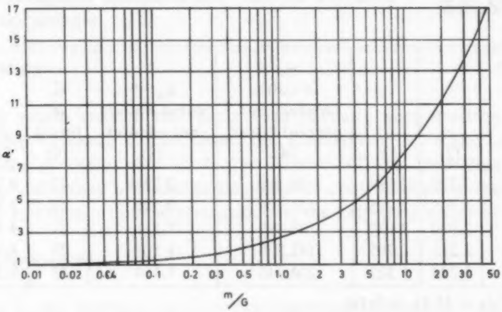

FIG. 6.—Aid to Solve for G When w, q, and m are Known

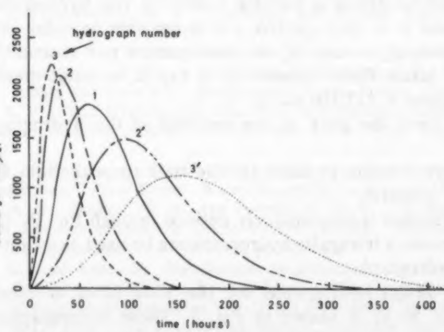

FIG. 7.—Few Members of Family of Hydrographs with Return Period of 50 yr

truncated sample = 56; and (8) number of years in the record = 54.

Calculations.—The following calculations can be made.

1. The mean number of events per year in the truncated sample, $\lambda = 56/54 = 1.037$.

2. Use of Eq. 32 gives the mean number of events in the underlying untruncated distribution: $\lambda^1 = 1.037/(1 - 0.447) = 1.875$.

3. The contour to use on Table 1 is therefore from Eq. 33: $T_R^{11} = 1.875 \times 50 = 94$.

4. As a check, use $T_R^{11} = 94$ in Eq. 31 to obtain T_R^1, in which $F_3^{11} = 1 - 1/T_R^{11} = 1 - 1/94 = 0.989$. So $T_R^1 = 1/\{1 - [(0.989 - 0.447)/(1 - 0.447)]\} = 51.982$. Use this value in Eq. 30 to obtain T_R: $T_R = 1/\{1 - \exp[-1.037(1/51.982)]\} = 50.6$ yr, which is close enough to the desired 50 yr.

5. Select pairs of the standardized variables x and y from Table 1 on the 94 contour (interpolate linearly for approximation between the 90 contour and the 100 contour) to define a suitable family of run hydrographs. Since $x = (u - \hat{\mu}_u)/\hat{\sigma}_u$ and $y = (v - \hat{\mu}_v)/\hat{\sigma}_v$, it is possible to solve directly for the actual flood peak, $q_o = \exp \hat{\mu}_u$ in cubic meters per second (1 m^3 = 35.31 cu ft). For the actual flood volume: $w_o = \exp \hat{\mu}_v$ in cubic meters per second hours (1 m^3/s hour = 127,116 cu ft).

TABLE 3.—Parameters for Family of Hydrographs with 50-Yr Return Period for Vaal River at Standerton

Hydrograph number (selected line) (1)	y (2)	x (3)	w_o, in cubic meters per second hours (4)	q_o, in cubic meters per second (5)	G, in hours (6)	α^1 (7)	m/G, in hours (8)
3	1.325	2.284	55,800	2,231	12	4.20	1.8
2	1.705	2.215	121,108	2,120	16	3.55	2.0
1	2.030	2.030	162,199	1,878	21	4.11	2.8
2^1	2.215	1.705	192,320	1,507	27	4.73	3.5
3^1	2.284	1.325	204,740	1,164	33	5.33	4.5

Note: (1 m^3/s = 35.31 cu ft/s).

6. The time from the peak to the centroid of the hydrograph is given by Eq. 27.

7. It now only remains to solve for the time to peak from Eqs. 28 and 29 in which Fig. 6 is useful.

8. Each hydrograph is now uniquely defined through Eq. 25. Otherwise, with q_o, w, and m known a triangular hydrograph ma be used as a first approximation to the design hydrograph.

A family of design hydrographs for the Vaal River at Standerton with a return period of 50 yr is shown in Fig. 7. These hydrographs are from the parameters which appear in Table 3. Note that hydrographs 2^1 and 3^1 are from mirror images of lines 2 and 3 on Fig. 2.

Conclusions

Run hydrograph theory was developed and demonstrated for application on fully-gaged catchments. The method allows for the synthesis of the whole family of design hydrographs for each desired return period. It is suggested that a few members of the family of design hydrographs with the desired return period be considered in practical applications instead of only the one member of the family with the highest peak. This method should be especially useful in flood problems where the flood volume plays a part.

In the development of the theory, hydrographs were analyzed as they occur in the record; thus the sample of hydrographs contains many composite hydrographs. This should result in realistic design hydrographs for practical applications.

In the estimation of the necessary parameters it was demonstrated how straightforward it can be to calculate the underlying probability distribution parameters from a truncated sample. Truncation is perhaps useful to emphasize the effect of the larger floods on the distribution and to ignore the smaller floods.

The run hydrograph technique may also be amenable towards extrapolation to ungaged catchments.

Acknowledgments

The study which lead to this paper was partially supported by the South African Water Research Commission, the Department of Water Affairs, and the University of Natal (6). G. G. S. Pegram of the Department of Civil Engineering, University of Natal made valuable contributions to the study. The writers wish to express their appreciation for the help they received.

Appendix I.—References

1. Aitchison, J., and Brown, J. A. C., "The Lognormal Distribution," *Monograph No. 5*, Cambridge University Press, Cambridge, England, 1976, pp. 87–90.
2. Cohen, A. C., "Restriction and Selection in Samples from Bivariate Normal Distributions," *Journal of the American Statistical Association*, No. 50, 1955, pp. 884–893.
3. Cramer, H., and Leadbetter, M. R., *Stationary and Related Stochastic Processes*, John Wiley and Sons, Inc., New York, N.Y., 1967, p. 259.
4. Dyck, S., and Kluge, C. R., "Investigations on the Structure of Frequency Distributions of Floods," *Mathematical Models in Hydrology*, Proceedings of the Warsaw Symposium, Vol. 1., Adlard and Sons Ltd., Bartholomew Press, Surrey, England, 1971.
5. Hiemstra, L. A. V., "Run Hydrographs from Poisson Generated Runlengths," *Journal of the Hydraulics Division*, ASCE, Vol. 100, No. HY11, Proc. Paper 10959, 1974, pp. 1617–1630.
6. Hiemstra, L. A. V., and Francis, D. M., "The Runhydrograph—Theory and Application for Flood Predictions," *Final Report*, Water Research Commission, Pretoria, 1979.
7. Hiemstra, L. A. V., Zuchini, W. S., and Pegram, G. G. S., "A Method of Finding the Family of Runhydrographs for Given Return Periods," *Journal of Hydrology*, Amsterdam, The Netherlands, No. 30, 1976, pp. 95–103.
8. Johnson, N. L., and Kotz, S., *Distributions in Statistics: Continuous Multivariate Distributions*, Houghton Mifflin Co., Boston, Mass., 1972, Chapter 36.
9. Reich, B. M., "Design Hydrographs for Very Small Watersheds from Rainfall," *Report No. CER 62 MNR 4150*, Civil Engineering Section, Colorado State University, Ft. Collins, Colo., 1962.
10. "Re-Evaluating Spillway Adequacy of Existing Dams," by the Task Committee on

the Re-evaluation of the Adequacy of Spillways of Existing Dams of the Committee on Hydrometeorology, R. W. Revell, Chmn., *Journal of the Hydraulics Division*, ASCE, Vol. 98, No. HY2, Proc. Paper 9571, 1973, pp. 337–372.
11. Sturges, H. A., "The Choice of the Class Interval," *Journal of the American Statistical Association*, Vol. 21, 1970, pp. 65–66.
12. Tihansky, D. P., "Properties of the Bivariate Normal Cumulative Distribution," *Rand Corporation Report*, Santa Monica, Calif., 1970.
13. Yevjevich, V. M., "Rate of Change of the Peak during Flood Progress along a Channel," *Memorandum to the United States Corps of Engineers, Geological Survey*, 1960.

Appendix II.—Notation

The following symbols are used in this paper:

A = catchment area in square kilometers (1 km^2 = 0.3861 sq mile);
E_i = expected number of events in class interval i;
F_f = probability distribution function for annual series of floods;
F_s = probability distribution function for partial duration series of floods;
f = probability density function;
G = time from hydrograph peak to its centroid, in hours;
G_f = exceedance probability distribution, $G_f = 1 - F_f$;
k = number of events;
m = time from beginning of flood hydrograph to its peak, in hours;
m^1 = number of parameters estimated from sample;
N = sample size;
n = sample size for truncated sample;
O_i = observed number of events in class interval i;
q = discharge rate in m^3/s (1 m^3/s = 35.31 cubic meters per second);
q_o = peak discharge rate in cu ft/sec;
q_{tr} = discharge rate in cu ft/sec at truncation level;
R^2 = coefficient of association between variables;
T_R = return period, in years;
T_R^1 = return period (not necessarily in years);
T_R^{11} = return period as approximation of T_R^1;
t = time;
u = natural logarithm of flood peaks;
u_{tr} = natural logarithm of discharge at truncation level;
v = natural logarithm of flood volumes;
w = flood volume in cubic meters (1 m^3 = 35.31 cu ft);
w_o = flood volume in cubic meters per second hours (1 cubic meters per second hour = 35.31 cu ft/sec hours);
x = standardized natural logarithm for peaks, $x = (u - \mu_u)/\sigma_u$;
y = standardized natural logarithm for volumes $y = (v - \mu_v)/\sigma_v$;
$Z(\hat{\xi})$ = function in truncation $\hat{\xi}$;
$\hat{\alpha}$ = estimate of population mean flood;
α^1 = hydrograph characteristic which equals $(w_o/q_o)/G$;
$\hat{\beta}$ = estimate of population bivariate characteristic which equals $\rho\,\sigma_v/\sigma_u$;
$\Gamma(\cdot)$ = gamma function;
γ = number of degrees of freedom;
$\hat{\xi}$ = estimate of truncation level on pdf;
Θ = estimate of area of pdf truncated;

λ = mean number of events per year in truncated sample;
λ' = mean number of events per year in untruncated sample;
μ = population mean;
$\hat{\mu}$ = estimate of population mean;
ν = moments round truncation level;
σ = population standard deviation;
$\hat{\sigma}$ = estimate of population standard deviation;
ρ = population cross-correlation coefficient;
$\hat{\rho}$ = estimate of population cross-correlation coefficient;
$\Phi(t)$ = standard normal density function; and
χ^2 = chi-square.

DISCUSSION

Note.—This paper is part of the Journal of the Hydraulics Division, Proceedings of the American Society of Civil Engineers, ©ASCE, Vol. 107, No. HY6, June, 1981. ISSN 0044-796X/81/0006-0779/$01.00.

Discussions

Discussions may be submitted on any Proceedings paper or technical note published in any *Journal* or on any paper presented at any Specialty Conference or other meeting, the *Proceedings* of which have been published by ASCE. Discussion of a paper/technical note is open to anyone who has significant comments or questions regarding the content of the paper/technical note. Discussions are accepted for a period of 4 months following the date of publication of a paper/technical note and they should be sent to the Manager of Technical and Professional Publications, ASCE, 345 East 47th Street, New York, N.Y. 10017. The discussion period may be extended by a written request from a discusser.

The original and three copies of the Discussion should be submitted on 8-1/2-in. (220-mm) by 1!-in. (280-mm) white bond paper, typed double-spaced with wide margins. The length of a Di.cussion is restricted to two *Journal* pages (about four typewritten double-spaced pages of manuscript including figures and tables); the editors will delete matter extraneous to the subject under discussion. If a Discussion is over two pages long it will be returned for shortening. All Discussions will be reviewed by the editors and the Division's or Council's Publications Committees. In some cases, Discussions will be returned to discussers for rewriting, or they may be encouraged to submit a paper or technical note rather than a Discussion.

Standards for Discussions are the same as those for Proceedings Papers. A Discussion is subject to rejection if it contains matter readily found elsewhere, advocates special interests, is carelessly prepared, controverts established fact, is purely speculative, introduces personalities, or is foreign to the purposes of the Society. All Discussions should be written in the third person, and the discusser should use the term "the writer" when referring to himself. The author of the original paper/technical note is referred to as "the author."

Discussions have a specific format. The title of the original paper/technical note appears at the top of the first page with a superscript that corresponds to a footnote indicating the month, year, author(s), and number of the original paper/technical note. The discusser's full name should be indicated below the title (see Discussions herein as an example) together with his ASCE membership grade (if applicable).

The discusser's title, company affiliation, and business address should appear on the first page of the manuscript, along with the *Proceedings* paper number of the original paper/technical note, the date and name of the *Journal* in which it appeared, and the original author's name.

Note that the discusser's identification footnote should follow consecutively from the original paper/technical note. If the paper/technical note under discussion contained footnote numbers 1 and 2, the first Discussion would begin with footnote 3, and subsequent Discussions would continue in sequence.

Figures supplied by the discusser should be designated by letters, starting with A. This also applies separately to tables and references. In referring to a figure, table, or reference that appeared in the original paper/technical note use the same number used in the original.

It is suggested that potential discussers request a copy of the *ASCE Authors' Guide to the Publications of ASCE* for more detailed information on preparation and submission of manuscripts.

Dispersion in Rivers as Related to Storage Zones[a]

Closure by George V. Sabol,[6] A. M. ASCE and Carl F. Nordin, Jr.,[7] M. ASCE

The writers appreciate the interest shown by the discussers. Some interesting points are addressed about the proposed model and dispersion theory in general that need clarifying: the physical significance and time range of values for the model parameters, the relative importance of velocity distribution and storage mechanism, and the distinction between models that are time dependent and models with time dependent parameters.

The parameter δ was defined as a measure of the average number of times a particle goes into storage per unit time. The range of the value of δ, as shown in Fig. 3, is over three log cycles, which is large and is justly criticized in a physical sense for this. However, this range is for a parameter evaluated for the 51 cases reported in Ref. 13. The range of channel length and flow conditions for these 51 cases is shown in Table 4. The time range for δ then is approximately the same as the physical range for the data base. The ratio of δ_{max} to δ_{min} for each of the 51 cases (13) is shown in Table 5. This ratio for a particular case had a range from 1.6 to 33.5 with an average of 7.2, as opposed to a ratio of over 1,000 for all data as shown in Fig. 3. The variation of δ is an exponentially decreasing function of time that changes relatively quickly during the start of dispersion and then undergoes only moderate change thereafter.

The parameter a_u is a measure of the time a particle is moving downstream relative to the total transit time. Holly and Tsai state that there is no apparent physical reason for this parameter to be as small as 0.75. Fig. 1 shows the vertical velocity profile simulated by the storage model. With this simplified velocity distribution, the parameter a_u becomes a lumped parameter that also takes into account the zone of very low velocities along the bed and banks along with storage zones. Holly and Tsai also questioned the independence of stage on the value of a_u. Based on limited data, a_u was fairly constant for specific river reaches independent of discharge and therefore stage. This may be explained by a a_u being indicative of inherent roughness and storage zones which considered in regards to the total cross section may change proportionally with stage. The ratio of $a_{u_{max}}$ to $a_{u_{min}}$ for each of the 51 cases (13) is shown in Table 5.

The parameters vary systematically with time, however this does not change their physical significance. The initial phase of dispersion occurs during the highest concentration of tracer material, and there is therefore a high probability for a transfer of a large mass of dispersant into storage. The concentration

[a]May, 1978, by George V. Sabol and Carl F. Nordin, Jr. (Proc. Paper 13758).

[6]Assoc. Prof. of Civ. Engrg., New Mexico State Univ., Box 3CE/Las Cruces, N.M. 88003.

[7]Hydro., U.S. Dept. of the Interior Geological Survey, Box 15047, Water Resources Div., Stop 413, Denver Federal Center, Denver, Colo. 80225.

decreases with time and it seems likely that the rate of transfer into storage would also decrease with time.

Prytch states that the writers used stochastic variables about which little information exists. The two parameters, δ and a_u, are diffusion coefficients with real physical meaning; the fact that these coefficients are not the same as those developed and investigated by others should not be important. While numerous studies have been undertaken to document diffusion coefficients, the dispersion solution still eludes us. This suggests that the answer may be found in other approaches—divergent from the traditional.

The relative importance of a storage mechanism to dispersion is difficult to evaluate, and possibly dispersion studies are the most direct measure of the importance of the storage mechanism. The significance of this storage may best be illustrated by the amount of tracer material that is recovered at the most distant point downstream. The recovery ration, RR, is defined as the ratio of mass of tracer material measured at a site to the mass of tracer injected. The recovery ratio for each of the most distant monitoring site for the 51 cases (13) is shown in Table 5. There are numerous difficulties and assumptions in calculating a recovery ratio and in fact some recovery ratios are greater than

TABLE 4.—Ranges of Channel Length and Flow Conditions for 51 Tracer Studies (13) Used to Determine Model Parameters

Variable (1)	Minimum (2)	Maximum (3)
Length, in miles	2	183
Discharge, in cubic feet per second	34	241,000
Mean width, in feet	40	2,400
Mean depth, in feet	1	60
Mean velocity, in feet per second	0.43	5.5

one, however, the high incidence of low recovery ratios indicates that a storage mechanism may be highly significant in open-channel dispersion.

The intent of the proposed model was to incorporate a storage mechanism, not to negate the importance of the velocity distribution. The velocity distribution was simplified as shown in Fig. 1. Prytch suggests that the numeric solution method of Fischer (6) could be used to simulate these storage zones by employing one or more streamtubes of zero velocity. By that method the ratio of zero velocity streamtubes to total streamtubes would have to be determined, and no method was suggested or is known for implementation of this.

It has been generally argued for some time that the dispersion process in open-channel flow procedes in two phases. The initial phase, termed the convective or advective period is characterized by incomplete mixing of the tracer in the cross section and a skewed concentration distribution. The second phase, termed the diffusive, dispersive, or Fickian period, is to obey the laws of a Fickian process given by Eq. 1. It is convenient and even physically appealing to consider the dispersion process to occur in these two phases; however, in reality it is doubtful that there is a distinct change between these, rather the change is probably gradual. The dispersion process changes with time and either

TABLE 5.—Relative Mixing Time, Recovery of Tracer Material, and Range of Model Parameters for 51 Tracer Studies (13) Used to Determine Model Parameters

Case (1)	L/X (2)	RR (3)	$\delta_{max}/\delta_{min}$ (4)	au_{max}/au_{min} (5)
1	40.0	0.32	10.8	1.46
2	27.3	0.44	15.6	1.30
3	59.4	0.50	4.1	1.35
4	10.7	0.56	2.2	1.10
5	3.5	1.22	3.6	1.09
6	1.8	0.93	2.8	1.19
7	3.8	1.25	2.1	1.09
8	2.3	0.96	5.0	1.31
9	3.2	0.44	2.6	1.21
10	3.2	0.57	13.4	1.09
11	2.8	0.93	4.0	1.11
12	3.2	0.78	5.6	1.04
13	9.9	0.93	6.3	1.08
14	10.6	0.98	4.9	1.09
15	4.1	0.51	2.8	1.09
16	2.6	1.06	2.7	1.46
17	48.6	0.65	4.4	1.22
18	1.9	1.00	5.6	1.26
19	18.4	0.61	1.6	1.09
20	38.3	0.24	7.8	1.10
21	67.6	1.40	19.2	1.21
22	15.8	0.34	4.4	1.12
23	55.4	0.78	6.9	1.18
24	36.7	0.87	6.7	1.21
25	17.4	0.70	3.6	1.20
26	3.5	0.59	6.2	1.20
27	3.3	0.77	4.1	1.30
28	7.1	0.85	4.8	1.24
29	1.5	0.62	3.7	1.15
30	2.8	0.40	5.6	1.20
31	5.0	1.00	33.5	1.42
32	232.2	0.18	3.8	1.07
33	110.6	0.16	2.7	1.15
34	49.3	0.57	3.4	1.08
35	1.1	0.50	—	—
36	0.9	0.64	5.2	1.11
37	1.1	0.59	1.6	1.11
38	21.0	0.75	6.4	1.27
39	23.8	0.52	7.8	1.26
40	7.0	1.18	13.1	1.25
41	1.7	1.03	9.4	1.22
42	18.6	0.68	8.0	1.09
43	4.1	0.71	2.1	1.12
44	1.1	0.71	5.3	1.12
45	4.5	0.86	3.5	1.32
46	1.0	1.31	5.6	1.16
47	1.9	0.85	28.4	1.14

TABLE 5.—*Continued*

(1)	(2)	(3)	(4)	(5)
48	1.9	0.88	16.7	1.26
49	1.3	1.13	13.3	1.13
50	5.6	0.72	14.3	1.24
51	2.5	0.72	2.7	1.06
Maximum	232.2	1.40	33.5	1.46
Minimum	0.9	0.16	1.60	1.04
Mean	18.7	0.743	7.198	1.186
Standard deviation	37.4	0.288	6.46	0.103

Note: L/X = total reach length to mixing length; (RR) = mass of tracer recorded at last site to mass of tracer injected, and $\delta_{max}/\delta_{min}$ and $a_{u_{max}}/a_{u_{min}}$ = minimum values of parameters for each case.

the model or the parameters should also change with time for an adequate simulation of the process.

A period of time is required in the convective phase before the dispersant can be considered completely mixed. This mixing length can be approximated by Eq. 32

$$X = 1.8 \frac{l^2 \bar{V}}{R_h u_*} \quad \quad (32)$$

in which X = the distance downstream from the source; l = the distance from the point of maximum surface velocity to the farthest bank; R_h = the hydraulic radius; and u_* = the shear velocity. The ratio of reach length to mixing length, L/X, for the 51 cases is given in Table 5.

Of the 51 cases reported (13) only two of these took place entirely in the convective period defined by Eq. 32. Of the 51 cases the minimum ratio of reach length to mixing length was 0.9, the maximum ratio was 232, and the average ratio was 18. The coefficient of skew did decrease in many of these cases, but the distributions were still highly skewed at the end of the test reach even after having been in the dispersive period for a magnitude of time larger than the convective period. Many of the 51 cases considered had been in the dispersive phase for an excessively long period and yet did not in general behave according to a Fickian process.

In discussing the convective period, Prytch states that Eq. 2 is not appropriate during that time and that it is incorrect to apply Eq. 2 directly even after passing through the convective period; rather, the concentration distribution that exists at the end of the convective period must be used as the initial condition for the diffusive period. This distribution nor its location can be accurately determined whereas the model as presented by Eq. 31 is valid throughout the complete dispersion process.

Open-channel dispersion is often considered a one-dimensional Fickian process and solutions obtained by using Eqs. 1, 2, and 3. The application of these equations however are time dependent, that is, only valid after the initial convective period. Fickian theory, as applied to river dispersion, then is itself time dependent. The proposed model can be applied without consideration to

these convective or dispersive periods; however, the parameters are time dependent. It seems then that both procedures are in fact time dependent; one by virtue of model applicability and the other by virtue of the parameters.

Holly states that "the model should not be expected to be applicable outside of the ranges of conditions and objectives for which it was calibered." Table 4 summarizes the range of hydraulic conditions used to forumulate the parameters of the model. Applicability based on this should be quite high.

Theory of Minimum Rate of Energy Dissipation[a]

Closure by Chih Ted Yang[7] and Charles C. S. Song,[8] Members, ASCE

The writers appreciate the interests shown in the paper. There is no dispute about the fact that solutions based on the general theory of minimum rate of energy dissipation or its simplified versions are in good agreement with observed data from both laboratory flumes and natural rivers. However, it seems that the discussers are not satisfied with some of the assumptions and approaches used by the writers in their derivations. Most of the disagreements between the discussers and the writers stem from different interpretations of terms used in the derivation and the concept used in the paper which is different from vectorial mechanics. A general comparison between the vectorial approach and the variational approach will be made to clarify basic concepts. Specific questions raised by each discusser will then be replied to separately.

The science of mechanics has been developed along two main lines, i.e., the vectorial and the variational approaches. The vectorial mechanics approach starts directly from Newton's laws of motion. Force and momentum are the basic concern of the vectorial approach. Thus, the motion of a particle can be uniquely determined by the known forces acting on it at every instant. The variational approach to mechanics replaces the force by the work of the force or the work function which is frequently replaceable by potential energy. At the same time, the momentum of Newton is replaced by kinetic energy. The variational approach is a scalar approach. In this approach, the law of mechanics is stated as the minimization of the action integral. In a classical formulation, for a nondissipative system, the action integral is the integral of kinetic energy minus potential energy. The mathematical tool used in the vectorial approach is the equation of motion, while the calculus of variation is used in solving minimization problems. Because the minimum value depends on the constraints

---

[a]July, 1979, by Chih Ted Yang and Charles C. S. Song (Proc. Paper 14677).

[7]Civ. Engr., U.S. Dept. of the Interior, Water and Power Resources Service, Engrg. and Research Center, P.O. Box 25007, Building 67, Denver Federal Center, Denver, Colo. 80225.

[8]Prof. of Civ. Engrg., St. Anthony Falls Hydr. Lab., Univ. of Minnesota, Mississippi River at 3rd Ave., SE, Minneapolis, Minn.

which define the optimum path, the scalar approach is that of minimization with constraints instead of solving differential equations with boundary conditions.

Most of the recent developments in fluid mechanics and hydraulics are based on the vectorial approach. This approach is well suited to solving problems which can be described easily in a rectangular coordinate system, but becomes cumbersome for curvilinear coordinates. The process and resulting equations based on the scalar approach remain valid for an arbitrary choice of coordinates. For systems with constraints, the scalar approach is often simpler and more economical. Thus, the scalar or minimization approach is especially suitable for solving complicated problems of natural rivers. A more detailed discussion of the two approaches and their merits is given by Lanczos (46).

The general theory of minimum rate of energy dissipation states that when a system is in equilibrium, its rate of energy dissipation is at its minimum. This minimum value depends on constraints applied to the system. When the system is not in an equilibrium condition, its rate of energy dissipation is not at its minimum, but will decrease with respect to time and reach a minimum to regain equilibrium. Depending on the constraints and environment, there are different means by which a river can minimize its rate of energy dissipation (48). The theoretical derivations made by the writers in the paper are limited to the case that the only means available to the system to minimize the rate of energy dissipation is through the velocity distribution. The intention of the writers' derivations is to show that the variational or minimization formulation of the problem is equivalent to the use of the equation of motion for the case of nonaccelerating open channel or closed conduit flows.

Silberman seems to imply that because the developers in turbulent theories in the past did not use so simple a formula for the rate of energy dissipation, the writers' approach could not be justified. The formulation of Eq. 7*a* is based on Boussinesq's concept which makes it possible to define eddy viscosity for turbulent flows. Boussinesq's concept or assumption has been widely used in turbulent theories. Whether this concept can be directly used to formulate the rate of energy dissipation and the theory of minimum rate of energy dissipation depends on whether the theoretical velocity profiles thus obtained agree with those observed in turbulent flows. The writers' verifications (41) indicate that the theoretical velocity profiles are in good agreement with the measurements. The theory of minimum unit stream power should be applied to one-dimensional open channel flows with constant width where sediment concentration is not too high. Where the sediment concentration is high, the power required to transport sediment can no longer be ignored and be treated as a constraint. In this case, the rate of energy dissipation for both water and sediment should be considered. For most natural rivers with variable width, the theory of minimum stream power, which is also a special case of the general theory, should be applied. Chang (43,44) applied the theory of minimum stream power by trial and error to determine river pattern and regime channel geometry. His results agree very well with those observed in the field. All these verifications (43,44) were made for turbulent flows in natural rivers and regime channels.

Davies considered laminar flow to be a linear process; turbulent flow is not. Actually, laminar flow can be a linear or nonlinear process depending on whether the inertia term can be neglected. In the writers' derivation, the eddy viscosity ϵ was not assumed to be a constant, thus, the flow could be a nonlinear one.

Because ϵ represents the inertia effect of turbulence and is included in the derivation, the inertia effect was not completely ignored. That is, the inertia effect of the mean flow was ignored in the derivation but not the inertia effect due to turbulence.

Parker raised several interesting points about the application of the theory of minimum stream power and minimum unit stream power. He has indicated in subsequent conversations with the writers that his discussion should not be construed as being a blanket condemnation of the approach of power minimization. He feels that worthwhile results have been obtained, but that the positive aspects of some of these might have been exaggerated. Parker's discussion was addressed to several specific points, and not the concept as a whole. The writers never stated that the theory of minimum unit stream power is equivalent to the theory of minimum stream power. However, both are special and simplified versions of the general theory of minimum rate of energy dissipation. As a result of using Eqs. 29 and 30, Figs. 3 and 4 show that the measured values approach the theoretical values gradually with decreasing sediment concentration. When sediment concentration is close to zero or when the bed is at incipient motion, the observed values are identical to the theoretical values. The gradual transition of agreement between observed and theoretical values as a function of sediment concentration is an indication that the general theory could be applied to both rigid and movable boundary conditions and might bridge the gap between them. In the determination of velocity profiles of open channel flows, the writers (41) treated the boundary as rigid without sediment movement. For low to medium sediment concentration, as in the case shown in the original paper, sediment concentration was treated as a constraint to the system. For the more general case, the total rate of energy dissipation due to water and sediment transportation may have to be considered (49). For all the aforementioned three categories verified by the writers, observed values are in good agreement with those determined from the theory of minimum rate of energy dissipation or its simplified versions. Thus, the theory does have the potential to bridge the gap between rigid and movable boundary fluid mechanics.

The writers do not believe that they have confused the minimization of functional with the minimization of functions. A more detailed and rigorous treatment of functional and function was made by the writers in a recent paper (47). Theoretically speaking, the general theory of minimum rate of energy dissipation should be applied wherever it is possible and the theory of minimum stream power and the theory of minimum unit stream power are special cases of the general theory. These two simplified versions of the general theory can be applied under certain special conditions. Based on comparisons with river and channel data, the theory of minimum stream power can be applied to channels with variable width while the theory of minimum unit stream power can be applied to channels with constant width. Among the sediment transport equations tested by the writers, only Eq. 30 can be used to determine the minimum unit stream power without using any resistance equation. Thus, Eq. 30 can serve the dual purpose of being a transport as well as a resistance equation. This was confirmed by Parker as shown in Fig. 5. Further studies on the conditions under which simplified theories of minimization can be applied are needed.

It is true that the use of Eq. 30 does not always assure the existence of

minimum unit stream power for subcritical flows. As shown in Figs. 3 and 4, the agreements between observed and theoretical values deteriorate as sediment concentration, which is related to Froude number, increases. For all the tests made by the writers, no minimum unit stream power can be found in supercritical flows. As sediment concentration or Froude number increased to a certain value, the treatment of sediment concentration merely as a constraint in the minimization process is not sufficient. In this case, the total rate of energy dissipation for water and sediment has to be minimized (49).

Chen raised some basic questions on the application of the variational principle to turbulent flows. A detailed and more rigorous treatment of this subject was published by the writers (47). The writers agree with Chen that the term of "gradually varied flow" used by the writers could cause some confusion and misunderstanding. The "gradually varied flow" used in the paper means nonaccelerating flow or the inertia terms in the equation of motion are small and can be ignored (47). The writers do not believe that the dissipation function for turbulent flow was incorrectly expressed by Eqs. 7*a* and 7*b*. There are at least two ways to demonstrate this point. The simplest way is to start with the Reynold's equation, Eq. 3, and the Boussinesq's assumption, Eq. 5. Substitution of Eq. 5 into Eq. 3 leads to an equation of the form identical to that of the original Navier-Stokes equation based on mean values with $\nu + \epsilon$ replacing ν. Eq. 6 is a simplified version of that equation after dropping the acceleration terms. The dissipation function based on the instantaneous values is known to be:

$$\Phi = \frac{1}{2}\rho\nu\left(\frac{\partial u_i}{\partial x_j} + \frac{\partial u_j}{\partial x_i}\right)^2 \quad \ldots\ldots\ldots\ldots\ldots\ldots\ldots\ldots\ldots\ldots \quad (43)$$

Eq. 43 is the dissipation function of the flow represented by the Navier-Stokes equation and the reduced equation of motion for turbulent flow is obtainable from the Navier-Stokes equation by substituting the instantaneous values with the mean values and ν by $\nu + \epsilon$. By the same substitution, Eq. 43 is transformed into Eq. 7*a*. That is, if Eq. 43 is the dissipation function of the Navier-Stokes equation, then Eq. 7*a* must be the dissipation function of the flow represented by Eq. 6. There should be no doubt that one can follow, step by step, the same procedure required for the derivation of Eq. 43 to arrive at Eq. 7*a* starting from Eq. 6.

The second approach is to base the argument on the energy balance equation as shown by Hinze (45). As Chen has correctly pointed out, the direct viscous dissipation of kinetic energy into heat energy from the mean velocity field and the turbulence field are, respectively, given by Eqs. 35 and 36. However, as Hinze (45) and other investigators have pointed out, the process of energy transfer within a unit volume of fluid is: mean flow → large scale turbulence → small scale turbulence → heat energy. The rate of turbulence production at the expense of mean flow energy per unit volume is:

$$\Phi_{tt} = -\rho\,\overline{u_i' u_j'}\,\frac{\partial \bar{u}_i}{\partial x_j} \quad \ldots\ldots\ldots\ldots\ldots\ldots\ldots\ldots\ldots\ldots \quad (44)$$

By Boussinesq's assumption, Eq. 44 reduces to the second part of Eq. 7*a* as pointed out by Chen. That is, Eq. 7*a* is equivalent to:

$$\Phi = \bar{\Phi} + \Phi_{tt} \quad (45)$$

Now all that remains to be shown is that $\Phi_{tt} = \Phi'$ under an equilibrium condition. Clearly, this is not strictly true because of the presence of other nondissipative work done terms. This is strictly true in a steady uniform turbulent flow because in this case there is no net work done between neighboring volumes of fluid and the turbulent energy of each unit volume remains constant. That is, the turbulence production is strictly balanced with the turbulence dissipation everywhere in this case. For the nonaccelerating flow case treated in the writers' paper, the relationship is only approximately true. When the system as a whole is in an equilibrium condition, the only source of error is the differential turbulent energy flux and the differential work done between the upstream and downstream ends. For a very long and nearly nonaccelerating river, these differences are likely to be much less than the total energy loss. The work done at the solid boundary as well as the free surface boundary is zero because either the velocity or the stress is zero there. The writers feel that Eq. 7*a* is a reasonably good representation of the total energy dissipation rate for the intended type of flows.

It appears that Chen might have misinterpreted the meaning of **V**. One must remember that $\mathbf{V} \cdot \mathbf{n} = l\hat{u}_1 + m\hat{u}_2 + n\hat{u}_3$ is the normal component of the velocity variation and not the velocity. Therefore, if the velocity distributions at both ends of a study reach are given, then **V** must be zero there. Because the free surface is a stream surface where the mean velocity $\bar{u}_i$, or $\mathbf{V} \cdot \mathbf{n}$ must be zero along the stream surface. If the velocity distributions at both ends are not given, the hydraulic heads at the upstream and downstream ends of a study reach or the difference between them must be given before the problem can be solved (47). The writers agree with Chen that the rigid boundary gradually varied flow problems of a given discharge with given roughness and specified boundary conditions can be solved without resorting to a minimization approach. The intent of the writers' derivations was to show that the variational or minimization approach can provide an alternative, and in some cases a more desirable and flexible approach to solving open channel hydraulic problems. The basic concept behind the minimization approach is not limited to seeking the best estimated value of roughness coefficient.

Appendix.—References

43. Chang, H. H., "Minimum Stream Power and River Channel Patterns," *Journal of Hydrology*, Vol. 41, 1979, pp. 303–327.
44. Chang, H. H., "Geometry of River in Regime," *Journal of the Hydraulics Division*, ASCE, Vol. 105, HY6, Proc. Paper No. 14640, June, 1979, pp. 691–706.
45. Hinze, J. O., *Turbulence*, 2nd ed., McGraw-Hill Publishing Co., Inc., New York, N.Y., 1975, pp. 22–23 and pp. 68–74.
46. Lanczos, C., *The Variational Principles of Mechanics*, 4th ed., University of Toronto Press, Toronto, Canada, 1974.
47. Song, C. C. S., and Yang, C. T., "Minimum Stream Power: Theory," *Journal of the Hydraulics Division*, ASCE, Vol. 106, No. HY9, Proc. Paper No. 15691, Sept., 1980, pp. 1477–1487.
48. Yang, C. T., "Theory of Minimum Rate of Energy Dissipation and Its Applications," post symposium lecture notes, International Symposium on River Sedimentation, Beijing, China, Mar., 1980.
49. Yang, C. T., Song, C. C. S., and Woldenberg, M. J., "Hydraulic Geometry and Minimum Rate of Energy Dissipation," paper accepted for publication in the *Water Resources Research*, 1981.

Interfacial Stability in Channel Flow[a]

Closure by Richard H. French,[4] A. M. ASCE

The writer appreciates the interest shown in the paper and wishes to thank the discussers, Jensen and McCutcheon, for their comments and suggestions. With regard to these discussions, the writer would like to note the following.

First, the suggestion of Jensen that interfacial stability at large Reynolds numbers should be a function of R_o and $u_*/\bar{u}$ would appear to be valid. Jensen is essentially claiming that interfacial stability is a function of the bottom boundary friction factor which is not a violation of the writer's basic hypothesis.

Second, McCutcheon correctly noted that the aspect ratio (width-to-depth) of the flume used by the writer was very small. McCutcheon (19) has demonstrated that a low aspect ratio can have a significant effect of $u_*/\bar{u}$ in stratified flows. This discusser's comments would indicate that the corrective procedures developed by Vanoni and Brooks (17) are not entirely applicable to stratified flows.

Third, McCutcheon noted that the writer's hypothesis showed no improvement on the work of Polk et al. (12) with regard to upstream warm water wedges at power plants. Although the writer noted and commented on the work of Polk, et al. (12), the specific subject of this paper was the stability of superposed turbulent layers with a zero velocity difference at the interface. In this case, there is a single mechanism of turbulence generation; the bottom boundary. In the case of upstream warm water wedges, there are two mechanisms of turbulence generation; the bottom boundary and interfacial shear. Because of this difference in turbulence generation, these two cases should be considered separately.

Fourth, the writer would like to thank McCutcheon for publishing additional data which were not available when the writer's work was published. In addition, the error analysis done by this discusser is interesting.

In conclusion, the writer would note the recent work of Abraham, et al. (24) in the areas of interfacial shear and stability.

Appendix.—Reference

24. Abraham, G., Karelse, M., and Van Os, A. G., "On the Magnitude of Interfacial Shear of Subcritical Stratified Flows in Relation with Interfacial Stability," *Journal of Hydraulic Research*, Vol. 17, No. 4, 1979, pp. 273–288.

[a]August, 1979, by Richard H. French (Proc. Paper 14768).

[4]Assoc. Research Prof., Desert Research Inst., Water Resources Center, Univ. of Nevada System, 4582 Maryland Parkway, Las Vegas, Nev. 89109.

Unconditional Stability in Convection Computations[a]

Closure by Victor Miguel Ponce,[9] Yung Hai Chen,[10] Members, ASCE, and Daryl B. Simons,[11] F. ASCE

The writers wish to thank Stelling, Arunachalam and Raman, and Barnett and McBride for their interest in this paper.

Stelling has addressed the question of terminology of explicit versus implicit schemes of the one-dimensional convection equation. In addition, he has pointed out some of the complications which may arise in calculations involving tidal areas. Arunachalam and Raman's discussion centers on the similarity (or perhaps, dissimilarity) of the writers' equations with the well-known Crank-Nicolson scheme. Barnett and McBride have correctly pointed out some of the difficulties encountered when attempting to model functions containing sharp gradients using neutrally stable schemes.

The semantic question regarding explicit and implicit schemes is one that, in the writers' opinion, needs to be put to rest. It has long been established (4) that explicit means point-by-point calculation; implicit, on the other hand, means line-by-line calculation. By this terminology, the schemes treated by the writers are all explicit. In a particular application the boundary conditions may be such that the solution necessitates the inversion of a matrix, in which case the associated scheme would be implicit. However, the basic difference between explicit and implicit schemes remains intact.

Arunachalam and Raman go through a lengthy and rather pointless mathematical exercise in an attempt to show that the writers' equations bear certain similarity with the Crank-Nicolson scheme. In fact, the writers treat explicit numerical schemes of the pure convection equation; Crank-Nicolson's method is a well-known *implicit* scheme of the diffusion equation. The only commonality between the writers' approach and that of Crank-Nicolson seems to be the feature of space and time centering.

Barnett and McBride's comments are well taken. The writers' aim was to show the numerical properties of a class of explicit schemes of the one-dimensional convection equation. In doing so, they may have inadvertedly misled the reader into thinking that schemes with vanishing numerical diffusion coefficient are to be preferred in all cases. In fact, as Barnett and McBride point out, there is something to say in favor of the introduction of some numerical diffusion, as long as it does not considerably impair accuracy.

The writers did not intend to use the schemes presented in connection with

[a]September, 1979, by Victor Miguel Ponce, Yung Hai Chen, and Daryl B. Simons (Proc. Paper 14807).

[9]Assoc. Prof. of Civ. Engrg., Coll. of Engrg., San Diego State Univ., San Diego, Calif. 92182.

[10]Assoc. Prof. of Civ. Engrg., Colorado State Univ., Fort Collins, Colo. 80521.

[11]Assoc. Dean of Engrg. and Prof. of Civ. Engrg., Colorado State Univ., Fort Collins, Colo. 80521.

the computation of "square waves." These waves contain, by definition, very sudden changes in properties, and no numerical method can fully account for these features. Barnett and McBride's choice of minimal phase error as being more desirable than amplitude preservation is at best a compromise, given the limitations inherent in the discrete computation.

Slurry Flow in Pipe Networks[a]

Closure by Don J. Wood,[3] M. ASCE

The discussion by Oner Yucel requests additional clarification of the nature of approximations applied to hydraulic graduates and flowrates which allows linearization of the nonlinear network equations. There are, in fact, no approximations involved because essentially an exact solution of the nonlinear network equations are obtained. Linearization of the nonlinear equations is utilized in an iterative procedure for solving these equations, but carrying out several trial results in the true solution of the nonlinear set of equations.

Certainly the ultimate goal of a cost optimization of slurry transport systems is desirable and the technique described in the paper for handling the hydraulic calculations is an essential component of this type of study.

Modified Fickian Model for Predicting Dispersion[b]

Discussion by Spyridon Beltaos[3]

The writer agrees with the main thesis of the paper, as stated in the following sentence: "The effects of dead zones as well as channel irregularity and nonuniformity can be regarded as a mere prolongation of the time required to reach the Taylor or diffusive periods." Using this same postulate, the writer (1,30) arrived by a different route to a variation of σ_t^2 with x which is equivalent to that of the authors. Putting $t_o = L/U$ and using the approximate transformation

[a]January, 1980, by Don J. Wood (Proc. Paper 15132).

[3]Prof. of Civ. Engrg., Coll. of Engrg., Univ. of Kentucky, Lexington, Ky. 40506.

[b]June, 1980, by Henry Liu and Alexander H. D. Cheng (Proc. Paper 15454).

[3]Research Scientist, Hydr. Div., National Water Research Inst., Canada Centre for Inland Waters, P.O. Box 5050, Burlington, Ontario L7R 4A6, Canada.

$x \approx Ut$ (also used by the authors implicitly), Eq. 6 reduces to Eq. 15 of Ref. 30; note that the writer's (30) coefficient "β"—not to be confused with the function β of the authors (therefore quotation marks are used in this discussion)—is equal to D_L / LU. It may be of interest to compare next the experimental values of corresponding model parameters.

Considering Eq. 18 and putting $l = 0.7\ \bar{W}$ and $t_o = L/U$ gives:

$$\frac{L}{\bar{W}} = 0.5\ \text{m} \left(\frac{\bar{W}}{R}\right)\left(\frac{U}{U_*}\right) \quad \ldots\ldots\ldots\ldots\ldots\ldots\ldots\ldots\ldots\ldots\ldots\ldots \quad (26)$$

which coincides with Eq. 37 of Ref. 30 if 0.5 m is set equal to the writer's coefficient α_L. Using $m = 5$, as recommended by the authors, gives $\alpha_L = 2.5$; this is about twice the average value implied in Fig. 8 of Ref. 30 but still within the range of scatter of the data points. Rearranging Eq. 19 with $A = \bar{W}R$ and $R \simeq d$, gives

$$\frac{D_L}{RU_*} = \gamma \left(\frac{\bar{W}}{R}\right)^2 \quad \ldots\ldots\ldots\ldots\ldots\ldots\ldots\ldots\ldots\ldots\ldots\ldots \quad (27)$$

which coincides with Eq. 6 of Ref. 30 if γ is set equal to the writer's coefficient B. The authors found γ to vary from 0.2 to 1.3, having an average value of about 0.6. These are close to corresponding values of B implied in Fig. 9 of Ref. 30, though B seems to scatter more than γ. Considering the writer's coefficient "β," Eqs. 26 and 27 may be used simultaneously to give

$$\text{"}\beta\text{"} = \frac{D_L}{LU} = \left(\frac{2\gamma}{m}\right)\left(\frac{U_*}{U}\right)^2 \quad \ldots\ldots\ldots\ldots\ldots\ldots\ldots\ldots\ldots\ldots \quad (28)$$

With $\gamma = 0.6$ and $m = 5$, Eq. 28 reduces to

$$\text{"}\beta\text{" (average)} = 0.24 \left(\frac{U_*}{U}\right)^2 \quad \ldots\ldots\ldots\ldots\ldots\ldots\ldots\ldots\ldots\ldots \quad (29)$$

which agrees closely with average values of "β" implied in Fig. 7 of Ref. 30. In summary, it may be stated that the experimental values of model parameters determined by the authors and the writer, respectively, are in agreement. In general, the writer's ranges of scatter appear wider than those of the authors; this is probably due to the fact that the authors have allowed larger scatter in evaluating individual test results as can be seen by comparing Figs. 5 and 6 with Figs. 8 and 10 of Ref. 1.

Concerning details of the model proposed by the authors, the writer suggests the following:

1. Introduction of the Pearson type-III distribution (Eq. 20) to predict C versus t variations appears arbitrary, especially in view of the fact that the model does provide a pertinent equation (Eq. 10). The advantage cited by the authors for Eq. 20, i.e., that it reproduces the skew better than does Eq. 10, is considered marginal from the practical point of view. In practice, the errors committed due to uncertainties in predicting σ_t^2 and $C_{\max}$ far outweigh discrepancies due to inaccurate predictions of skew. Therefore, use of Eq. 20 is considered an unnecessary refinement.

2. By direct substitution and some algebra, it can be shown that Eq. 10 is not a solution of Eq. 11; the correct version of Eq. 11, such that it is satisfied by Eq. 10, can be shown to be:

$$\frac{\partial C}{\partial t} + U\frac{\partial C}{\partial x} = \left[\frac{d}{dt}(D_L^* t)\right]\frac{\partial^2 C}{\partial x^2} \quad \ldots\ldots\ldots\ldots\ldots\ldots\ldots\ldots \quad (30)$$

Note that, by Eq. 9, $d(D_L^* t)/dt = 0.5\,(d\sigma_x^2/dt)$ which is consistent with the definition of the diffusion or dispersion coefficient; and that $d(D_L^*/t)/dt$ does not coincide with D_L^* unless β is a constant. According to Eq. 8*a*, β is a function of t, approaching the constant value $\beta = 1$ only when $t/t_o \to \infty$. Using the definition of D_L^* and performing the differentiation indicated in Eq. 30 gives:

$$\frac{\partial C}{\partial t} + U\frac{\partial C}{\partial x} = D_L(1 - e^{-t/t_o})\frac{\partial^2 C}{\partial x^2} \quad \ldots\ldots\ldots\ldots\ldots\ldots\ldots\ldots \quad (31)$$

which shows that the dispersion coefficient, $D_L(1 - e^{-t/t_o})$, increases with time to the asymptotic value of D_L. For practical purposes, the dispersion coefficient can be considered equal to D_L when $t \geq 3t_o$. The correct version of Eq. 13 is

$$\frac{\partial C'}{\partial t'} + \frac{\partial C'}{\partial x'} = D'_L(1 - e^{-t/t_o})\frac{\partial^2 C'}{\partial x'^2} \quad \ldots\ldots\ldots\ldots\ldots\ldots\ldots\ldots \quad (32)$$

It is noted, however, that these modifications do not affect later results because the analysis has been based on Eqs. 10 and 15 which are correct.

Appendix.—Reference

30. Beltaos, S., "Longitudinal Dispersion in Rivers," *Journal of the Hydraulics Division*, ASCE, Vol. 106, No. HY1, Proc. Paper 15118, Jan., 1980, pp. 151–172.

Transverse Mixing Tests in Natural Streams[a]

Discussion by Hugo B. Fischer,[2] M. ASCE

The writer welcomes the new experimental data given in this paper, as accurate observations of transverse mixing in real streams are indeed few. Nevertheless the writer is concerned that the author's computed results are so strongly dependent on the factor ψ, and would like to be more certain that the reported values of the transverse mixing coefficient E_z are accurate. In earlier work

[a]October, 1980, by Spyridon Beltaos (Proc. Paper 15731).

[2]Prof. of Civ. Engrg., Hydr. and Coastal Engrg., 412 O'Brien Hall, Univ. of California, Berkeley, Calif. 94720.

(16) the author has also used the stream tube method to ascertain the value of E_z, but did not require the assumption that $h^2 U_d \epsilon_{zd}$ is constant. Since $U_d \approx h^{1/2}$ and $\epsilon \approx u^* h \approx h^{3/2}$, it is more reasonable to expect that $h^2 U_d \epsilon_{zd}$ is proportional to h^4, which is far from constant. In addition, it should be noted that Eq. 6 follows from Eq. 5 only if $\epsilon_{zd} = e_z$ is constant, since otherwise the averaging process yields an additional term resulting from the correlation of ϵ_{zd} with $h^2 U_d$. The definition of ψ (given incorrectly in Eq. 8 and the derivation of Eq. 12 depend in turn on Eq. 6, Eq. 12 being the crucial equation for the determination of E_z from the observations. Without access to the complete set of data the writer is unable to evaluate the inaccuracy introduced by the several averaging processes. The author notes briefly that in one instance he checked his value of E_z using a numerical algorithm. Any further evidence that could be offered in the closure to establish the validity of the reported values of E_z would be most helpful. Use of the numerical algorithm described by the writer in Ref. 16, e.g., would avoid the questions of accuracy just raised.

The writer hopes that maps of the test reaches for tests 3-4 and 5-6 can be included in the closure, as he suspects few readers will have access to Ref. 2 and thinks maps of the study reaches essential to evaluate results.

Finally, the writer wishes to suggest an explanation for the result that $K(=E_z/RV_*)$ increases due to an ice cover. In a wide stream $R \approx H$ and $K \approx E_z/HV_*$, the nondimensional representation commonly used since Elder's (1959) work. In a wide ice-covered stream, however, $R \approx H/2$. The question then arises whether R or H is the correct length scale, i.e., whether it is more logical to report a dimensionless dispersion coefficient as $K = E_z/RV_*$ or $K' = E_z/HV_* \approx K/2$. In the writer's opinion the choice is clear. Taylor's theory of diffusion by continuous movements (21) shows that the magnitude of a turbulent diffusion coefficient depends on the product of a length scale and a velocity scale (see Ref. 20, p. 71). In turbulent channel flow the velocity scale is generally accepted to be the shear velocity. The length scale is generally taken as the distance between the boundaries, which means between the free surface and the channel bottom in the case of a free surface flow, or between the upper ice boundary and the channel bottom in the case of an ice-covered stream. The author's use of R implies that the effect of the ice cover is to halve the length scale of the turbulence. This seems unlikely, since the turbulent motions can be expected to persist over the whole distance between the boundaries, and the writer suggests that H is the logical choice.

Table 3 gives information computed from the author's Table 1, but the nondimensional result is given in terms of $K' = E_z/HV_*$. The shear velocity, $V_* = \sqrt{gRS}$, was computed from the author's table assuming, for lack of more exact information, that $R = H$ for open water and $R = H/2$ for ice-covered conditions.

The range of K' is nearly within that of previous experiments

$$K' = 0.6 \pm 50\% \quad \ldots\ldots\ldots\ldots\ldots\ldots\ldots\ldots\ldots\ldots \quad (26)$$

as reviewed by the writer (Ref. 20, p. 112). In two of the three pairs, K' is smaller for the ice-covered test, but no consistent relationship is shown. The writer concludes that the author's data support the previously established approximate relationship, and demonstrate that an ice cover has no great effect. At the same time the author's data demonstrate once again our inadequate

TABLE 3.—Recomputed Dimensionless Dispersion

Test number (1)	Riversite and channel description (2)	Flow condition (3)	Discharge, in cubic meters per second (4)	Width, in meters (5)	Depth, in meters (6)
1	Athabasca River below Fort McMurray; straight with occasional bars, islands	Ice-covered	240	252	1.9
2	Same as Test 1	Open water	776	373	2.2
3	Beaver River near Cold Lake; regular meanders, point bars and large dunes	Open water	20.5	42.7	0.96
4	Same as Test 3	Ice-covered	6.5	38.7	0.61
5	Athabasca River below Athabasca; irregular meanders with occasional bars, islands	Open water	566	320	2.05
6	Same as Test 5	Ice-covered	105	276	0.96

Notes: 1 m = 3.28 ft. Col. 1–6, 8, 9, and 11 are taken directly from Table 1.

understanding of the nature of transverse mixing, as exemplified by the range of the dimensionless coefficient over a factor of 4.

APPENDIX.—REFERENCES

19. Elder, J. W., "The dispersion of marked fluid particles in turbulent shear flow," J. Fluid Mech. *5*, 544–460 (1959).
20. Fischer, H. B., List, E. J., Koh, R. C. Y., Imberger, J., and Brooks, N. H., *Mixing in Inland and Coastal Waters*, Academic Press, New York, N.Y., 1979.
21. Taylor, G. I., "Diffusion by Continuous Movements," *Proceedings*, London Mathematical Society, Series A., Vol. 20, 1921, pp. 196–211.

Coefficients for Author's Tests

Hydraulic radius, in meters (7)	Velocity, in meters per second (8)	Slope $\times 10^4$ (9)	Shear velocity, in meters per second (10)	Transverse mixing coefficient, in square meters per second (11)	E_z/RU^* (12)	E_z/HU^* (13)
0.95	0.49	1.44	0.0366	0.041	1.18	0.59
2.2	0.95	1.44	0.0557	0.093	0.76	0.76
0.96	0.50	2.1	0.0444	0.043	1.01	1.01
0.305	0.28	2.1	0.025	0.020	2.62	1.31
2.05	0.86	3.1	0.0789	0.067	0.41	0.41
0.48	0.40	3.1	0.0382	0.010	0.55	0.27

Bar Resistance of Gravel-Bed Streams[a]

Discussion by Peter Engel[3] and Y. Lam Lau[4]

The authors have presented a method for predicting the stage discharge for gravel-bed streams. Their contribution has been greatly enhanced by the use of relatively rare and comprehensive data from actual river reaches. Fundamental to the authors' analysis was the determination of the bar resistance C_B and it is on this aspect of their paper that the writers wish to comment.

[a]October, 1980, by Gary Parker and Allan W. Peterson (Proc. Paper 15733).

[3]Research Engr., Environmental Hydr. Section, Hydr. Div., National Water Research Inst., Canada Centre for Inland Waters, P.O. Box 5050, Burlington, Ontario L7R 4A6, Canada.

[4]Head, Environmental Hydr. Section, Hydr. Div., National Water Research Inst., Canada Centre for Inland Waters, P.O. Box 5050, Burlington, Ontario L7R 4A6, Canada.

One of the two fundamental assumptions made by the authors is that C_B is a unique function of the dimensionless shear stress τ_G^* due to the granular bed material. The values of C_B obtained were plotted against τ_G^* in Fig. 6 to arrive at a relationship between C_B and τ_G^*. The writers wish to suggest a simpler variable which may correlate just as well with C_B.

The authors have assumed that $C_B = f(\tau_G^*) = f(RS_G)$ in which $R = H/D_{50}$. The submerged specific gravity will be neglected as it was taken to be a constant. Following Keulegan's relation for grain resistance the authors obtained Eq. 10 which gives S_G as a function of H/D_{50} and the Froude number F. Therefore, the authors are in effect assuming that C_B is a function of a variable which is itself a function of H/D_{50} and F, i.e.:

$$C_B = f\left[\frac{H}{D_{50}}, \phi\left(\mathsf{F}, \frac{H}{D_{50}}\right)\right] \quad \ldots\ldots\ldots\ldots\ldots\ldots\ldots\ldots\ldots\ldots \quad (20)$$

with ϕ given by Eq. 10.

The fact that C_B should depend on H/D_{50} and F can be obtained from a dimensional analysis for C_B and then neglecting the effects of Reynolds number and the specific gravity of the bed material. However, it has been shown by Engel and Lau (35) that, for Froude numbers up to 0.5, the total resistance for flow over dunes was independent of the Froude number. As the grain resistance coefficient is also independent of the Froude number (Eq. 2), one would expect that, in the present case, the bar resistance coefficient C_B will also be independent of the Froude number. As a result, it should be possible to express C_B as a function of H/D_{50} only i.e.:

$$C_B = f\left[\frac{H}{D_{50}}\right] \quad \ldots\ldots\ldots\ldots\ldots\ldots\ldots\ldots\ldots\ldots\ldots\ldots\ldots\ldots \quad (21)$$

The authors' Fig. 4 for Old Man River shows that even though the effect of H/D_{50} on C_G is not too large, H/D_{50} has a large effect on the total C and therefore C_B. Therefore, it may be better to try and correlate C_B with H/D_{50} which is a more basic variable as opposed to the more complicated τ_G^*. This would also more directly reflect the authors' premise that C_B becomes more important at successively lower stages of the flow.

A second point on which the writers wish to comment is the authors' assumption that, at flood stages, C_B is negligible. The authors sought to confirm their assumption by a comparison of S and S_G in their Fig. 5, and observed that the S_G which they calculated was approximately equal to the observed S at flood stages. These results are in contrast with observations made on artificial dunes by the writers from laboratory measurements (35). In Ref. 35 the writers' experimental data, as well as those of Vadagodakumbura for values of H/D_{50} up to 1,000 and dune steepness (i.e., dune height/dune length) down to 0.02, indicate clearly that the total friction factor is larger than that computed from the authors' Eq. 2. It may be that, because of errors in determining the slope S and grain-size D_{90} in the field, the difference between S and S_G could not be detected by the authors. It seems only logical that even at high flows there must be some form resistance due to the shape of the bars. Therefore,

depending upon the shape of the bars, C_B may be small but may not always be negligible.

APPENDIX.—REFERENCE

35. Engel, P. and Lau, Y. L., "Friction Factor for Two-Dimensional Dune Roughness," *Journal of Hydraulic Research*, Delft, The Netherlands, Vol. 18, No. 3, 1980, pp. 213–225.

Technical Papers

Original papers should be submitted in triplicate to the Manager of Technical and Professional Publications, ASCE, 345 East 47th Street, New York, N.Y. 10017. Authors must indicate the Technical Division or Council, Technical Committee, Subcommittee, and Task Committee (if any) to which the paper should be referred. Those who are planning to submit material will expedite the review and publication procedures by complying with the following basic requirements:

1. Titles must have a length not exceeding 50 characters and spaces.

2. The manuscript (an original ribbon copy and two duplicate copies) should be double-spaced on one side of 8-1/2-in. (220-mm) by 11-in. (280-mm) paper. Three copies of all figures and tables must be included.

3. Generally, the maximum length of a paper is 10,000 word-equivalents. As an *approximation*, each full manuscript page of text, tables or figures is the equivalent of 300 words. If a particular subject cannot be adequately presented within the 10,000-word limit, the paper should be accompanied by a rationale for the overlength. This will permit rapid review and approval by the Division or Council Publications and Executive Committees and the Society's Committee on Publications. Valuable contributions to the Society's publications are not intended to be discouraged by this procedure.

4. The author's full name, Society membership grade, and a footnote stating present employment must appear on the first page of the paper. Authors need not be Society members.

5. All mathematics must be typewritten and special symbols must be identified properly. The letter symbols used should be defined where they first appear, in figures, tables, or text, and arranged alphabetically in an appendix at the end of the paper titled Appendix.—Notation.

6. Standard definitions and symbols should be used. Reference should be made to the lists published by the American National Standards Institute and to the *Authors' Guide to the Publications of ASCE*.

7. Figures should be drawn in black ink, at a size that, with a 50% reduction, would have a published width in the *Journals* of from 3 in. (76 mm) to 4-1/2 in. (110 mm). The lettering must be legible at the reduced size. Photographs should be submitted as glossy prints. Explanations and descriptions must be placed in text rather than within the figure.

8. Tables should be typed (an original ribbon copy and two duplicates) on one side of 8-1/2-in. (220-mm) by 11-in. (280-mm) paper. An explanation of each table must appear in the text.

9. References cited in text should be arranged in alphabetical order in an appendix at the end of the paper, or preceding the Appendix.—Notation, as an Appendix.—References.

10. A list of key words and an information retrieval abstract of 175 words should be provided with each paper.

11. A summary of approximately 40 words must accompany the paper.

12. A set of conclusions must end the paper.

13. Dual units, i.e., U.S. Customary followed by SI (International System) units in parentheses, should be used throughout the paper.

14. A practical applications section should be included also, if appropriate.